

Density stratification, suspended-sediment transport, and downstream fining in large,  
low-slope, sand-bed rivers

A THESIS  
SUBMITTED TO THE FACULTY OF THE GRADUATE SCHOOL  
OF THE UNIVERSITY OF MINNESOTA  
BY

Scott Alan Wright

IN PARTIAL FULFILLMENT OF THE REQUIREMENTS  
FOR THE DEGREE OF  
DOCTOR OF PHILOSOPHY

Gary Parker, Adviser

May 2003

## **ABSTRACT**

Large sand-bed rivers typically display an upward concave longitudinal profile and a downstream decrease in median bed sediment grain diameter. This thesis contains four journal ready papers related to the study of these phenomena.

Chapter 1 focuses on the effects of density stratification on the vertical velocity and concentration profiles in open-channel flows. It is found that in general density stratification effects tend to be greater in large, low-slope rivers than in their smaller, steeper brethren. The effect on the total suspended load and size distribution of suspended-sediment can be significant, and thus density stratification should be included in sediment transport predictions for these conditions. Chapter 2 incorporates density stratification into new formulations for the prediction of the flow depth and grain-size specific suspended-sediment transport rate in sand-bed rivers. The new formulation also includes new predictive equations for near-bed entrainment rate into suspension and form drag.

Chapter 3 presents a numerical model for the simulation of the longitudinal profile and bed sediment distribution in sand-bed rivers over the past 5,000 years of relatively stable sea-level. In Chapter 4 the model is applied to a generic river reach typical of a large, sand-bed river flowing into the ocean in order to investigate the effects of sea-level rise and tectonic subsidence on the degree of profile concavity and downstream fining. Also, several other physical mechanisms that may affect fining are studied, including the relative importance of the suspended versus bed load, the effect of the loss of sediment overbank, and the influence of the delta bottom slope.

# TABLE OF CONTENTS

OVERVIEW .....	1
CHAPTER 1: DENSITY STRATIFICATION EFFECTS IN SAND-BED RIVERS .....	3
ABSTRACT .....	4
INTRODUCTION.....	4
THEORY .....	7
Governing equations .....	7
Turbulence closure .....	8
Non-dimensional forms.....	11
Comparison with previous models.....	12
Generalization for sediment mixtures .....	16
Governing dimensionless parameters.....	17
COMPARISON WITH LABORATORY DATA.....	19
Clear-water flows .....	19
Sediment suspensions.....	20
APPLICATION TO SAND-BED RIVERS .....	23
Use of field measurements .....	23
Accounting for flow variability.....	27
Calculation results .....	28
CONCLUSIONS .....	31
ACKNOWLEDGEMENTS.....	34
REFERENCES .....	34
NOTATION.....	39

TABLES .....	43
FIGURES.....	45
CHAPTER 2: FLOW RESISTANCE AND SUSPENDED LOAD IN SAND-BED	
RIVERS: SIMPLIFIED STRATIFICATION MODEL .....	54
ABSTRACT .....	55
INTRODUCTION.....	55
DENSITY STRATIFICATION .....	61
RELATION FOR NEAR-BED CONCENTRATION .....	65
Limitations of the Garcia and Parker (1991) entrainment relation .....	66
Skin friction/form drag partitioning .....	68
New entrainment relation .....	71
DEPTH-DISCHARGE RELATION .....	72
RELATION FOR SUSPENDED SEDIMENT TRANSPORT.....	75
CONCLUSIONS .....	78
ACKNOWLEDGEMENTS.....	79
REFERENCES .....	79
NOTATION.....	82
TABLES .....	85
FIGURES.....	86
CHAPTER 3: MODELING DOWNSTREAM FINING IN SAND-BED RIVERS I:	
FORMULATION .....	94
ABSTRACT .....	95
INTRODUCTION.....	95

MODEL DESCRIPTION .....	97
Primary governing equations .....	97
Prograding delta boundary .....	101
Moving boundary formulation .....	102
Numerical solution scheme .....	104
Flow intermittency factor .....	105
CONCLUSIONS .....	106
REFERENCES .....	108
NOTATION.....	112
TABLES .....	115
FIGURES.....	116
 CHAPTER 4: MODELING DOWNSTREAM FINING IN SAND-BED RIVERS II:	
APPLICATION .....	119
ABSTRACT .....	120
INTRODUCTION.....	120
MODEL PRELIMINARIES .....	123
Generic study reach.....	123
Active width.....	124
RESULTS I: DRIVING MECHANISMS.....	125
Prograding delta .....	125
Sea-level rise .....	126
Tectonic subsidence .....	127
Comparison with field cases .....	127

RESULTS II: IMPORTANCE OF OTHER MECHANISMS .....	128
Bed load versus suspended load.....	128
Active width.....	129
Overbank sediment loss .....	130
Delta bottom slope .....	132
Density stratification .....	132
SENSITIVITY ANALYSIS .....	133
CONCLUSIONS .....	136
REFERENCES .....	138
NOTATION.....	140
FIGURES.....	142

## OVERVIEW

Large sand-bed rivers typically display downstream decreases in bed slope and characteristic bed sediment grain diameter (such as the median). Two examples, the Mississippi and Fly Rivers, are illustrated in Figures 1 and 2 of Chapter 3. In this thesis the mechanisms controlling the development of the concave upward longitudinal profile and downstream fining are investigated. The thesis consists of four chapters, where each chapter is a journal-ready formatted paper. The first two papers relate to the prediction of size-selective, suspended-sediment transport, a key process driving downstream fining. The third and fourth papers detail the development and application of a numerical model of downstream fining, which makes use of the relations developed in the first two papers.

In Chapter 1, the effects of density stratification are studied through the application of a one-dimensional (vertical) numerical model of momentum and mass balance in an open-channel, which incorporates a turbulence closure that retains the buoyancy terms. The primary new finding is that in general density stratification effects tend to be greater in large, low-slope rivers than in their smaller, steeper brethren. Under high flow conditions the total suspended load and size distribution of suspended-sediment can be significantly affected by density stratification.

In Chapter 2, new methods are presented for the prediction of the flow depth and grain-size specific suspended-sediment transport rate. The improvements all relate to the need to modify existing formulations in order to extend their ranges of applicability to large, low-slope, sand-bed rivers. They can be summarized as follows: a) inclusion of density stratification effects using a simplified version of the model developed in Chapter

1; b) a new predictor for near-bed entrainment rate into suspension; and c) a new predictor for form drag.

In Chapter 3 a numerical model is presented for the simultaneous simulation of the longitudinal profile and bed sediment distribution in sand-bed rivers over the past 5,000 years of relatively stable sea-level. The model formulation contains several mechanisms that can drive the development of an upward concave profile and downstream fining, including a delta prograding into standing water, sea-level rise, and tectonic subsidence. A moving boundary formulation is used to track the two moving boundaries associated with the prograding delta. The set of equations is solved using a four-point implicit finite difference scheme and Newton iteration, which allows for the use of large time steps.

In Chapter 4 the model presented in Chapter 3 is applied to a generic river reach typical of a large, sand-bed river flowing into the ocean in order to investigate the mechanisms controlling longitudinal profile development and downstream fining. Various rates of sea-level rise (typical of the late Holocene) and tectonic subsidence are modeled in order to quantify their effects on the degree of profile concavity and downstream fining. Also, several other physical mechanisms which may affect fining are studied, including the relative importance of the suspended versus bed load, the effect of the loss of sediment overbank, and the influence of the delta bottom slope. Finally, sensitivity analysis is used to show that the grain-size distribution at the interface between the active layer and substrate has a significant effect on downstream fining.

# **CHAPTER 1: DENSITY STRATIFICATION EFFECTS IN SAND-BED RIVERS**

Scott Wright and Gary Parker

## **ABSTRACT**

In this paper the effects of density stratification in sand-bed rivers are studied by the application of a model of vertical velocity and concentration profiles, coupled through the use of a turbulence closure that retains the buoyancy terms. By making the governing equations dimensionless, it is revealed that the slope is the additional dimensionless parameter introduced by inclusion of the buoyancy terms. The primary new finding is that in general density stratification effects tend to be greater in large, low-slope rivers than in their smaller, steeper brethren. Under high flow conditions the total suspended load and size distribution of suspended sediment can be significantly affected by density stratification, and should be accounted for in any general theory of suspended transport.

## **INTRODUCTION**

The velocity and concentration profiles in uniform, open-channel, sediment-laden flows have been the subject of many theoretical, experimental, and numerical studies over the past 50 years. A primary reason for such interest is that accurate prediction of the profiles allows for accurate prediction of the flow depth and suspended sediment discharge, key parameters for morphological prediction models. Early on, Vanoni (1946) and Einstein and Chien (1955) experimentally observed an increase in the velocity gradient in the presence of suspended sediment. The phenomenon was also observed in measurements of velocity profiles in the field, including the Missouri and Atchafalaya Rivers (Einstein and Chien 1954, 1955), the Rio Grande (Nordin 1964) and the Mississippi River (Jordan 1965, Scott and Stephens 1966). It was hypothesized that the effect was due to a “damping” of the turbulence, thus decreasing turbulent mixing (see

e.g. ASCE 1975). One mechanism typically cited as a cause for this “damping” is the vertical density stratification induced by the concentration gradient. The density gradient creates a buoyancy force that makes it more difficult to flux heavier fluid/sediment upward into lighter fluid/sediment, and similarly restricts the downward flux of lighter fluid/sediment into heavier fluid/sediment. The early experimental results led Einstein and Chien (1954, 1955) to propose an empirical correlation between an “apparent” von Karman parameter and the ratio of the power to hold a sediment grain in suspension to the power to overcome friction. In their study this apparent von Karman parameter was determined by fitting the overall logarithmic velocity profile to measured data. Here this is distinguished from the traditional definition of the von Karman constant ( $\kappa$ ) as a near-wall value associated with a constant shear layer. The apparent von Karman parameter,  $\kappa_a$ , is here defined as the inverse of the slope of the straight line fit to velocity versus distance above the bed over the entire flow depth on semi-log paper, that is:

$$\frac{I}{\kappa_a} = \frac{d\left(\frac{u}{u_*}\right)}{d(\ln y)} \quad (1)$$

where  $u$  is streamwise velocity,  $u_*$  is shear velocity, and  $y$  is vertical distance from the bed.

The experimental correlation of Einstein and Chien is reproduced as Figure 1 herein. Several important features of this figure are now noted, and will be returned to frequently throughout this paper. First, the ordinate of Figure 1 may be considered to be a form of the Richardson number, which expresses the ratio of energy lost working against a density gradient to the turbulent kinetic energy produced by shear. This implies

that density stratification is indeed the physical process underlying the empirical correlation. Second, the presence of the slope in the denominator of the abscissa is significant. It will be shown that slope is the additional dimensionless parameter introduced by the inclusion of density stratification effects. Finally, it is noted that the largest decreases in  $\kappa_a$  are in general realized for the field conditions of the Missouri and Atchafalaya Rivers, both of which represent examples of large, low-slope sand-bed rivers.

The conclusions detailed above will be drawn primarily from numerical integration of the time-averaged momentum and mass-balance equations with a turbulence closure due to Mellor and Yamada (1982) as modified by Galperin et al. (1988), along with data from various sand-bed rivers. The turbulence closure accounts for the presence of a density gradient, and has been applied to many geophysical flows in which density stratification effects are important (e.g. atmospheric and oceanic boundary layers). The stratification model is first compared with some previous models, then to data from flume experiments exhibiting both weak and strong stratification effects. The model is quite similar to previous models that have been compared extensively with flume data (see e.g. Villaret and Trowbridge 1991), so a comprehensive comparison is not presented here. The objective of this study is not a strict validation of the stratified flow analogy for open-channel, sediment-laden flows, but rather the exploration of some of the implications of density stratification on grain-size specific suspended sediment discharge under field conditions. To this end, the model is generalized for mixtures of sand, and applied to a range of conditions typical of sand-bed rivers, as determined from several field studies detailed in the literature. A new figure similar to Figure 1 is

produced from the theory and data, indicating that density stratification is the major factor responsible for the correlation originally developed by Einstein and Chien (1954, 1955). Also a more general analysis is performed at the discharge with a 5% exceedence probability in order to estimate the magnitude of density effects under comparable high flow conditions across a wide range of sand-bed rivers.

## THEORY

### Governing equations

The balances governing turbulent, steady, uniform, open-channel sediment-laden flows are Reynolds-averaged water momentum and sediment mass conservation, given as follows for a uniform grain-size (see Figure 2 for a definition sketch):

$$0 = \frac{d(\overline{-u'v'})}{dy} + gS_o(1 + RC) \quad (2)$$

$$0 = \overline{-v'c'} + v_s C \quad (3)$$

where  $C$  is time-averaged volumetric concentration,  $u'$ ,  $v'$ , and  $c'$  are the streamwise and vertical turbulent velocity fluctuations and turbulent concentration fluctuation, respectively, the overbar represents time averaging,  $\overline{-u'v'} = \tau/\rho$  is the Reynolds stress,  $\tau$  is shear stress,  $\rho$  is water density,  $g$  is acceleration due to gravity,  $S_o$  is slope,  $R = (\rho_s/\rho - 1)$  is submerged specific gravity,  $\rho_s$  is sediment density,  $\overline{-v'c'}$  is Reynolds flux of sediment, and  $v_s$  is particle settling velocity. Integration of (2) and application of zero shear stress at the water surface yields:

$$\frac{-\overline{u'v'}}{ghS_o} = \left(1 - \frac{y}{h}\right) + \frac{R}{h} \int_y^h C dy \quad (4)$$

where  $h$  is the flow depth. It is seen that the maximum effect of the sediment on the local stress is realized as  $y \rightarrow 0$ , in which case the second term on the right-hand side of (4) becomes  $R\bar{C}$ , where  $\bar{C}$  is the depth-averaged concentration. Herein the suspension is assumed dilute such that  $\bar{C} \ll 1$ , and therefore the linear clear-water stress profile is retained:

$$\frac{-\overline{u'v'}}{u_*^2} = 1 - \eta \quad (5)$$

where  $u_* \equiv \sqrt{\tau_o/\rho} = \sqrt{ghS_o}$  is the shear velocity,  $\tau_o$  is the bed shear stress, and  $\eta = y/h$ . Though the model will be applied to situations later in which dunes are present, no attempt is made to model the details of the flow structure over the dunes (e.g. Smith and McLean 1977, Nelson et al. 1993). As will be seen later, the model near-bed boundary conditions are specified at 5% of the depth, and it is assumed (but not rigorously verified) that this is a distance far enough from the bed so that (5) is roughly applicable with the total shear stress computed from the depth-slope product (i.e. internal boundary layer dynamics due to bedforms are neglected).

### **Turbulence closure**

Closure relationships are now required to relate Reynolds stress and flux to the time-averaged velocity and concentration. The standard mixing length closure of Prandtl leads to the well-known law of the wall velocity profile (log-law) and the Rouse distribution for suspended sediment (see e.g. ASCE 1975). To account for density stratification effects, the closure scheme of Mellor and Yamada (1982), as modified by

Galperin et al. (1988) is used. Mellor and Yamada (1974, 1982) have derived a series of “levels” of closure of decreasing complexity. Details of the assumptions and scaling arguments leading to the closure relations can be found in the references cited, but are not presented here. The “Level 4” model is a full Reynolds stress closure, consisting of transport equations for all components of the Reynolds stress tensor and Reynolds flux vector. Scaling arguments and data are then used to simplify the closure. Here we find the “Level 2” model, which assumes a direct balance between turbulent kinetic energy production and dissipation, to perform well for open-channel suspensions. Preliminary calculations were performed with the “Level 2½” model, which retains a diffusion term in the energy balance. The results differ only in a region near the surface where the production-dissipation balance does not hold due to very low shear production. Near the surface the concentration is typically quite small, so that differences in suspended sediment discharge between the two levels are generally small. It was concluded that the small differences in sediment transport do not justify the additional numerical complexity (initial value problem becomes boundary value problem).

The “Level 2” model for steady, uniform flow for a uniform grain-size suspension consists of the following turbulent kinetic energy balance, and algebraic relations for the individual stresses and fluxes:

$$0 = -\overline{u'v'} \frac{du}{dy} - Rg\overline{v'c'} - \frac{k^{3/2}}{B_I\ell} \quad (6)$$

$$\overline{u'v'} = -\frac{3A_I\ell}{\sqrt{k}} \left[ (\overline{v'^2} - C_I k) \frac{du}{dy} + Rg\overline{u'c'} \right] \quad (7)$$

$$\overline{v'^2} = \frac{k}{3} \left( 1 - 6 \frac{A_1}{B_1} \right) - 6 \frac{A_1 \ell}{\sqrt{k}} Rg \overline{v'c'} \quad (8)$$

$$\overline{u'c'} = -\frac{3A_2 \ell}{\sqrt{k}} \left( \overline{u'v'} \frac{dC}{dy} + \overline{v'c'} \frac{du}{dy} \right) \quad (9)$$

$$\overline{v'c'} = -\frac{3A_2 \ell}{\sqrt{k}} \left( \overline{v'^2} \frac{dC}{dy} + Rg \overline{c'^2} \right) \quad (10)$$

$$\overline{c'^2} = -\frac{B_2 \ell}{\sqrt{k}} \overline{v'c'} \frac{dC}{dy} \quad (11)$$

where  $k \equiv \overline{u'^2} + \overline{v'^2} + \overline{w'^2}$  is turbulent kinetic energy,  $\ell$  is the master turbulence length scale, and  $A_1, A_2, B_1, B_2,$  and  $C_1$  are model constants. The constants relate all length scales to the master length scale, and have been determined from neutral data by Mellor and Yamada (1982). The constants  $A_2$  and  $B_2$  are dependent on the turbulent Prandtl number, or Schmidt number in this case, which is the ratio of the turbulent diffusivity of momentum to that of mass. Mellor and Yamada chose 0.80 for the turbulent Prandtl number, a value generally accepted for heat. Little agreement is available on the value of the Schmidt number in sediment-laden flows (see e.g. van Rijn 1984, Brush et al. 1952, Cellino and Graf 1997, Greimann et al. 1999, Singamsetti 1966, Coleman 1970); given the significant debate on this subject, here the simplest choice of unity is made. Though this assumption may be proven somewhat erroneous in the future, the general conclusions presented herein are not expected to change greatly. This choice leads to the following set of model constants:

$$(A_1, A_2, B_1, B_2, C_1) = (0.92, 0.59, 16.6, 8.1, 0.08) \quad (12)$$

For the master turbulent length scale the algebraic relation suggested by Mellor and Yamada (1982) is chosen:

$$\ell = \ell_o \frac{\kappa y}{\kappa y + \ell_o} \quad \ell_o = \alpha \frac{\int_0^h y \sqrt{k} dy}{\int_0^h \sqrt{k} dy} \quad (13)$$

where  $\kappa=0.4$  is the von Karman constant, and  $\alpha$  is an empirical constant to be determined. Note that (13) reduces to the Prandtl mixing length near the wall.

### Non-dimensional forms

The governing equations and closure are now made dimensionless as follows:

$$\hat{u} = \frac{u}{u_*} \quad \hat{k} = \frac{k}{u_*^2} \quad \hat{v}_s = \frac{v_s}{u_*} \quad \hat{\ell} = \frac{\ell}{h} \quad \eta = \frac{y}{h} \quad (14)$$

Substitution of (3) and (5) into (6) and application of (14) yields the non-dimensional form of the turbulent kinetic energy balance:

$$0 = (1 - \eta) \frac{d\hat{u}}{d\eta} - \frac{R}{S_o} \hat{v}_s C - \frac{\hat{k}^{3/2}}{B_1 \hat{\ell}} \quad (15)$$

Substitution of the closure relations, (7)-(11), into the momentum balance (5) yields:

$$\left[ \frac{\chi_4 \hat{\ell} \hat{k}^{1/2} - \chi_5 R \hat{\ell}^2 \hat{v}_s C}{\hat{k} S_o} \right] \frac{d\hat{u}}{d\eta} = 1 - \eta \quad (16)$$

$$\left[ 1 - \frac{\chi_3 R \hat{\ell}^2}{\hat{k} S_o} \frac{dC}{d\eta} \right]$$

and for sediment mass balance (3):

$$\left[ \chi_1 \hat{\ell} \hat{k}^{1/2} - \frac{\chi_2 R \hat{\ell}^2 \hat{v}_s C}{\hat{k} S_o} \right] \frac{dC}{d\eta} = -\hat{v}_s C \quad (17)$$

where  $\chi_1 = A_2 - 6A_1A_2/B_1$ ,  $\chi_2 = 18A_1A_s + 3A_2B_2$ ,  $\chi_3 = 9A_1A_2$ ,  
 $\chi_4 = A_1 - 6A_1^2/B_1 - 3A_1C_1$ , and  $\chi_5 = 18A_1^2 + 9A_1A_2$ . With the use of (12) and (13),  
(15)-(17) comprise three equations in three unknowns,  $\hat{k}$ ,  $C$ , and  $\hat{u}$  which require near-  
bed velocity and concentration boundary conditions. All model results presented here are  
obtained using fourth-order Runge-Kutta numerical integration for (16) and (17),  
combined with a Newton iteration for (15).

### **Comparison with previous models**

Several models have been proposed in the literature to account for the effects of  
sediment on velocity and concentration profiles. Itakura and Kishi (1980) applied a  
direct analogy to the Monin-Obukhov theory for the stably stratified atmosphere (see e.g.  
Turner 1973). The theory assumes constant shear and buoyancy flux layers, which  
results in a log-linear velocity profile, i.e. only the outer flow region is affected.  
Coleman (1981, 1986) proposed a similar velocity profile to that of Itakura and Kishi,  
whereby the outer-flow “wake” coefficient is increased to account for the presence of  
sediment, while the conventional log-law holds near the bed. The wake coefficient is  
correlated with a gross flow Richardson number, therefore the effect is assumed due to  
density stratification. However, other researchers (Soulsby and Wainwright 1987,  
McLean 1991, 1992) have shown (through theory and modeling, not data) that  
stratification effects may be restricted to either the inner- or outer-region of the flow, or  
span the entire flow depth, depending on the flow and sediment conditions. van Rijn  
(1984) proposed an empirical modification to the sediment diffusivity to account for  
damping of turbulence and the resultant effect on the concentration profile, while

assuming that the effects on the velocity profile can be neglected for the computation of suspended sediment transport.

Smith and McLean (1977) appear to be the first to apply a more rigorous analogy to the thermally stratified atmospheric boundary layer. The governing equations are set in the form:

$$K_m \frac{du}{dy} = u_*^2 (1 - \eta) \quad (18)$$

$$K_s \frac{dC}{dy} = -v_s C \quad (19)$$

where  $K_m$  is the eddy viscosity and  $K_s$  is the sediment diffusivity. The clear-water eddy viscosity and sediment diffusivity are then modified as a function of the flux Richardson number. Typically it is assumed that the adjustments to eddy viscosity and diffusivity are the same (i.e. Schmidt number equal to unity), so here for simplicity eddy viscosity only is compared. The general form of the adjustment is as follows:

$$K_m = K_{mo} f(Ri_f) \quad (20)$$

where  $K_{mo}$  is the clear-water eddy viscosity, and  $f(Ri_f)$  denotes a functional relationship of the flux Richardson number:

$$Ri_f = \frac{Rg v_s C}{u_*^2 (1 - \eta) \frac{du}{dy}} \quad (21)$$

Smith and McLean (1977) used the following form:

$$f(Ri_f) = (1 - \beta Ri_f) \quad (22)$$

where  $\beta$  is an empirical constant. It is noted that Smith and McLean formulated (20) in terms of the gradient Richardson number, which is identical to the flux Richardson

number for a Schmidt number equal to one. The empirical constant  $\beta=4.7$  in accordance with the measurements of Businger et al. (1971) in the thermally stratified atmospheric surface layer. Gelfenbaum and Smith (1986) followed with a similar approach, stating that a scaling analysis of the turbulent kinetic energy equation was used to derive the following form:

$$f(Ri_f) = (1 + \gamma\zeta)^{-1} \quad (23)$$

$$\zeta = \frac{Ri_f}{1 - \gamma Ri_f} \quad (24)$$

where  $\gamma$  is an empirical constant. However, (23) and (24) can be manipulated into the exact same form as (22), that is:

$$f(Ri_f) = (1 - \gamma Ri_f) \quad (25)$$

Gelfenbaum and Smith (1986) found that  $\gamma=4.7$  as per Businger et al. (1971) and  $\gamma=6.9$  as per Wierenga (1980) both worked well for cases of weak stratification, but  $\gamma=10.0$  was required when stratification effects were strong. This result is based on comparison with the flume experiments of Vanoni (1946) and Einstein and Chien (1955). McLean (1991, 1992) used a similar model with dependence on a stratification parameter closely related to the flux Richardson number, which cannot be set in the form of (20). However it is expected that the dependence will be similar to (23), as stated by McLean (1992).

The model given by (15)-(17) can be recast in the form of (19) by assuming a turbulent length scale analogous to Prandtl's mixing length for an open-channel flow:

$$\hat{l} = \kappa\eta\sqrt{1-\eta} \quad (26)$$

Note that this prescription of the length scale is used here only to compare with previous models. The length scale given by (13) is used in all subsequent model applications. Substitution of (26) into (15)-(17) results in the following form of (20):

$$f(Ri_f) = [B_1(1 - Ri_f)]^{-1/2} \left[ \frac{\chi_1 B_1(1 - Ri_f) + (\chi_3 - \chi_2) Ri_f}{(\chi_4 B_1(1 - Ri_f) - \chi_5 Ri_f)(\chi_1 B_1(1 - Ri_f) - \chi_2 Ri_f)} \right]^{-3/4} \quad (27)$$

The three models are compared in Figure 3, with  $\gamma=10.0$  for the Gelfenbaum and Smith (1986) model. It is seen that (27) is quite similar to the model of Smith and McLean (1977), while the model of Gelfenbaum and Smith (1986) predicts a much larger effect of stratification for smaller Richardson number, due to the choice of the empirical constant. For the present model and that due to Smith and McLean, turbulence is extinguished for  $Ri_f \cong 0.21$ . One advantage of the present approach is that the empirical constants are determined from neutral data, i.e. under conditions where stratification is absent. It is then assumed that the physically based model can be applied to conditions where stratification is present, an assumption which must of course be validated by comparison with data. A more empirical approach such as that of Gelfenbaum and Smith (1986) relies on data from a range of flows where stratification is present. As shown by Villaret and Trowbridge (1991), determining these coefficients from laboratory experiments on sediment suspensions has proven difficult. Unfortunately, both approaches suffer from a lack of data on turbulence in sediment suspensions. The similarity of the dependence shown in Figure 3 is at least partially due to the fact that constants for both models are derived from heat flux data.

## Generalization for sediment mixtures

Gelfenbaum and Smith (1986) and McLean (1991, 1992) have shown that the effects of the grain-size distribution must be addressed in the calculation of suspended sediment transport. The present model can be readily generalized for a mixture of grain-sizes  $D_i$ ,  $i=1, n$  where  $n$  is the number of individual grain-sizes. The water momentum and turbulent energy balances are affected through a summation over all grain-sizes, while a sediment mass balance equation is attained for each grain-size. Thus (15)-(17) become, respectively:

$$0 = (1 - \eta) \frac{d\hat{u}}{d\eta} - \frac{R}{S_o} \sum_{i=1}^n \hat{v}_{si} C_i - \frac{\hat{k}^{3/2}}{B_1 \hat{\ell}} \quad (28)$$

$$\left[ \frac{\chi_4 \hat{\ell} \hat{k}^{1/2} - \frac{\chi_5 R \hat{\ell}^2}{\hat{k} S_o} \sum_{i=1}^n v_{si} C_i}{1 - \frac{\chi_3 R \hat{\ell}^2}{\hat{k} S_o} \frac{d}{d\eta} \sum_{i=1}^n C_i} \right] \frac{d\hat{u}}{d\eta} = 1 - \eta \quad (29)$$

$$\left[ \chi_1 \hat{\ell} \hat{k}^{1/2} - \frac{\chi_2 R \hat{\ell}^2}{\hat{k} S_o} \sum_{i=1}^n v_{si} C_i \right] \frac{dC_i}{d\eta} = -\hat{v}_{si} C_i \quad i=1, n \quad (30i)$$

where  $v_{si}$  and  $C_i$  are settling velocity and volumetric concentration of grain-size  $i$ , respectively. The generalized flux Richardson number becomes:

$$Ri_f = \frac{Rg \sum_{i=1}^n v_{si} C_i}{u_*^2 (1 - \eta) du/dy} \quad (31)$$

A near-bed concentration boundary condition is now required for each size fraction.

## Governing dimensionless parameters

To understand how density stratification is embedded into the problem, it is instructive to examine the dimensionless parameter groupings that must be specified in order to solve the system of equations. One interesting property of the governing equations is that the velocity appears only as a derivative. Also, the dimensionless grouping which indicates the strength of stratification, the flux Richardson number, also contains the velocity only as a derivative. Therefore in terms of assessing the effects of stratification only the velocity derivative is of importance. Indeed, substitution of (16) into (15) and (17) allows for integration of (17) to obtain the concentration profile independent of the velocity. This solution, along with (16), may then be used to compute the flux Richardson number.

Based on the above, the discussion of the dimensionless parameters governing stratification will focus on the concentration profile. Neglecting the buoyancy terms in (15) and (17), with the aid of (26) results in:

$$\frac{dC}{d\eta} = \frac{-v_s C}{u_* \kappa \eta (1 - \eta)} \quad (32)$$

Again it is noted that (26) is used here in place of (13) only for illustrative purposes.

Integration of (32) gives the Rouse equation:

$$\frac{C}{C_a} = \left[ \frac{1 - \eta}{\eta} \frac{\eta_a}{1 - \eta_a} \right]^{Z_R} \quad (33)$$

$$Z_R = \frac{v_s}{\kappa u_*} \quad (34)$$

where  $C_a$  is the concentration at some near-bed point  $\eta_a$ , which should correspond to the top of the bedload layer. Thus in the absence of stratification three parameters must be specified to compute the concentration profile:  $C_a$ ,  $\eta_a$ , and  $v_s/u_*$ . To determine if any additional parameters are required in the presence of density stratification, (15) and (17) are examined. It is quickly recognized that the terms representing stratification all contain one additional dimensionless parameter, the slope (or more precisely, the ratio  $S_o/R$ ). It should be borne in mind, however, that  $C_a$  itself could theoretically be a function of slope in such a way that it mitigates stratification effects.

Most near-bed concentration predictors assume the primary dependence to be on bed shear stress, or equivalently shear velocity, and do not include slope directly in the formulation. The following thought experiment helps to understand the role of slope in mediating stratification effects. A uniform flow and equilibrium suspension is attained in a flume with sediment size  $D$ , slope  $S_o$ , and unit water discharge  $q$ . The water temperature, depth and concentration profiles are measured, and  $v_s/u_*$  is computed. The slope is then decreased, but the unit discharge is increased so that the depth-slope product is held constant, so insuring that  $u_*$  is unmodified. If sediment size also remains the same, then the ratio  $v_s/u_*$  does not change. If the near-bed concentration is primarily a function of  $v_s/u_*$  and sediment size (e.g. van Rijn 1984, Garcia and Parker 1992), and  $\eta_a \cong \text{constant}$ , then  $C_a$  will be approximately the same. Under these conditions, the Rouse equation would predict the same dimensionless concentration distribution for both experiments. However, the model with density stratification terms would not predict the same concentration distribution, since the stratification terms would be increased by the

decrease in slope, as indicated by (15) – (17). As illustrated below, the neglect of slope effects in  $C_a$  are an oversimplification, but the above thought experiment serves to illustrate the essential point: decreasing slope accentuates stratification effects.

The influence of the slope can also be quickly seen by rearranging the flux Richardson number using the non-dimensional parameters given in (14):

$$Ri_f = \frac{R}{S_o} \left( \frac{v_s}{u_*} \right) \frac{C}{(1-\eta) d\hat{u}/d\eta} \quad (35)$$

Here again we see the presence of the governing dimensionless parameters. Recall that the Richardson number represents the ratio of energy lost working against the density gradient to energy produced by shear. It is difficult to ascertain directly from (35) how the governing parameters interact to affect the Richardson number. Slope may decrease over orders of magnitude from small to large sand-bed rivers, potentially yielding much higher Richardson numbers in the large rivers, since slope appears in the denominator. It is shown below, however, that low-slope rivers tend to have systematically lower concentrations than steeper rivers for the same value of  $v_s/u_*$ . This fact mitigates but by no means eliminates stratification effects mediated by the Richardson number through the slope. The problem can be further clarified by considering laboratory and field data.

## COMPARISON WITH LABORATORY DATA

### Clear-water flows

Before the model can be applied to sediment suspensions, the empirical coefficient  $\alpha$  in the turbulent length scale equation (13) must be determined for open-

channel flows. Clear-water calculations were compared with the flume experiments of Nezu and Rodi (1986), and with a standard log-law combined with a wake function:

$$\frac{u}{u_*} = \left( \frac{u}{u_*} \right)_a + \frac{1}{\kappa} \ln \left( \frac{\eta}{\eta_a} \right) + \frac{2II}{\kappa} \sin^2 \left( \frac{\pi}{2} \eta \right) \quad (36)$$

where  $(u/u_*)_a$  is the non-dimensional velocity at  $\eta_a$ , which is determined from the data, and  $II$  is the wake strength (set equal to 0.2 here as per Nezu and Rodi 1986). Figure 4 shows the comparison for Run P4 with  $\alpha=0.7$ , which is the value adopted for the remainder of the calculations presented. For this and all calculation results presented hereafter,  $\kappa=0.4$ .

### **Sediment suspensions**

Many laboratory experiments have been conducted to study velocity and suspended sediment profiles in open-channel flows. Villaret and Trowbridge (1991) provide a summary of the most often cited studies. The objective of their work was to determine the empirical coefficient for a model such as Smith and McLean (1977), as presented earlier. They concluded that few experiments have been conducted under conditions in which stratification effects are strong, and thus it is difficult to distinguish stratification effects in the presence of experimental error for these experiments (see their Figure 18). The set of experiments found most promising by Villaret and Trowbridge (1991) for detecting stratification effects is the fine sand series of Coleman (1981, 1986). These experiments may be criticized for the effects of the sidewalls due to a width to depth ratio of approximately two, which results in a velocity maximum well below the surface. It is desirable to also compare the model to data where stratification is weak; for this purpose the experiments of Lyn (1986) and Barton and Lin (1955) are chosen.

Settling velocity for this and all further calculations reported herein are computed from the empirical relation due to Dietrich (1982).

Figures 5 and 6 compare the model velocity and concentration profiles with the measurements of Lyn for experiment EQ1565, Barton and Lin Run 36, and Coleman’s Run 20 (see Table 1 for experimental conditions). The boundary conditions were set according to the measured near-bed values (but not always to the exact value of the measurement made nearest the bed). The increased velocity gradient can be clearly discerned in the Coleman velocity profile (note also the sidewall effects near the surface). While the fit looks quite good for each run, Lyn (2000) has pointed out that better comparisons can be made by first subtracting out the clear-water profile, or in the case of sediment the profile without stratification effects. Comparing the “total” profile can be misleading in terms of the goodness of fit since the deviations can be small. It is more appropriate to compare the part of the profile due to stratification effects only, since this is the feature of the model of prime interest here. Comparisons of these deviations from the profiles without stratification are shown in Figures 7 and 8, as follows:

$$U_{dev} = \frac{u_s - u_{ns}}{u_s} \quad (37)$$

$$C_{dev} = \frac{C_s - C_{ns}}{C_s} \quad (38)$$

where the subscripts  $s$  and  $ns$  denote with and without stratification, respectively. Clearly there is more scatter about the model predictions when the profile without stratification is subtracted out. In particular the deviation from the log-law near the bed noted by Lyn (1986) is most apparent, and is clearly not a stratification effect. However, the general

trend of deviation from the profile without stratification is captured by the model. This is particularly so for the experiment of Coleman, for which stratification effects are strongest. As stated in the introduction, the objective here is not to validate the stratified flow analogy for sediment suspensions. More rigorous comparisons with data for a model similar to the one presented here can be found in Villaret and Trowbridge (1991). One of the difficulties in comparing models of stratification with flume data is that experiments showing strong stratification are simply very rare. One might initially assume that this is because stratification effects are not important in equilibrium, open-channel suspensions. However, another assumption might be that the conditions conducive to strong stratification effects (low-slope and/or high concentration, as shown below), are simply not attainable in the laboratory. The presence of the sidewall effects in the Coleman experiments, the only experiments to show strong stratification, is telling. In order to model low-slopes in the laboratory under conditions where sand-size sediment will go into suspension (i.e. sufficiently high shear stresses) the depth needs to be quite large, thus requiring an extremely wide flume to avoid sidewall effects. Using sand and water, one simply cannot model the governing dimensionless parameters conducive to significant stratification in a small flume.

Because low-slope, sand suspensions do exist in the field, it would seem logical to resort to field data for comparison with stratification models. However this raises an entirely new set of difficulties. First, profile measurements are relatively rare, particularly at high flows, and typically only a few points in the vertical are sampled. Also, field conditions are typically not very uniform, such that two- and three-dimensional effects are greater than in controlled flume experiments. Finally,

measurement uncertainty is expected to be greater in the field than in the laboratory. These complications make direct comparisons against detailed field data quite difficult. An approach that requires less detailed field data is pursued below. In particular, the model is used to compute the bulk effect of stratification on the eddy viscosity, similar to the apparent von Karman parameter  $\kappa_a$  illustrated in Figure 1.

## **APPLICATION TO SAND-BED RIVERS**

### **Use of field measurements**

Some evidence for density stratification effects in sand-bed rivers has been measured in the field and reported for various river reaches (Einstein and Chien 1954, Nordin 1964, Jordan 1965, and Scott and Stephens 1966) The primary evidence reported in these studies is a reduction in the apparent von Karman parameter, i.e. the best-fit slope of the velocity profile over the entire depth on semi-log paper. Fitting the log-law to measurements provides no insight into the mechanism underlying the decrease. However, by applying the stratification model to conditions similar to the ones reported in these studies, it can be determined whether or not density stratification is contributing to the measured phenomenon. The model also allows a study of the conditions under which the effects are strongest, similar to the line of reasoning followed by Soulsby and Wainright (1987) for coastal environments. The field measurements suggest a reduction in the apparent von Karman parameter of 30-50% for rivers such as the Missouri, Atchafalaya, Mississippi, and the Rio Grande. If the model predicts similar effects on the velocity profile to those observed in the field, it can be considered strong evidence that density stratification is the physical mechanism underlying these measurements.

For the model to be applied in a purely predictive sense, near-bed velocity and concentration boundary conditions must be specified in terms of the independent flow and bed sediment conditions. Here, however, the goal is simply to deduce the conditions under which stratification effects are strongest. Therefore measurements of velocity and sediment transport from several sand-bed rivers are used to specify the boundary conditions. Ideally the procedure would be similar to that used for the flume experiments. Field data sets including near-bed point velocity and concentration measurements are, however, relatively rare. The goal of most sediment sampling programs is to measure the total suspended load; therefore transport rates are most often measured with a depth-integrating sampler at several equal discharge (or width) verticals, which results in a discharge-weighted mean concentration for the entire cross-section, for each grain-size range:

$$C_{mi} = \frac{Q_{si}}{Q} \quad (39)$$

where  $Q_{si}$  is the volume suspended sediment transport rate of grain-size  $D_i$ , and  $Q$  is the water discharge. If the channel width is assumed relatively constant with depth, and the lateral variation in vertical distribution of velocity and suspended sediment are neglected (as in a wide channel), (39) can be approximated by:

$$C_{mi} = \frac{q_{si}}{q} = \frac{\int_{\delta}^h u C_i dy}{\int_{\delta}^h u dy} \quad (40)$$

where  $\delta$  is the top of the bedload layer or some near-bed position. Field velocity profiles are also rarely reported, but discharge often is, either by measuring velocity profiles at several verticals and computing the total discharge, or by using of a rating curve

developed from previous direct measurements. The mean depth and width are also often measured, allowing for calculation of the mean velocity. Again assuming a roughly rectangular cross-section and wide channel, the mean velocity can be approximated by:

$$U = \frac{Q}{bh} = \frac{1}{h} \int_{\delta}^h u dy \quad (41)$$

Measured mean velocity and mean concentration by grain-size can be used to specify the near-bed boundary conditions in an iterative fashion. The boundary conditions are guessed, and the profiles are computed from the model. Computed mean velocity and concentrations from (40) and (41) are compared to the measured values. Since the sediment samplers cannot be applied all the way to the bed, the comparisons using (40) are restricted to the region of flow outside of this distance (i.e. above the unsampled zone). The boundary conditions are then updated using a Newton procedure, and the iteration is continued until the computed values match the measurements to a specified tolerance.

The near-bed boundary conditions are specified at 5% of the flow depth for all calculations presented here. This height is typically near or below the unsampled zone height. Theoretically this position should be closer to the bed, but this becomes particularly difficult for flows with bedforms where the position above the bed must be defined with respect to the spatially averaged bed elevation. Also, specification at a significant distance from the bed (such as 5%) helps to justify the neglect of the internal boundary layer and wake dynamics of the flow over dunes (Smith and McLean 1977, Nelson et al. 1993). Though the internal boundary layer may extend outside the lower 5% of the flow depth for many cases, the additional complexity involved in rigorously

treating this region is not considered warranted here, given the uncertainty and error associated with the field data. The use of 5% of the depth also serves to restrict the calculations to a region where the concentrations do not violate the dilute suspension assumption, and should not have a major effect on transport rates.

Although this technique ignores lateral variations which may indeed be strong under many field conditions (e.g. in meander bends), it does provide an approximation of the average velocity and concentration profiles across the channel. The use of the measured mean velocity and concentrations assures that gross errors will not be made in terms of the bulk properties of the suspension. A basic assumption here then is that the average profiles determined as described above are adequate for assessing the relative strength of density stratification across a range of conditions representative of sand-bed rivers.

Sediment transport data collection programs have been instituted on various sand-bed rivers in the U.S., primarily in the 1950's and 60's. Six locations are chosen for comparison here: the Niobrara River at Cody, NE (Colby and Hembree 1956), the Middle Loup River at Dunning, NE (Hubbell and Matejka 1959), the Rio Grande River at Bernallilo, NM (Nordin 1964), and the Red River at Alexandria, LA, the Atchafalaya River at Simmesport, LA, and the Mississippi River at Tarbert Landing, MS (Toffaletti 1968). The Niobrara and Middle Loup are both shallow, relatively steep sand-bed rivers in the upper Mississippi River basin, while the Red, Atchafalaya, and Mississippi (at Tarbert Landing) are large, deep, low-slope rivers in the lower Mississippi basin. The Rio Grande falls in between in terms of depth and slope, with larger depths and lower

slopes than the small rivers, but not nearly as deep as the large rivers. The range of parameters for each river are summarized in Table 2.

### **Accounting for flow variability**

One problem with using measurements as described above is that there is no guarantee that flow events of similar magnitude are being compared between rivers. This makes it difficult to generalize the results and make direct comparisons between different rivers. Comparisons between rivers should be made for a similar flow event, such as the bankfull flow or flows with equal exceedence probability. Here the flow with a 5% exceedence probability,  $Q_5$ , is chosen to compare the rivers. The 5% probability is chosen because it is a high flow event where stratification effects are expected to be greatest, but not such a large flow that no measurements would be available at or above the discharge. U.S. Geological Survey daily discharge gages have been in operation over a period of time at all of the river locations listed in the previous section. The daily discharge records were used to construct the flow-duration curve (cumulative distribution function) for each river. The gage number, period of record, and computed  $Q_5$  for each river are listed in Table 3. Then for each river the pertinent dimensionless parameters,  $S_o$ ,  $C_m$ , and  $v_{s50}/u_*$ , were determined by plotting each versus  $Q/Q_5$ , visually fitting a line through the scatter, and estimating the parameter at  $Q/Q_5=1$ . It can be seen in Tables 2 and 3 that sediment measurements were made on the Atchafalaya, Niobrara, and Rio Grande at flows greater than  $Q_5$ . However, for the Middle Loup, Red, and Mississippi all sediment measurements were made at flows less than  $Q_5$ , such that extrapolation was required to determine the parameters at  $Q_5$ . The Middle Loup and Mississippi each had measured flows very near  $Q_5$ , so that the extrapolation was straightforward. The highest

flow event for the Red was only approximately 50% of  $Q_5$ , making the extrapolation more difficult. However, for the purposes of the general comparison desired here, the extrapolation procedure is considered appropriate. The results of the estimation procedure are shown in Table 3. A similar procedure was used for estimating the bulk stratification effects at  $Q_5$  for each river, as discussed in the following section.

### Calculation results

Before analyzing model results, some observations can be made regarding the relationships between the governing dimensionless parameters. First, as was mentioned previously, concentration tends to increase with slope, as shown by Figure 9. Figure 10 shows the variation of  $v_{s50}/u_*$  with slope ( $v_{s50}$  is settling velocity based on  $D_{50}$ ); no clear trend can be discerned. This is in accordance with previous studies (Parker, et al. 1998, Dade and Friend 1998), where it has been shown that dimensionless bed shear stress based on  $D_{50}$  at bankfull flow is loosely constant across a wide range of sand-bed rivers. The importance of these interrelationships becomes apparent when a “sand river” Richardson number is defined as follows:

$$Ri_{sr} = R \frac{v_{s50}}{u_*} \frac{C_m}{S_o} \quad (42)$$

where  $C_m$  is the total discharge-weighted concentration of sand by volume. Note that (42) is essentially a depth-averaged version of (35), if it is assumed that the dimensionless velocity derivative does not change greatly between flows. It is also important to recognize the similarity between (42) and the parameter used by Einstein and Chien (1954, 1955), shown here in Figure 1. Now it is clear that the ratio  $C_m/S_o$  is of primary importance, since  $v_{s50}/u_*$  is relatively unchanged between rivers. Figure 9

shows that slope and concentration both vary over about two orders of magnitude for the rivers used here. However, it can be seen in Figure 11 that this ratio tends to be larger for the low-slope rivers at the 5% exceedence discharge. Based on this, it is expected that in general the largest decreases in turbulent mixing predicted by the model should be realized in the larger, low-slope rivers when comparable flow events are compared.

The model was applied to each observation for the rivers in Table 2, specifying the boundary conditions iteratively as described. The bulk strength of density stratification is estimated by analyzing the predicted reduction in turbulent mixing, averaged over the depth. The degree of turbulent mixing is indicated by the eddy viscosity, so that the reduction in depth-averaged eddy viscosity is given by:

$$\bar{K}_{red} = \frac{\bar{K}_m}{\bar{K}_{mo}} \quad (43)$$

where  $\bar{K}_m$  is the depth-averaged eddy viscosity with stratification effects, and  $\bar{K}_{mo}$  is the depth-averaged eddy viscosity for the equivalent clear-water flow. Note that  $\bar{K}_{red}$  is roughly equivalent to the reduction in the apparent von Karman parameter which would be attained if a log-law were fit to the modeled velocity profiles, i.e.:

$$\kappa_a \cong \bar{K}_{red} \kappa \quad (44)$$

This methodology provides a bulk measure of stratification, but it is not meant to suggest that stratification effects are constant throughout the flow depth. Now a figure reminiscent of the Einstein and Chien figure (Figure 1 here) can be constructed, and is presented in Figure 12. As expected, the largest decreases in turbulent mixing (or  $\kappa_a$ ) are realized for the large, low-slope rivers. Figure 12 also shows the importance of

comparing rivers at similar flow events, as it is seen that the Rio Grande realized some significant stratification effects since the measurements were made at very high flows.

Comparing the model results at the 5% exceedence discharge provides an opportunity to determine the general conditions under which stratification effects are expected to be greatest for sand-bed rivers. The bulk measure of stratification,  $\bar{K}_{red}$ , was plotted versus  $Q/Q_5$ , and the value for each river was estimated at  $Q/Q_5=1$ . Figure 13 shows the reduction in eddy viscosity versus slope for all of the measurements, and for each river at  $Q_5$ . Here it is seen that the reduction in turbulent mixing is greatest for the lowest slopes. The reduction can approach 30% however for steeper streams at very high flows as seen for the Rio Grande, so that stratification effects for the steeper rivers may not be uniformly discounted.

While the reduction in eddy viscosity is a good measure of the bulk stratification effects, the most important assessment is the effect of stratification on sediment transport. To this end, the model was applied both with and without the stratification terms in the formulation. The boundary conditions used were the same as those determined from the simulations presented previously. The results of this analysis are presented in Figure 14, where the ratio of suspended transport with stratification effects ( $q_s$ ) to that without stratification effects ( $q_{so}$ ) is plotted versus slope. By reducing mixing, stratification increases mean velocity (which tends to increase the suspended sediment load at the same mean concentration) and decreases mean concentration (which would tend to decrease the suspended sediment load at the same mean velocity). The effect on the concentration dominates the suspended load, such that the load with the stratification effects is less than without stratification. Stratification also affects the distribution of sediment in

suspension as illustrated in Figure 15, where the ratio of median diameter in suspension with ( $D_{50s}$ ) to without ( $D_{50so}$ ) stratification is plotted versus slope. It is seen that the distribution with stratification tends to be somewhat finer than without stratification, since the reduced mixing has the greatest effect on the sizes with the largest concentration gradients, i.e. the largest sizes. Again the analysis at the 5% exceedence discharge shows that the greatest effects are realized for the rivers with the lowest slopes.

## CONCLUSIONS

The Mellor-Yamada “Level 2” turbulence closure (Mellor and Yamada, 1982) was applied to the conditions of steady, uniform, open-channel flow in the presence of sediment. It was shown that for a specified turbulent length scale (parabolic eddy viscosity), the buoyancy effects as modeled by the turbulence closure are quite similar to the empirical models employed by previous researchers (Smith and McLean 1977, Gelfenbaum and Smith 1986). Here a slightly different length scale equation is used which allows for inclusion of wake effects in the velocity profile. The non-dimensional form of the governing equations reveals that one additional dimensionless parameter is introduced through inclusion of the buoyancy terms: the slope. That is, to calculate the non-dimensional profiles from the standard log-law and Rouse equation, slope is not required directly. Inclusion of buoyancy terms requires direct specification of the slope, independent of the shear velocity. In the absence of stratification effects, two flows with identical sediment and shear velocity (one shallow and steep, one deep and mild), would have identical dimensionless profiles according to the log-law and Rouse equation

(assuming identical roughness). However, if buoyancy terms are included the profiles could be quite different, as the low-slope flow would have a higher Richardson number.

The model presented was briefly compared with flume experiments for two reasons. First, the comparison provides a test of the performance of the model under conditions of weak and strong stratification. Because the model is quite similar to previous approaches, however, a rigorous comparison with all available flume experiments was not presented. For this, the reader is referred to the paper by Villaret and Trowbridge (1991), where a similar model is compared to a large set of data from experiments. The second goal was to illustrate a fundamental problem with studies of stratification effects in the laboratory. Very few experiments have been conducted under conditions conducive to strong stratification effects. Coleman (1981, 1986) was able to produce relatively strong effects in his fine sand series, but only at the expense of a small width to depth ratio and concomitant severe sidewall effects. The reason Coleman was able to produce significant stratification effects was a combination of small sediment (i.e. high concentration), and low-slope (less than other similar flume studies). In order to have this low-slope and still entrain sediment (high enough shear velocity), the depth must be greater, thus introducing width to depth ratio problems. As shown herein, the ratio of concentration to slope is of primary importance in determining the strength of stratification. The greater this ratio, the greater the buoyancy effects will be. In the laboratory, however, depth is restricted by the width of the flume (typically one-quarter of the width) in order to avoid sidewall effects. As the slope is decreased, in order to maintain a bed shear stress which will transport sand the depth must be increased accordingly. Thus the depth restriction essentially becomes a slope restriction, since the

use of sizes smaller than sand introduces other factors (i.e. cohesion). Einstein and Chien (1955) were also able to produce what may be stratification effects by conducting experiments under supercritical flow conditions resulting in extremely high concentrations. However, it is difficult to extract stratification effects from these experiments since the high concentrations typically violate the dilute suspension assumption, introducing other phenomena such as hindered settling and particle-particle interaction. The study of stratification in the laboratory may require innovative uses of fluids other than water, and/or sediment other than river sand.

The primary focus of this study was the application of the model to a range of conditions typical of sand-bed rivers. Data were compiled for high flow conditions for six sand-bed rivers which span a spectrum of hydraulic conditions. Further, comparisons between rivers were made at a comparable discharge by determining the 5% exceedence discharge for each river, and estimating the results at this discharge. The bulk strength of density stratification was measured by comparing the reduction in turbulent mixing (i.e. eddy viscosity), averaged over the depth. The reduction was plotted versus a bulk flow Richardson number, resulting in a plot (Figure 12) reminiscent of the seminal work by Einstein and Chien (1954, 1955), reproduced as Figure 1 here. The most significant finding of this analysis is the conclusion that that the ratio of concentration (not including wash load) to slope is a primary indicator of the strength of stratification in sand bed rivers. Further, this ratio tends to be greatest in large, low-slope rivers since the decrease in slope tends to be greater than the decrease in concentration as one moves downstream in a river system. It is shown that stratification tends to decrease the overall transport rate, such that predictions made without stratification effects would tend to over-predict

the transport rate. Also the distribution of suspended sediment is finer when stratification effects are included. Again, the effects tend to be greatest for low-slope rivers compared to comparable flow events in steeper rivers.

It is noted that sediment-mediated effects not due to density stratification have also been measured in various flume experiments, such as the work of Lyn (1986). The present model does not capture the magnitude of increase in the velocity gradient near the bed measured by Lyn. Also, phenomena such as particle slip and turbulence modulation due to direct particle-flow interactions that have been measured (Best et al. 1997, Muste 1997) are not accounted for in the model presented here. The focus here has been the determination of the conditions under which density stratification effects are important. Similar studies of these other phenomena and their potential geomorphic significance would be a welcome contribution.

## **ACKNOWLEDGEMENTS**

The bulk of this research was conducted while the first author was supported through the Graduate Assistance in Areas of National Need (GAANN) Fellowship, a program of the Department of Education. Further support was provided by National Science Foundation Grant CTS-0096916. Dennis Lyn is thanked for his helpful discussions and insightful comments.

## **REFERENCES**

ASCE (1975). *Sedimentation Engineering*, V.A. Vanoni, ed., New York.

- Barton, J.R., and Lin, P.N. (1955). "A study of the sediment transport in alluvial streams." *Civil Engineering Department Report*, Colorado A&M College, Fort Collins.
- Best, J., Bennet, S., Bridge, J., and Leeder, M. (1997). "Turbulence modulation and particle velocities over flat sand beds at low transport rates." *J. Hydraulic Eng.*, 123(12), 1118-1129.
- Brush, L.M., Jr., Ho, H.W., and Singamsetti, S.R. (1952). "A study of sediment in suspension." *Extract of Publication No. 59*, IASH Commission on Land Erosion, 293-310.
- Businger, J.A., Wyngaard, J.C., Izumi, Y., and Bradley, E.F. (1971). "Flux relationships in the atmospheric surface layer." *J. Atmospheric Science*, 28, 190-201.
- Cellino, M., and Graf, W.H. (1997). "Sediment-laden flow in open-channels under noncapacity and capacity conditions." *J. Hydraulic Eng.*, 125(5), 455-462.
- Colby, B.R., and Hembree, C.H. (1956). "Computations of total sediment discharge Niobrara River near Cody, Nebraska." *U.S. Geol. Survey Water-Supply Paper* 1357.
- Coleman, N.L. (1970). "Flume studies of the sediment transfer coefficient." *Water Resources Research*, 6(3), 801-809.
- Coleman, N.L. (1981). "Velocity profiles with suspended sediment." *J. Hydraulic Res.*, 19(3), 211-229.
- Coleman, N.L. (1986). "Effects of suspended on the open-channel velocity distribution." *Water Resources Research*, 22(10), 1377-1384.

- Dietrich, W.E. (1982). "Settling velocity of natural particles." *Water Resources Research*, 18(6), 1615-1626.
- Einstein, H.A., and Chien, N. (1954). "Second approximation to the solution of the suspended load theory." *MRD Sediment Series No. 3*, University of California Berkeley, Institute of Engineering Research, Berkeley, California.
- Einstein, H.A., and Chien, N. (1955). "Effects of heavy sediment concentration near the bed on velocity and sediment distribution." *MRD Sediment Series No. 8*, University of California, Institute of Engineering Research, Berkeley, California.
- Galperin, B., Kantha, L.H., Hassid, S., and Rosati, A. (1988). "A quasi-equilibrium turbulent kinetic energy model for geophysical flows." *J. Atmospheric Sciences*, 45(1), 55-62.
- Gelfenbaum, G., and Smith, J.D. (1986). "Experimental evaluation of a generalized suspended-sediment transport theory." *Shelf Sands and Sandstones*, R.J. Knight and J.R. McLean, eds., Canadian Society of Petroleum Geologists, Memoir II, 133-144.
- Greimann, B.P., Muste, M., and Holly, F.M. (1999). "Two-phase formulation of suspended sediment transport." *J. Hydraulic Res.*, 37(4), 479-500.
- Hubbell, D.W., and Matejka, D.Q. (1959). "Investigations of Sediment Transportation Middle Loup River at Dunning, Nebraska." *U.S. Geol. Survey Water-Supply Paper 1476*.
- Itakura, T., and Kishi T. (1980). "Open channel flow with suspended sediment." *J. Hydraulics Division ASCE*, 106(HY8), 1325-1343.

- Jordan, P.R. (1965). "Fluvial sediment of the Mississippi River at St. Louis, Missouri." *U.S. Geol. Survey Water-Supply Paper 1802*.
- Karim, F. (1998). "Bed material discharge prediction for nonuniform bed sediment." *J. Hydraulic Eng.*, 124(6), 597-604.
- Lyn, D.A. (2000). "Regression residuals and mean profiles in uniform open-channel flows." *J. Hydraulic Eng.*, 126(1), 24-32.
- Lyn, D.A. (1986). "Turbulence and Turbulent Transport in Sediment-Laden Open-Channel Flows." *Report No. KH-R-49*, W.M. Keck Laboratory of Hydraulics and Water Resources, Division of Engineering and Applied Science, California Institute of Technology, Pasadena, California.
- McLean, S.R. (1991). "Depth-integrated suspended-load calculations." *J. Hydraulic Eng.*, 117(11), 1440-1458.
- McLean, S.R. (1992). "On the calculation of suspended load for noncohesive sediments." *J. Geophysical Res.*, 97(C4), 5759-5770.
- Mellor, G.L., and Yamada, T. (1974). "A hierarchy of turbulence closure models for planetary boundary layers", *J. Atmospheric Science*, 31, 1791-1806.
- Mellor, G.L., and Yamada, T. (1982). "Development of a turbulence closure model for geophysical fluid problems", *Reviews of Geophysics and Space Physics*, 20(4), 851-875.
- Muste, M., and Patel, V.C. (1997). "Velocity profiles for particles and liquid in open-channel flow with suspended sediment", *J. Hydraulic Eng.*, 123(9), 742-751.
- Nakato, T. (1990). "Tests of selected sediment-transport formulas", *J. Hydraulic Eng.*, 116(3), 362-379.

- Nelson, J., McLean, S., and Wolfe, S. (1993). "Mean flow and turbulence fields over two-dimensional bed forms." *Water Resources Research*, 29(12), 3935-3953.
- Nezu, I, and Rodi, W. (1986). "Open-channel flow measurements with a laser doppler anemometer", *J. Hydraulic Eng.*, 112(5), 335-355.
- Nordin, C.F. (1964). "Aspects of flow resistance and sediment transport Rio Grande near Bernallilo, New Mexico." *U.S. Geol. Survey Water-Supply Paper 1498-H*.
- Parker, G., Paola, C., Whipple, K.X., and Mohrig, D. (1998). "Alluvial fans formed by channelized fluvial and sheet flow I: Theory." *J. Hydraulic Eng.*, 124(10), 985-995.
- Scott, L.H., and Stephens, H.D. (1966). "Special Sediment Investigations Mississippi River at St. Louis, Missouri, 1961-1963." *U.S. Geol. Survey Water-Supply Paper 1819-J*.
- Singamsetti, S.R. (1966). "Diffusion of sediment in a submerged jet", *J. Hydraulics Division ASCE*, 92(HY2), 153-168.
- Smith, J.D., and McLean, S.R. (1977). "Spatially averaged flow over a wavy surface." *J. Geophysical Research*, 82(12), 1735-1746.
- Soulsby, R.L., and Wainright, B.L.S.A. (1987). "A criterion for the effect of suspended sediment on near-bottom velocity profiles.", *J. Hydraulic Res.*, 25(3), 341-356.
- Toffaletti, F.B. (1968). "A procedure for computation of the total river sand discharge and detailed distribution, bed to surface." *Technical Report No. 5*, Committee on Channel Stabilization, Corps of Engineers.
- Turner, J.S. (1973). *Buoyancy Effects in Fluids*. Cambridge University Press.

- Vanoni, V.A. (1946). "Transportation of suspended sediment by water", *Trans. ASCE*, 111, Paper no. 2267, 67-133.
- van Rijn, L.C. (1984). "Sediment transport, part II: Suspended load transport." *J. Hydraulic Eng.*, 110(11), 1613-1641.
- Villaret, C., and Trowbridge, J.H. (1991). "Effects of stratification by suspended sediments on turbulent shear flows." *J. Geophysical Res.*, 96(C6), 10,659-10,680.
- Wieringa, J. (1980). "A reevaluation of the Kansas Mast influence on measurements of stress and cup anemometer overspeeding." *Boundary Layer Meteorology*, 18, 411-430.

## NOTATION

- $A_1, B_1, C_1, A_2, B_2$  turbulence closure model constants;
- $b$  channel width;
- $C$  sediment concentration by volume;
- $c'$  turbulent concentration fluctuation;
- $\bar{C}$  depth-averaged concentration by volume;
- $C_i$  concentration by volume of grain-size  $i$ ;
- $\bar{C}_i$  depth-averaged concentration by volume of grain-size  $i$ ;
- $C_a$  concentration by volume at near-bed point  $\eta_a$ ;
- $C_m$  total discharge-weighted suspended sand concentration;
- $C_{mi}$  discharge-weighted suspended sand concentration of grain-size  $i$ ;
- $C_{dev}$  relative deviation of concentration from the without stratification case;
- $C_s$  concentration with stratification effects;

$C_{ns}$	concentration without stratification effects;
$D$	sediment grain diameter;
$D_i$	diameter of grain-size $i$ ;
$D_{50}$	median grain-size of bed material;
$D_{50s}$	median grain-size of suspended sediment;
$D_{50so}$	median grain-size of suspended sediment without stratification effects;
$g$	acceleration due to gravity;
$h$	flow depth;
$k$	turbulent kinetic energy;
$K_m$	eddy viscosity;
$K_s$	sediment diffusivity;
$K_{mo}$	clear-water eddy viscosity;
$\bar{K}_m$	depth-averaged eddy viscosity;
$\bar{K}_{mo}$	depth-averaged clear-water eddy viscosity;
$\bar{K}_{red}$	reduction in depth-averaged eddy viscosity from the clear-water case;
$\ell$	turbulence length scale;
$q$	water discharge per unit width;
$q_s$	total suspended sand transport rate per unit width;
$q_{si}$	suspended sand transport rate per unit width of grain-size $i$ ;
$q_{so}$	total suspended sand transport rate per unit width without stratification effects;
$Q$	water discharge;
$Q_{si}$	total suspended sand transport rate;

$Q_5$	discharge with a 5% probability of exceedence;
$R$	sediment submerged specific gravity;
$Ri_f$	flux Richardson number;
$Ri_{sr}$	sand river Richardson number;
$S_o$	slope;
$T$	water temperature;
$u$	streamwise velocity;
$u'$	streamwise turbulent velocity fluctuation;
$u^*$	shear velocity;
$U$	depth-averaged velocity;
$U_{dev}$	relative deviation of velocity from the without stratification case;
$u_s$	velocity with stratification effects;
$u_{ns}$	velocity without stratification effects (clear water);
$v'$	vertical turbulent velocity fluctuation;
$v_s$	sediment settling velocity;
$v_{si}$	settling velocity of grain-size $i$ ;
$v_{s50}$	settling velocity based on the median grain diameter;
$y$	height above bed;
$Z_R$	Rouse number;
$Z_{mi}$	entrainment relation parameter;
$\alpha$	turbulence length scale constant;
$\beta$	stratification model constant;
$\delta$	top of the bedload layer

- $\gamma$  stratification model constant;
- $\kappa$  von Karman constant;
- $\kappa_a$  apparent von Karman parameter;
- $\eta$  non-dimensional height above bed;
- $\eta_a$  non-dimensional near-bed height;
- $\Pi$  Coles wake strength parameter;
- $\rho$  water density;
- $\rho_s$  sediment density;
- $\tau$  local shear stress;
- $\tau_o$  bed shear stress;
- $\chi_1, \chi_2, \chi_3, \chi_4, \chi_5$  combinations of turbulence model constants;
- $\wedge$  denotes non-dimensional quantity, using  $u_*$  and  $h$  as scales;

## TABLES

Table 1 Flow and sediment properties for three laboratory experiments.

	Run #	$b$ (cm)	$h$ (cm)	$S_o$ ( $\times 1000$ )	$D$ (mm)	$T$ (°C)
Lyn (1986)	1565EQ	26.7	6.45	2.4	0.15	20.7
Barton and Lin (1955)	36	121.9	16.2	2.1	0.18	26.1
Coleman (1981, 1986)	20	35.6	17.0	1.0	0.105	23.9

Table 2 Range of conditions spanned by measurements from six sand-bed rivers.

River	$Q$ ( $m^3/s$ )	$b$ (m)	$h$ (m)	$S_o$ ( $\times 1000$ )	$D_{50}$ (mm)
Niobrara (10)*	6.6 – 16.1	21.0 – 21.9	0.47 – 0.58	1.1 – 1.8	0.25 – 0.31
Middle Loup (26)	9.3 – 12.9	37.5 – 46.3	0.25 – 0.40	0.93 – 1.6	0.20 – 0.42
Rio Grande (20)	35.1 – 286	40.5 – 83.2	0.71 – 1.5	0.74 – 0.89	0.15 – 0.39
Red (26)	190 – 1540	130 – 183	3.0 – 7.4	0.066 – 0.082	0.10 – 0.22
Atchafalaya (48)	1450 – 14,200	317 – 503	6.9 – 14.8	0.014 – 0.051	0.09 – 0.29
Mississippi (35)	4330 – 28,800	896 – 1110	6.7 – 16.4	0.022 – 0.043	0.18 – 0.32

\* parentheses indicate the number of observations at each river

Table 3 Estimated values of several parameters at the 5% exceedence discharge.

				Estimated values at $Q_5$			
	<i>USGS</i> <i>Gage ID</i>	<i>Period of</i> <i>Record</i>	$Q_5$ <i>(m<sup>3</sup>/s)</i>	$S_o$ <i>(x1000)</i>	$C_m$ <i>(mg/L)</i>	$v_{s50}/u_*$	$\bar{K}_{red}$
Niobrara	06459000	1941 – 1953	13.0	1.7	860	0.31	0.94
Middle Loup	06775500	1945 – 2000	15.0	1.2	2100	0.42	0.84
Rio Grande	08329500	1941 – 1969	120	0.81	1730	0.40	0.80
Red	07355500	1928 – 1983	2950	0.073	600	0.23	0.67
Atchafalaya	07381490	1963 – 1988	13,100	0.050	360	0.25	0.63
Mississippi	07373291	1928 – 1986	29,100	0.038	230	0.27	0.64

## **FIGURES**

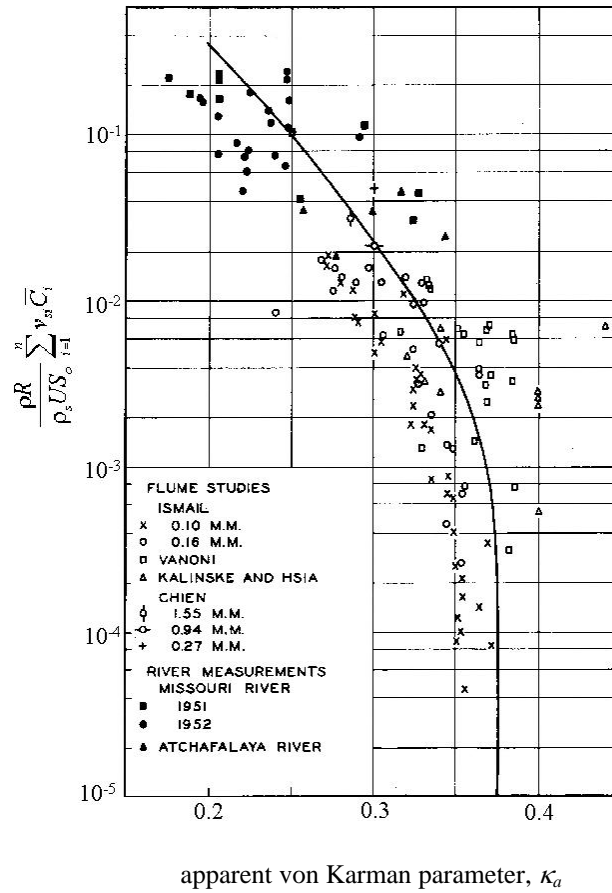


Figure 1 Empirical correlation between apparent von Karman parameter  $\kappa_a$  and the ratio of the power to hold a sediment grain in suspension to the power to overcome friction. Reproduced from Einstein and Chien (1955).

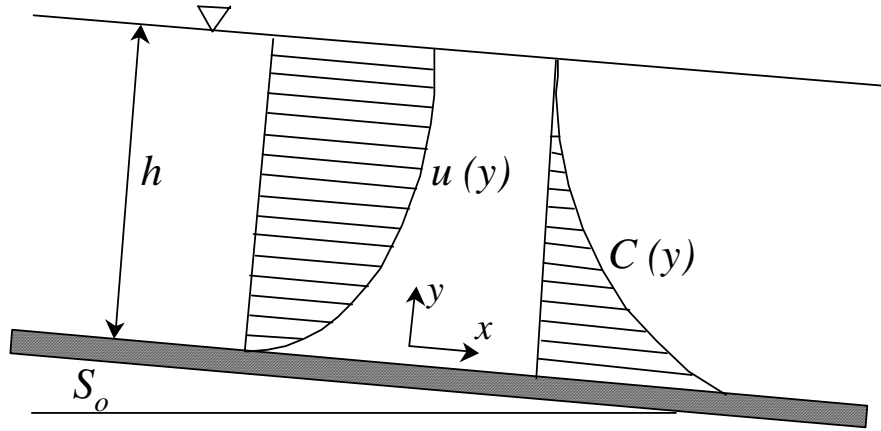


Figure 2 Steady, uniform, open-channel suspension definition sketch.

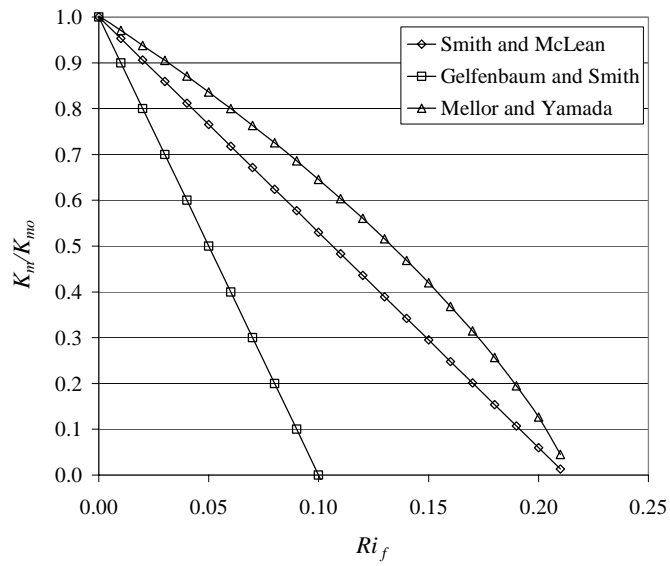


Figure 3 Comparison of previous models of density stratification with the model presented herein (Mellor and Yamada closure).

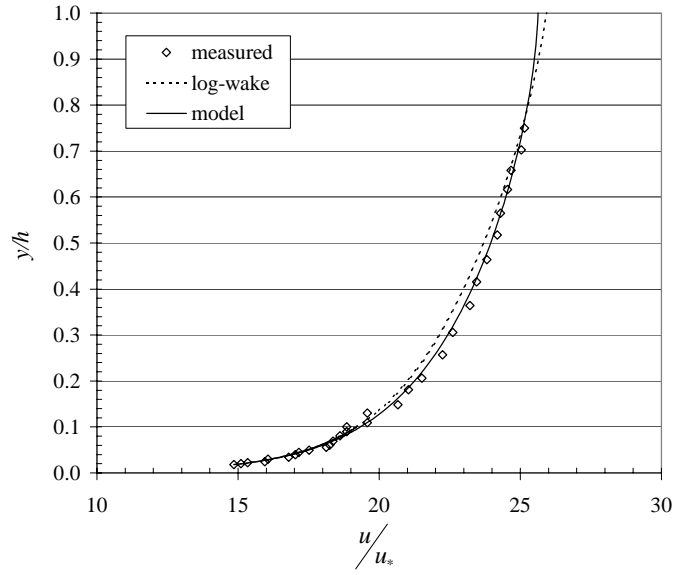


Figure 4 Comparison of the model with  $\alpha=0.7$  and a log-wake velocity profile to the clear-water flow Run P4 of Nezu and Rodi (1986).

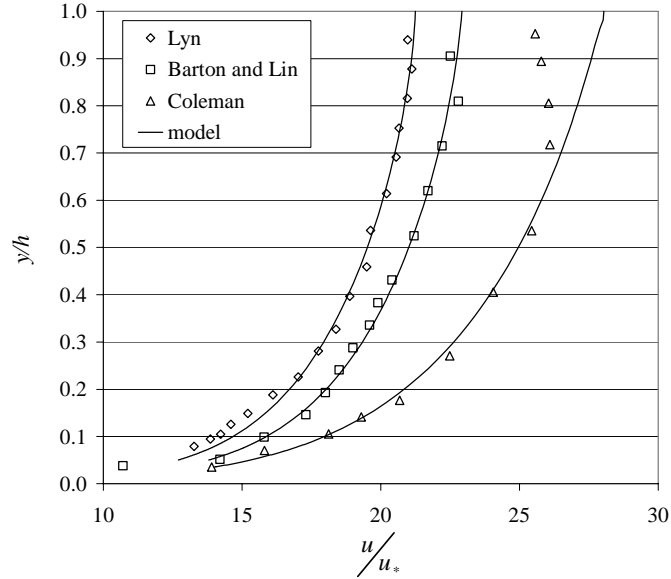


Figure 5 Comparison of model predictions with measured velocity profiles from Lyn (1986), Barton and Lin (1955), and Coleman (1981, 1986).

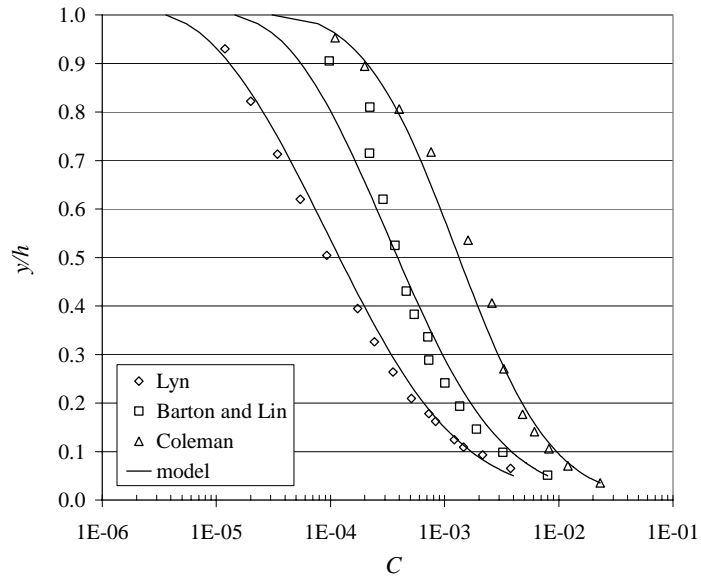


Figure 6 Comparison of model predictions with measured concentration profiles from Lyn (1986), Barton and Lin (1955), and Coleman (1986).

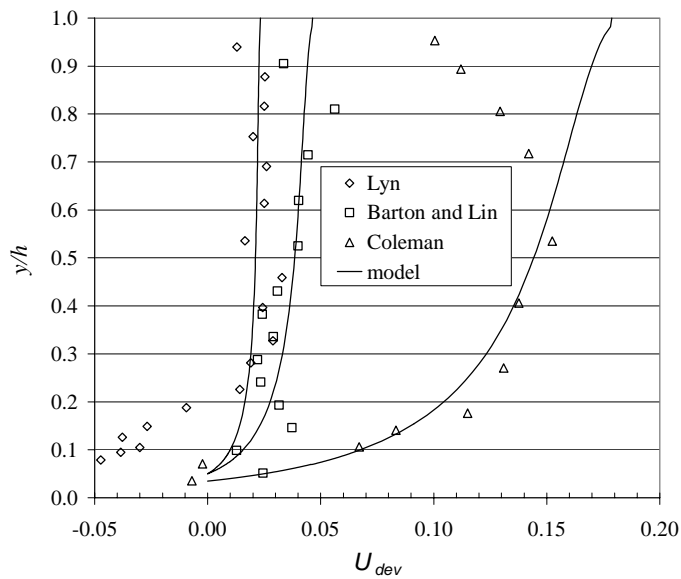


Figure 7 Comparison of predicted and measured relative deviation from the clear-water velocity profile for the three profiles shown in Figure 5.

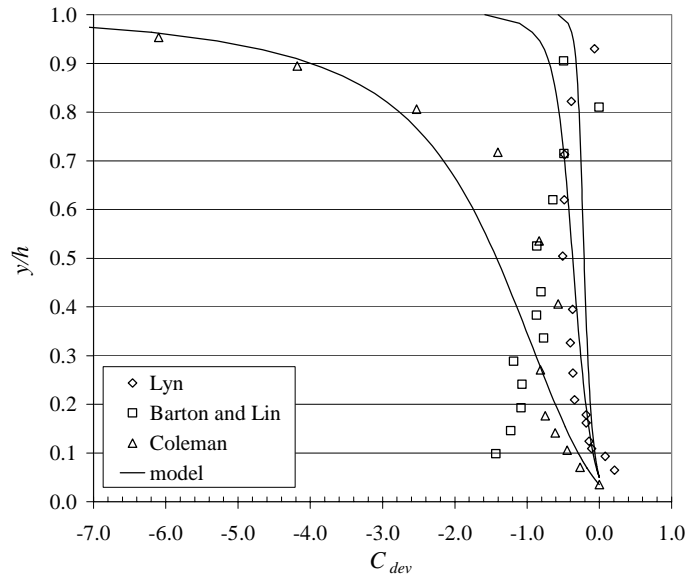


Figure 8 Comparison of predicted and measured relative deviation from the without stratification concentration profile for the three profiles shown in Figure 6.

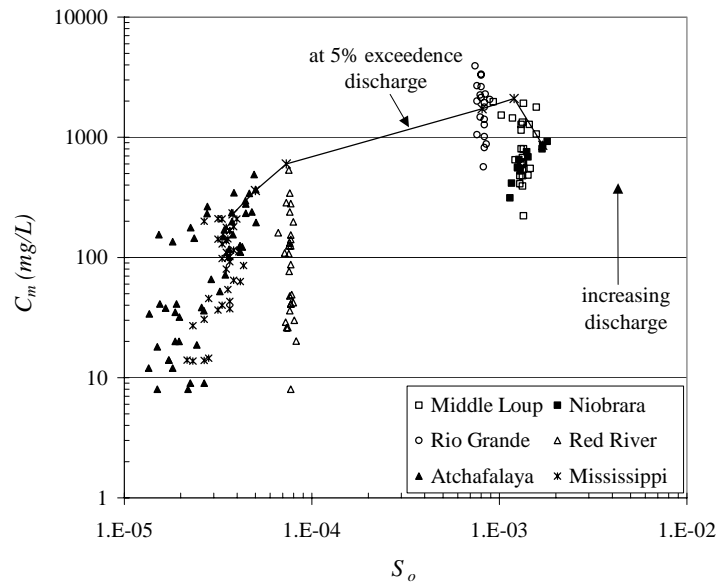


Figure 9 Total discharge-weighted suspended sand concentration versus slope for several events from six sand-bed rivers, and estimated values at the 5% exceedence discharge.

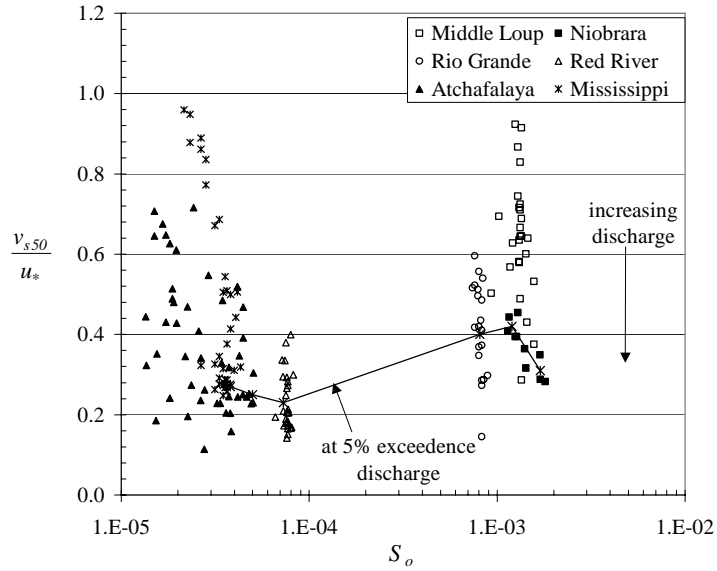


Figure 10 Ratio of settling velocity based on  $D_{50}$  to shear velocity versus slope for several events from six sand-bed rivers, and estimated values at the 5% exceedence discharge.

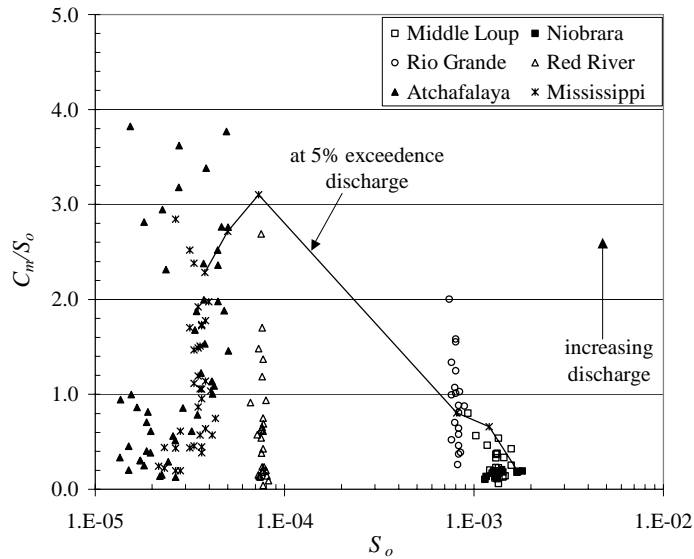


Figure 11 Ratio of total discharge-weighted suspended sand concentration to slope versus slope for several events from six sand-bed rivers, and estimated values at the 5% exceedence discharge.

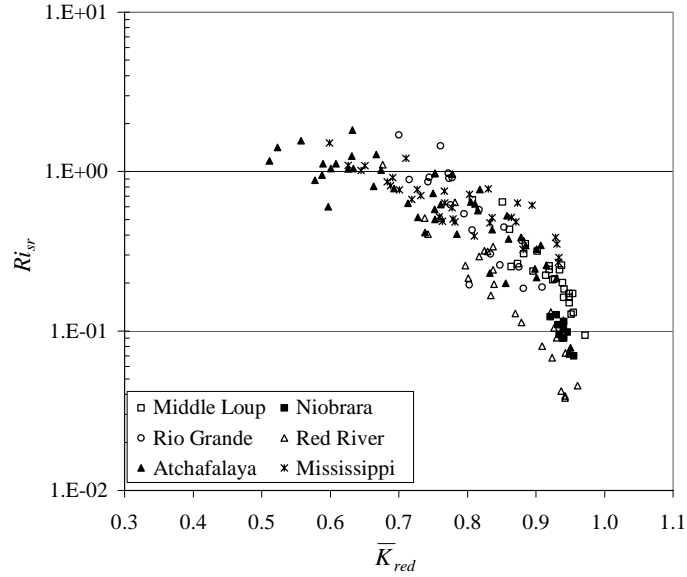


Figure 12 Bulk (depth-averaged) reduction in turbulent mixing (eddy viscosity) computed from the model versus the sand river Richardson number for several flow events from six sand-bed rivers.

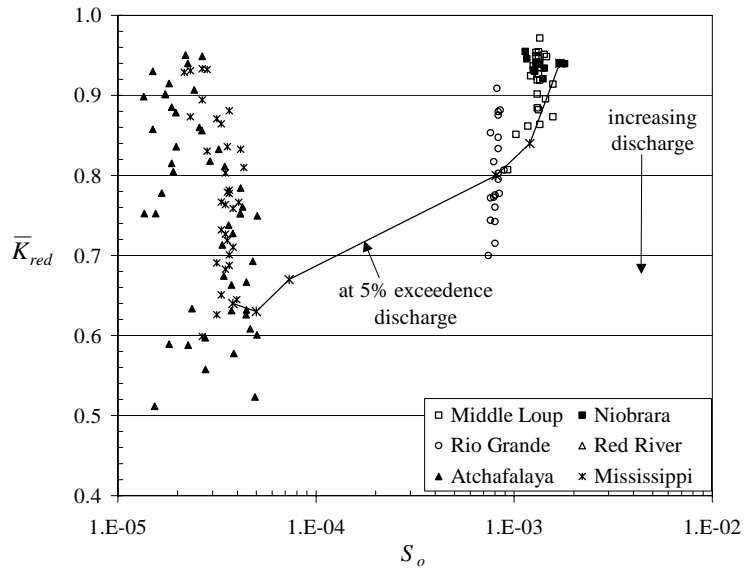


Figure 13 Bulk (depth-averaged) reduction in turbulent mixing (eddy viscosity) versus slope for several events from six sand-bed rivers, and estimated values at the 5% exceedence discharge.

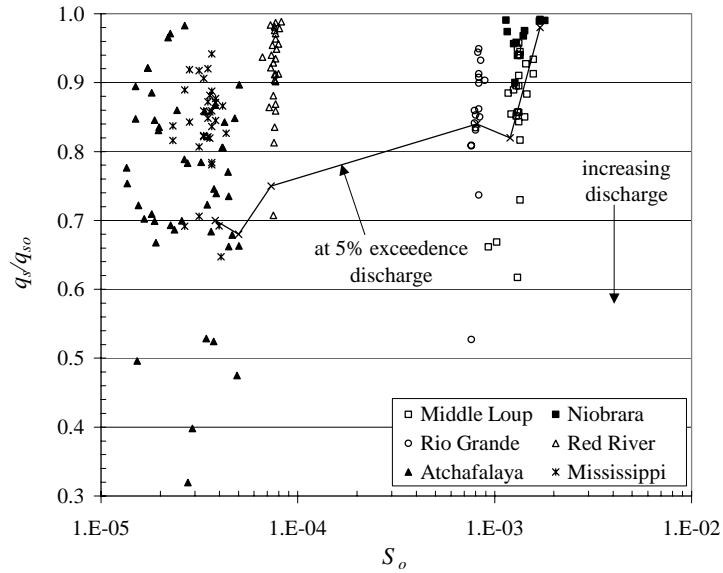


Figure 14 Ratio of total suspended transport rate with and without stratification effects versus slope for several events from six sand-bed rivers, and estimated values at the 5% exceedence discharge.

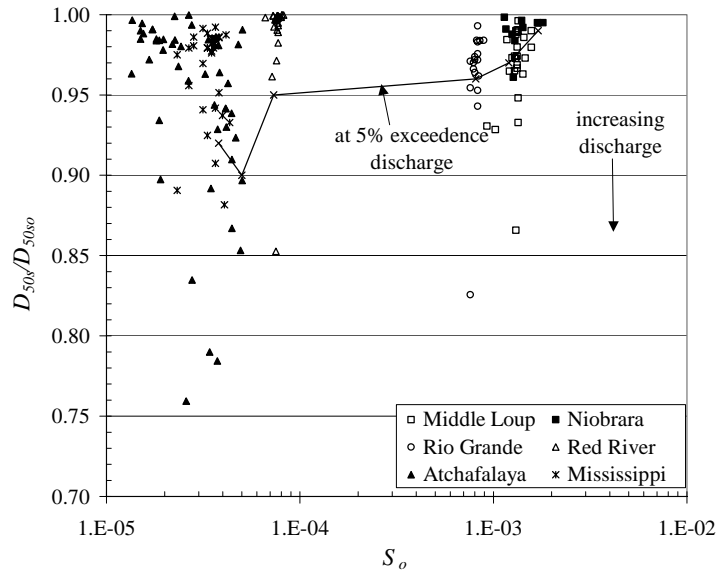


Figure 15 Ratio of median grain-size in suspension with and without stratification effects versus slope for several events from six sand-bed rivers, and estimated values at the 5% exceedence discharge.

**CHAPTER 2: FLOW RESISTANCE AND SUSPENDED LOAD IN  
SAND-BED RIVERS: SIMPLIFIED STRATIFICATION MODEL**

Scott Wright and Gary Parker

## **ABSTRACT**

New methods are presented for the prediction of the flow depth, grain-size specific near-bed concentration, and bed-material suspended sediment transport rate in sand-bed rivers. The salient improvements delineated here all relate to the need to modify existing formulations in order to encompass the full range of sand-bed rivers, and in particular large, low-slope sand-bed rivers. They can be summarized as follows: a) the inclusion of density stratification effects in a simplified manner, which have been shown in the companion paper to be particularly relevant for large, low-slope, sand-bed rivers; b) a new predictor for near-bed entrainment rate into suspension which extends a previous relation to the range of large, low-slope sand-bed rivers, and c) a new predictor for form drag which again extends a previous relation to include large, low-slope sand-bed rivers. Finally, every attempt has been made to cast the relations in the simplest form possible, including the development of software, so that the methods may be easily used by practicing engineers.

## **INTRODUCTION**

Prediction of the grain-size specific sediment transport of sand mixtures is of primary importance in studies of sorting processes in rivers. For example, the grain-size distribution of the suspended load plays a major role in controlling the longitudinal sorting pattern in the downstream reaches of large, sand-bed rivers, where sediment transport is dominated by suspension. Thus a method for accurately predicting this distribution for such a river type would be of use. The method presented here is based on

the calculation of the velocity and concentration profiles, and thus leads to the development of a depth-discharge predictor as well, through integration of the velocity profile over the flow depth.

Einstein (1950) was probably the first to propose a method for the calculation of sediment transport on a grain-size specific basis, proposing separate relations for bed and suspended load. For the suspended load, Einstein used estimators of the vertical velocity and concentration profiles to determine the suspended load by grain-size:

$$q_{si} = \int_{\delta}^h u C_i dy \quad (1)$$

where  $u$  is flow velocity,  $C_i$  is volume concentration of grain-size  $i$ ,  $\delta$  is the top of the bedload layer, and  $h$  is the flow depth. The log-law velocity profile and Rouse concentration profile (e.g. ASCE 1975) were used, along with the Einstein bed-load equation for the near-bed concentration.

McLean (1991, 1992) followed a similar approach, with several improvements. First, McLean accounted for density stratification effects in both the velocity and concentration profiles. Further, the effects of dunes on flow resistance (i.e. skin friction/form drag partitioning) were addressed using the spatial averaging technique of Smith and McLean (1977). Also, McLean used a near-bed concentration predictor which assumes a direct relation with bed shear stress due to skin friction. While the method of McLean provides significant improvements physically, the improvements come at a cost to the ease of solution. In particular, the inclusion of stratification effects as implemented by McLean results in the need for an iterative solution for the velocity and concentration profiles, along with the numerical integration required for (1). Finally, the near-bed

concentration predictor used therein, while adapted for multiple grain-sizes, does not account for relative exposure/hiding effects on entrainment of different grain-sizes from the bed.

Another class of relations take a more empirical approach. There are several methods for partitioning the total sediment transport on a grain-size specific basis, using a variety of relations for predicting the total sediment transport. A review of these methods can be found in Molinas and Wu (2000). While these methods predict the total sediment transport by grain-size, there are also methods which predict the grain-size specific bedload and/or suspended load separately. Samaga et al. (1986) developed such relations based on a set of flume experiments. The suspended load is assumed to be related to the bed shear stress, and several adjustments are used to account for the effective shear stress and uniformity of the sand mixture. Even though the method is relatively simple and empirically based, it is not particularly easy to use as it requires reading values off of a series of plots. Recently, Wu et al. (2000) have proposed a method for the prediction of bedload and suspended load for nonuniform sediment for alluvial rivers. Their technique assumes a relation between the suspended load and the excess shear stress (i.e. above the critical value for entrainment) and ratio of mean flow velocity to settling velocity of the particular grain-size. Shear stress partitioning is accomplished through a standard Einstein (1950) decomposition using Manning's equation, and a new procedure is introduced for accounting for hiding/exposure effects using probability concepts. The relation is calibrated using a set of laboratory and field data, and tested against several previously proposed relations for an independent dataset.

The method proposed here attempts to strike a balance between the two types of methods discussed above. That is, the salient physical processes of the McLean method are retained in a simplified manner in order to develop a relation which is nearly as easy to use as the more empirically based methods of e.g. Samaga or Wu. The effects of density stratification are accounted for using a simple semi-empirical adjustment to the velocity and concentration profiles, based on the more elaborate model of Wright and Parker (companion paper, in press a) and data from several sand-bed rivers. A new grain-size specific near-bed sediment entrainment relation, which includes hiding and exposure effects is introduced. The entrainment relation is a modification to the relation of Garcia and Parker (1991), so that it performs better for large, sand-bed rivers. Shear stress partitioning is accomplished through a newly developed empirical relation between skin friction and total Shields stress. The relation is similar to that developed by Engelund and Hansen (1967), but includes a further dependence on Froude number in order to account for the differences in dune behavior over the range slopes spanned by sand-bed rivers. Similar to the findings of Julien and Klaasen (1995), it is shown here that bedforms tend to wash out at lower total shear stresses in the steeper sand-bed rivers. A modified Einstein decomposition, including density stratification effects, is used to compute the skin friction shear stress for a large dataset of field measurements, which is then used to develop the empirical relation.

Because the suspended sediment transport relation proposed relies on the calculation of the vertical velocity profile and a partitioning between skin friction and total shear stress, it is conducive to the development of a depth-discharge relation, i.e. a

relation for hydraulic resistance, as well. The relation is formulated in terms of the depth-averaged velocity obtained by integrating the velocity profile over the flow depth:

$$U = \frac{1}{h} \int_{\delta}^h u dy \quad (2)$$

Using continuity,  $q=Uh$ , (2) is transformed into a relation between depth and discharge, assuming the velocity profile is known. To compute the velocity profile, the near-bed velocity boundary condition must be specified. For a flow over a sand-bed with no bedforms, the point of zero velocity is typically taken to be proportional to the equivalent sand-grain roughness height,  $k_s$ . For a river with bed forms, a relation between the sand-grain roughness height (skin friction) and the total roughness height (form drag plus skin friction) is required. Here this is accomplished through the empirical relation mentioned above. It is noted that method of McLean (1991, 1992) has been applied in a similar manner. McLean included a method for shear stress partitioning if the bed form dimensions are known. Bennett (1995) used the McLean model, along with the bed form predictor of van Rijn (1984), to develop an algorithm for hydraulic resistance and sediment transport which is similar to the method presented here. Again, however, the solution for the depth using this more complicated method requires iteration and numerical integration due to the technique for accounting for density stratification. Here the density stratification adjustment is simple enough to allow for an analytical integration of (2). The final relation requires one level of iteration, and a software package has been developed for public use.

Many depth-discharge relations have been proposed previously for open-channel flows, beginning with the Chezy, Manning, and Darcy-Weisbach equations for clear-

water, rigid-bed flows (e.g. Henderson 1960). Subsequently relations have been proposed for alluvial rivers, including those of Einstein (1950), Engelund and Hansen (1967), and Brownlie (1983), to name only a few. The primary improvement of the proposed method is the accounting for density stratification effects, as will be demonstrated by comparison with predictions using the Brownlie method. The improvement will be seen to be greatest for large, sand-bed rivers at high flows, which is not surprising since it has been shown by Wright and Parker (companion paper, in press a) the density stratification effects are strongest under these conditions. Further, the proposed method accounts for the tendency of dunes to wash out at lower shear stresses in steeper rivers, and is thus applicable over the range of slopes typical of sand-bed rivers.

This paper focuses only on that part of the suspended load that is also contained in measurable quantities in the stream bed, i.e. the suspended part of the bed material load. Suspended sediment that is too fine to be contained in measurable quantities in the bed, i.e. wash load, does not exchange with the bed. In addition, it tends to be distributed uniformly in the vertical, and thus does not contribute to stratification effects. While the precise cutoff between bed material load and washload is a matter of some debate, and appears to be weakly dependent on flow conditions (e.g. Einstein and Chien 1953), the traditional cutoff size of 0.062 mm (e.g. Colby 1975, ASCE 1975, Raudkivi 1976) is used here as the divide between the two.

## DENSITY STRATIFICATION

The vertical gradient in suspended sediment concentration results in a density gradient which in turn induces a buoyancy force that inhibits vertical mixing by turbulence. In the context of uniform open-channel flow, this translates to a reduction in the turbulent eddy viscosity (for momentum) and sediment diffusivity. The effect of density stratification on the eddy viscosity can be written in following general functional form:

$$K_m = K_{mo} f(Ri_f) \quad (3)$$

where  $K_m$  is eddy viscosity,  $K_{mo}$  is the eddy viscosity of an equivalent clear-water flow, and  $Ri_f$  is the flux Richardson number, which represents the ratio of turbulent kinetic energy lost working against the density gradient to the kinetic energy generated by shear. For suspended sediment mixtures, the flux Richardson number is given by (Wright and Parker, in press a):

$$Ri_f = \frac{Rg \sum v_{si} C_i}{u_*^2 (1 - \eta) du/dy} \quad (4)$$

where  $R = (\rho_s/\rho - 1)$  is submerged specific gravity,  $g$  is gravity,  $v_{si}$  and  $C_i$  are the settling velocity and local volumetric concentration of grain-size  $i$ , respectively,  $n$  is the number of grain-sizes in suspension,  $u_* = \sqrt{ghS_o}$  is shear velocity,  $h$  is flow depth,  $S_o$  is slope,  $u$  is local streamwise velocity,  $y$  is vertical distance from the bed, and  $\eta = y/h$  is the non-dimensional distance from the bed.

The vertical velocity and concentration profiles for equilibrium flows can be computed using (3) and momentum balance for water and mass balance for sediment, respectively:

$$K_m \frac{du}{dy} = u_*^2 (1 - \eta) \quad (5)$$

$$K_m \frac{dC_i}{dy} = -v_{si} C_i \quad (6)$$

where it has been assumed that sediment diffusivity equals eddy viscosity (i.e. Schmidt number of unity). As noted in the companion paper (Wright and Parker, in press a), various researchers have proposed various values for the Schmidt number, and thus the choice of unity is open to debate. For a flow with no density stratification, application of the standard parabolic eddy viscosity leads to the logarithmic velocity profile and Rouse concentration profile (see e.g. ASCE 1975). In the companion paper, several functional forms for (3) are presented, including that of McLean (1991, 1992) and that resulting from the use of the Mellor-Yamada turbulence closure. The dependence of the eddy viscosity on the Richardson number, and thus local sediment concentration, leads to the need for iteration and numerical integration in order to compute the profiles. Here a simplified stratification adjustment is introduced which allows for analytical integration of (5) and (6), and thus stratification-modified forms of the log-law and Rouse profile.

The simplest stratification adjustment is one that is constant in the vertical, i.e. a constant reduction in the parabolic eddy viscosity throughout the flow depth. Many authors have treated this in terms of a reduction in the von Karman constant, because the assumption of a parabolic eddy viscosity given by the relation:

$$K_m = \kappa u_* y (1 - \eta) \quad (7)$$

where  $\kappa=0.4$  is the von Karman constant leads to the standard logarithmic velocity profile over the entire depth of flow. It is important to realize, however, that formally the von Karman constant is a near-wall parameter which is likely to be unmodified by stratification. For this reason Wright and Parker (companion paper, in press a) have termed the parameter obtained by fitting the logarithmic velocity law to data over the entire depth the apparent von Karman parameter  $\kappa_a$ . This parameter is no longer a constant, in that it varies with the degree of flow stratification. Wright and Parker also showed that the relationship developed by Einstein and Chein (1955) for the apparent von Karman parameter can indeed be explained by density stratification.

Given the functional form of (3), it is clear that a reduction in eddy viscosity that is constant in the vertical implies constant flux Richardson number throughout the flow depth. To test this hypothesis, several  $Ri_f$  profiles developed using the model described in the companion paper for the conditions of several sand-bed rivers are plotted in Figure 1. While  $Ri_f$  is clearly not strictly constant over the depth, it is concluded that averaging over the flow depth is an appropriate assumption for the objectives detailed here. It should be noted that the abrupt increase in  $Ri_f$  near the surface (where shear production of turbulent energy approaches zero) has little effect on the profiles, since both velocity and concentration gradients are small in this region. This is illustrated in Figure 2, where velocity profiles are shown corresponding to the Red and Atchafalaya River  $Ri_f$  profiles of Figure 1. It is seen that the stratification adjusted logarithmic profile approximates the profile from the full model quite well, and captures the primary deviation from the clear-water profile.

For a vertically constant  $Ri_f$  then the parabolic eddy viscosity becomes:

$$K_m = \alpha \kappa u_* y (1 - \eta) \quad (8)$$

where  $\alpha$  is a constant stratification adjustment which depends on a bulk form of the Richardson number, e.g. that used by Einstein or in the companion paper (in which  $\bar{K}_{red} = \alpha$ ). In the companion paper (Wright and Parker, in press a), a sand-river Richardson number was defined which used the depth-averaged total discharge-weighted concentration. Here an even simpler approach is employed, which recognizes the primary role of the ratio of concentration to slope in controlling stratification effects. This ratio is a surrogate for the Richardson number, whereby concentration and slope parameterize buoyancy and shear, respectively. Again primarily to avoid the need for iteration, the near-bed concentration is used in place of the depth-averaged concentration. The results obtained from the more elaborate model presented in the companion paper for the six sand-bed rivers are used to develop the stratification adjustment. The range in parameters for the rivers are summarized in Table 2 of the companion paper (Wright and Parker, in press a). The reduction in eddy viscosity computed by the model was averaged over the flow depth in order to determine  $\alpha$  for each event. The results are plotted in Figure 3, which can be characterized by the following relation:

$$\alpha = \begin{cases} 1 - 0.06 \left( \frac{C_{5t}}{S_o} \right)^{0.77} & \text{for } \frac{C_{5t}}{S_o} \leq 10 \\ 0.67 - 0.0025 \left( \frac{C_{5t}}{S_o} \right) & \text{for } \frac{C_{5t}}{S_o} > 10 \end{cases} \quad (9)$$

Now (5) and (6) can be integrated, with the use of (8), to yield the stratification corrected log-law and Rouse profile, respectively:

$$\frac{u}{u_*} = \frac{1}{\alpha \kappa} \ln\left(\frac{\eta}{\eta_o}\right) \quad (10)$$

$$\frac{C_i}{C_{ai}} = \left[ \frac{1-\eta}{\eta} \frac{\eta_a}{1-\eta_a} \right]^{Z_{Ri}} \quad (11)$$

where  $\eta_o$  is the non-dimensional height where  $u=0$ ,  $C_{ai}$  is the concentration of grain-size  $i$  at near-bed point  $a$ ,  $\eta_a = a/h$ , and

$$Z_{Ri} = \frac{v_{si}}{\alpha \kappa u_*} \quad (12)$$

is the stratification adjusted Rouse number for grain-size  $i$ .

## RELATION FOR NEAR-BED CONCENTRATION

The eddy viscosity stratification adjustment presented in the previous section is dependent on the near-bed suspended sediment concentration. Here 5% of the flow depth, i.e.  $\eta_a=0.05$  is used to define the point at which the near-bed concentration is evaluated. This choice is motivated primarily by the paucity of field concentration measurements below this level. Extrapolation of concentration profiles to very near the bed is difficult because of the large gradients and uncertainty of near-bed processes for flows over bedforms.

Several relations have been presented for predicting the near-bed concentration for an open-channel sand suspension, and most assume some form of relationship between the bed shear stress due to skin friction and concentration. Garcia and Parker (1991) reviewed several of these relations, developed a new relation, and compared them against a set of laboratory data. They found the relations of van Rijn (1984) and Smith

and McLean (1977), along with their newly developed relation, performed best in comparison with the laboratory data. Further, their newly developed relation was generalized for the case of sediment mixtures by accounting for relative hiding/exposure effects of different grain-sizes as well as an overall suppression of entrainment characteristic of sediment mixtures. Here it will be shown that the Garcia-Parker relation is inadequate under conditions typical of large, low-slope, sand-bed rivers, so motivating the development of a modified version.

### **Limitations of the Garcia and Parker (1991) entrainment relation**

The relation of Garcia and Parker (1991) for sediment mixtures is given as follows:

$$E_{si} = \frac{A(\lambda X_i)^5}{1 + \frac{A}{0.3}(\lambda X_i)^5} \quad (13)$$

$$X_i = \left( \frac{u_{*sk}}{v_{si}} Re_{pi}^{0.6} \right) \left( \frac{D_i}{D_{50}} \right)^{0.2} \quad (14)$$

where  $E_{si}$  denotes the dimensionless entrainment rate of sediment in the  $i$ th grain-size range (volume entrainment per bed area per unit time per unit fractional bed content, made dimensionless by  $v_{si}$ ),  $\lambda = 1 - 0.28\sigma_\phi$  represents the overall suppression of entrainment due to mixture effects,  $\sigma_\phi$  is the standard deviation of the bed sediment on the sedimentological  $\phi$ -scale,  $u_{*sk}$  is the shear velocity due to skin friction,  $Re_{pi} = \sqrt{RgD_i} D_i / \nu$  is the particle Reynolds number,  $\nu$  is kinematic viscosity,  $D_i$  is the characteristic diameter of the  $i$ th grain-size range,  $D_{50}$  is median grain diameter of the bed material, and  $A = 1.3 \times 10^{-7}$ . In the case of equilibrium suspensions  $E_{si} = C_{5i} / F_{bi}$ ,

where  $C_{5i}$  is the volumetric concentration at 5% of the flow depth and  $F_{bi}$  is the volume bed fraction for the  $i$ th grain-size range. Note that the normalization with bed content fraction implies that the relation applies only to the bed-material part of the suspended load. Shear stress partitioning was accomplished by Garcia and Parker using the Einstein decomposition with a logarithmic velocity law and equivalent sand-grain roughness equal to twice the median bed material grain diameter (see Garcia and Parker, 1991, for details).

The relation given in (13) and (14) was developed from laboratory data and field data from the Rio Grande (Nordin and Dempster 1963) and Niobrara Rivers (Colby and Hembree 1956). It was found during the course of this work that the use of this relation for prediction of sediment transport for large sand-bed rivers resulted in the over-prediction of transport rates. This was investigated by comparing the relation with near-bed concentration data from the Mississippi River at St. Louis (Jordan 1965, Scott and Stephens 1966), as well as the Rio Grande data used by Garcia and Parker. For comparison, typical depths and slopes for the Rio Grande are  $0.5\text{ m}$  and  $1 \times 10^{-3}$ , while for the Mississippi they are  $8\text{ m}$  and  $6 \times 10^{-5}$ , respectively. Figure 4 shows the variation of near-bed entrainment ( $E_{si} = C_{5i}/F_{bi}$ ) with the Garcia-Parker entrainment parameter,  $\lambda X_i$ , for both rivers. Clearly the relation is not applicable to both cases, as the Mississippi River has a significantly lower near-bed entrainment than the Rio Grande for an equivalent  $X_i$  (note  $X_i$  is representative of bed shear stress). The primary difference between the Mississippi and Rio Grande Rivers is the slope, or equivalently the depth.

In the development of the Garcia-Parker relation, the ratio  $h/D_{50}$  was dropped because the range of this variable in the laboratory and field data was too narrow to

discern any dependence. The Mississippi data indicates that this parameter may need to be retained. Also, the method used for partitioning skin friction ignores stratification effects, which may be expected to be significant for the Mississippi River based on the findings of the companion paper (Wright and Parker, in press a). Both of these possibilities are investigated in the next section and a new relationship is developed as a result.

### **Skin friction/form drag partitioning**

The shear velocity due to skin friction is computed here in a manner similar to that used by Garcia and Parker (1991), the major difference being the inclusion of stratification effects. In Garcia and Parker, the shear stress partitioning is computed by considering a flow with equivalent mean velocity without bed forms *and* without stratification effects (the standard Einstein decomposition). Here the inconsistency of neglecting stratification effects is overcome by using a depth-averaged version of (10), which includes stratification effects. Integrating (10) over the flow depth leads to a logarithmic form for the mean velocity (i.e. Keulegan equation). Several authors have shown the near equivalence of the logarithmic velocity law and a one-sixth power-law (Engelund and Hansen 1967, Brownlie 1983). Here a stratification adjusted form of the equation given by Brownlie is used, primarily because it is simpler to work with analytically than the logarithmic form:

$$\frac{U}{\sqrt{gh_{sk}S_o}} = \frac{8.32}{\alpha} \left( \frac{h_{sk}}{k_s} \right)^{1/6} \quad (15)$$

where  $U$  is the depth-averaged velocity,  $h_{sk}$  is the depth due to skin-friction, and  $k_s$  is the sand grain equivalent roughness height (i.e. the skin-friction roughness height). Here

$k_s=3D_{90}$  is used (van Rijn 1984). The shear velocity due to skin friction is computed by solving (15) for  $h_{sk}$ , and applying  $u_{*sk} = \sqrt{gh_{sk}S_o}$ .

The use of (15) determines the skin friction component of the stress by considering a flow with equivalent mean velocity *and* stratification effects without bed forms. The drawback of including stratification effects is that now  $\alpha$  must be known to compute  $u_{*sk}$ . However  $\alpha$  is dependent on near-bed concentration through (9), so that iteration is required even when the depth is known *a priori*.

The need for iteration to determine  $u_{*sk}$  when depth is known can be avoided by looking for a more direct relationship between total shear stress and skin friction shear stress, which can then be used to close the depth-discharge relation as well. Engelund and Hansen (1967) used similarity principles to propose  $\tau_{*sk} = f(\tau_*)$ , where  $\tau_* = hS_o/RD_{50}$  is dimensionless bed shear stress (i.e. Shields stress) and  $\tau_{*sk} = h_{sk}S_o/RD_{50}$  is the skin friction component. To determine the form of the relationship, Engelund and Hansen computed  $\tau_{*sk}$  from laboratory data and a power velocity law similar to (15), but without the stratification adjustment. They then deduced the following form:

$$\tau_{*sk} = 0.06 + 0.4\tau_*^2 \quad (16)$$

Because the Einstein decomposition (i.e. (15)) was used to compute the skin-friction Shields stresses that went into developing (16), the two methods must provide roughly equivalent results for  $\tau_{*sk}$  when the depth is known. The usefulness of an equation like (16) is that it provides the additional link required to compute an unknown depth, as will

be demonstrated in a subsequent section. It is introduced here because it also provides a convenient way to compute  $\tau_{*sk}$  and thus  $u_{*sk}$  when the depth is known. However the entrainment relation which is developed in the subsequent section could be accomplished using the Einstein decomposition only.

Garcia (1995) found (16) to perform poorly for the large river data collected in his study. It was found that (16) tends to over-predict the skin friction shear stress for large rivers at high flows, indicating that large rivers do not make the transition from dunes to a flat bed at shear stresses as low as those observed in laboratory flumes. Julien and Klaasen (1995) have similarly shown that dunes are not washed out during floods for several large, sand-bed rivers. This same behavior is found here using the sand-bed river data introduced in the companion paper (Wright and Parker, in press a). Figure 5 shows  $\tau_{*sk}$ , computed from (15), versus  $\tau_*$  for the data set in question. It seen that (16) performs adequately for the small, steeper rivers such as the Rio Grande and Middle Loup. However, the skin friction shear stress is over-predicted by (16) for the large rivers such as the Mississippi and Atchafalaya, particularly at high shear stress. This suggests that the transition from dunes to upper regime occurs in these rivers at a much larger shear stress, as found by Julien and Klaasen (1995). Many such streams have a bankfull depth that is too low to allow for them to ever make the transition to upper-regime.

One major difference between large, low-slope rivers and small, steeper, sand-bed rivers is the magnitude of the Froude number,  $Fr = U/\sqrt{gh}$ , realized during high flows. This is shown in Figure 6, where Froude number is plotted versus slope. The Froude

number has been shown to be an important parameter in regards to the stability of dunes (Engelund 1970, Smith 1970), and has been used to characterize the transition between bedform regimes (Vanoni 1974). Because the Froude number remains small even at high flows in larger rivers, the transition to upper regime is expected to occur less frequently, if at all. Thus the skin friction shear stress will be less for greater total shear stress in large rivers, as was documented by Garcia (1995) and shown here in Figure 5. Based on this evidence, the Froude number has been incorporated into the relationship. The collapse is shown in Figure 7, and the best fit relation is given by:

$$\tau_{*sk} = 0.05 + 0.7(\tau_* Fr^{0.7})^{0.8} \quad (17)$$

The above relation is appropriate only for lower-regime conditions. As noted above, upper regime conditions are not commonly encountered in large, low-slope sand-bed streams. They are encountered in their smaller, higher-slope cousins, however, in which case the upper-regime formulation of Engelund and Hansen (1967) remains appropriate.

### **New entrainment relation**

It was previously shown that the Garcia and Parker (1991) relation tends to over-predict the near-bed concentration for large, low-slope rivers. One possible explanation is the neglect of stratification effects in the shear stress partitioning, which is addressed in the previous section. It was found, however, that the discrepancy shown in Figure 4 was still apparent when (15) was used. Thus another dependence on depth (or slope) is evident.

Though included in their dimensional analysis, the range of  $h/D_{50}$  in the data used by Garcia and Parker was too narrow to identify any dependence. Here the inclusion of the Mississippi River data allows for the elucidation of this effect. The ratio  $h/D_{50}$  is

replaced by  $S_o$  in the dimensional analysis (which is nearly equivalent and just a matter of choice of independent variables), and then simply lumped into the entrainment parameter (14). It was then assumed that the overall mixture entrainment suppression ( $\lambda$  in (13)) is the same as that found by Garcia and Parker. The final collapse of the data is shown in Figure 8, and the final relation becomes:

$$E_{si} = \frac{B(\lambda X_i)^5}{1 + \frac{B}{0.3}(\lambda X_i)^5} \quad (18)$$

$$X_i = \left( \frac{u_{*sk} Re_{pi}^{0.6}}{v_{si}} \right) S_o^{0.08} \left( \frac{D_i}{D_{50}} \right)^{0.2} \quad (19)$$

where  $B=7.8 \times 10^{-7}$ , and the exponent on  $D_i/D_{50}$  (0.2) is the same as that in the original Garcia-Parker relation. The relation in (18) and (19) represents a slight modification to that given in Wright and Parker (in press b), based on some further analysis.

Finally, it should be mentioned that the new relation can also be applied to uniform sediment, as the mixture effects disappear from (18) and (19) in this case. The new relation was applied to the flume data reported by Garcia and Parker (1991), yielding a goodness of fit quite similar to that found for their relation, , as well as for the van Rijn (1984) and Smith and McLean (1977) relations also included therein. This is expected since the range of  $S_o$  is small for the laboratory data.

## DEPTH-DISCHARGE RELATION

The relationship between depth and discharge appropriate for lower-regime conditions is developed by first assuming that the velocity profile over a bed with dunes has roughly the same shape as that over a flat bed. Thus the sand-grain roughness,  $k_s$  in

(15) may be replaced by a composite roughness,  $k_c$ , encompassing both skin friction and form drag:

$$\frac{U}{u_*} = \frac{8.32}{\alpha} \left( \frac{h}{k_c} \right)^{1/6} \quad (20)$$

Now using continuity,  $q=Uh$ , (20) can be rearranged into the following form:

$$\frac{h}{D_{50}} = \left[ \frac{\alpha}{8.32} \frac{q_*}{\sqrt{S_0}} \left( \frac{k_c}{D_{50}} \right)^{1/6} \right]^{3/5} \quad (21)$$

where  $q_* = q/\sqrt{gD_{50}}D_{50}$  is the dimensionless unit discharge. The composite roughness is related the sand-grain roughness by eliminating  $U$  between (15) and (20), which yields:

$$\frac{k_c}{k_s} = \left( \frac{h}{h_{sk}} \right)^4 = \left( \frac{\tau_*}{\tau_{*sk}} \right)^4 \quad (22)$$

The relationship between  $\tau_*$  and  $\tau_{*sk}$  is given by (17), which provides all of the information to solve (21) iteratively for the depth as outlined below. The required known parameters are the unit discharge,  $q$ , the slope,  $S_0$ , and the grain-size distribution of the bed ( $F_{bi}$ ,  $D_i$ ). The last of these allows for the determination of  $D_{50}$ ,  $D_{90}$ , and  $\sigma_\phi$ . To implement the calculation, guess the depth,  $h$ , and calculate  $\tau_*$  and  $Fr$ . Then calculate  $\tau_{*sk}$  from (17) and  $k_c$  from (22) (using  $k_s=3D_{90}$ ). Next, calculate the total near-bed concentration,  $C_{5t} = \sum E_{si}/F_{bi}$ , from (18), which allows for the calculation of the stratification correction,  $\alpha$ , from (9). Finally, calculate the new depth from (21) and iterate to convergence.

This new formulation was validated against the large river dataset of Toffaleti (1968), which includes the Mississippi, Atchafalaya, and Red Rivers, and was introduced in the companion paper and used in the development of the formulation itself. In addition, the data set of Garcia (1995) which was not used to develop the formulation, was employed to provide independent validation. It contains 85 measurements made from 1987-1990 at various locations along the Mississippi River, Illinois River, Missouri River, Ohio River, and several others. The data used for comparison is primarily from large, deep rivers, because these are the conditions under which the proposed method is expected to yield the greatest improvement upon previous methods. Figures 9 and 10 show the agreement between the measurements and predictions for the two datasets; the agreement is seen to be quite good for both.

To illustrate the advantage of the new relation it is compared with the relation of Brownlie (1983), which uses a similar power-law form and is based on a large data set including many sand-bed rivers, e.g. the Toffaleti large river data. Figure 11 shows the agreement between measurements and predictions by the Brownlie equation for the same large river data from Toffaleti.. It is seen that Brownlie tends to over-predict the depth at the highest flows, where stratification effects are expected to be greatest. Comparison with Figure 9 reveals that accounting for density stratification in the newly proposed relation eliminates this over-prediction. It is also apparent that the proposed method and Brownlie relation under predict the Red River depths. The reasons for this discrepancy are unknown; however it is noted that the proposed method performs well for similar depth flows in Figure 10.

## RELATION FOR SUSPENDED SEDIMENT TRANSPORT

The stratification adjusted velocity and concentration profiles, and near-bed concentration predictor can now be used to develop a relation for the grain-size specific suspended sediment transport rate. Again an equivalent power-law form of the velocity profile is used in place of the logarithmic profile:

$$\frac{u}{u_*} = \frac{9.70}{\alpha} \left( \frac{y}{k_c} \right)^{1/6} \quad (23)$$

which leads to (20) when integrated over the depth. Substitution of (23) and (11) into (1) and integration yields the bed-material suspended sediment transport rate:

$$\frac{q_{si}}{u_* h} = \frac{9.70}{\alpha} C_{si} \left( \frac{h}{k_c} \right)^{1/6} I \quad (24)$$

$$I = \int_{\eta_a}^1 \eta^{1/6} \left( \frac{1-\eta}{\eta} \frac{\eta_a}{1-\eta_a} \right)^{Z_{Ri}} d\eta \quad (25)$$

The integral in (24) and (25) has no analytical solution and thus must be determined numerically. Since  $\eta_a$  is a constant set equal to 0.05 here,  $I$  is a function of  $Z_{Ri}$  only. The integral was computed numerically for a range of  $Z_{Ri}$  typical of sand suspensions and the following expression approximates the integral to within about 10%:

$$I \cong \begin{cases} 0.679 \exp\{-2.23Z_{Ri}\} & \text{for } Z_{Ri} \leq 1 \\ 0.073Z_{Ri}^{-1.44} & \text{for } Z_{Ri} > 1 \end{cases} \quad (26)$$

The new relation was tested against the same set of measurements used for comparison of the depth-discharge relation, i.e. the large river data of Toffaleti (1968). The initiation of suspension criterion of van Rijn (1984) was used for all calculations. Figure 12 shows measured versus predicted total discharge-weighted sand concentration,

$C_m = \sum q_{si}/q$ . Figure 13 presents measured versus predicted fraction in suspended transport of each grain-size,  $F_{ii} = q_{si}/\sum q_{si}$ , for the three rivers. In Figure 13, very fine sand is sizes 0.0625 – 0.125 mm, fine sand is 0.125 – 0.25 mm, and medium sand is 0.25 – 0.5 mm.

Figure 12 indicates that the new method tends to under-predict the total transport at low transport rates. This notwithstanding, it performs quite well at the higher concentrations, which are generally of greatest interest for morphological computations. Figure 13 indicates that the new method does relatively well at predicting the distribution of the suspended load for each of the rivers. There is a tendency to under-predict the transport of the larger sizes in suspension (medium sand), which has only a slight effect on the total concentration predictions because the finer sizes dominate the transport. For the data used here, the average distribution is 69% very fine sand, 25% fine sand, and only 5% medium sand. These results provide confidence that the method may be useful for the study of suspension driven sorting phenomena.

A more quantitative description of the performance of the method is achieved by analyzing the ratio of predicted to measured values, termed the discrepancy ratio. The discrepancy ratio was computed for the total sand concentration,  $C_m$ , and for each fraction in transport,  $F_{ii}$ . For comparison, the relationship of Wu et al. (2000) was also applied to the same data set. The Wu method represents a relatively new method which takes a more empirical approach. Unlike most other methods for predicting grain-size specific transport, the Wu method distinguishes between bedload and suspended load, and thus is directly comparable to the method presented here, which treats suspended load only. It is

noted that the measured depths were used for calculations using the Wu method, while the depths predicted from (21) were used for calculations with the new method.

The discrepancy ratio results (mean and standard deviation) for each method are given in Table 1. A value of unity for the mean and zero for the standard deviation would represent perfect agreement. The discrepancy ratio results confirm what is seen in Figures 12 and 13, i.e. the proposed method predicts relatively well the total transport and grain-size distribution of the suspension. The results also confirm the under-prediction of the transport of the larger sizes. This is likely due to the increased diffusion of larger sizes which has been noted by several authors (van Rijn 1984, Greimann et al. 1999, Cellino and Graf 2002). Typically this has been accounted for through the use of the  $\beta$  factor in the Rouse number (van Rijn 1984, Graf and Cellino 2002). This track was not pursued here for several reasons: 1) the simplified stratification adjustment was developed using a model which assumed  $\beta=1$ , and thus the use of a relation which specifies  $\beta \neq 1$  would be inconsistent the relation for  $\beta$  proposed by van Rijn (1984) does not isolate stratification effects from the increased diffusion, which is required to be compatible with the proposed method, 2) existing relations for  $\beta$  (such as van Rijn 1984) do not isolate increased diffusion effects from stratification effects, which would be required for compatibility with the proposed method, 3) there is still a good amount of uncertainty related to the  $\beta$  factor for flows with bed forms (Graf and Cellino 2002), and probably most importantly 4) the larger sizes that are most affected by the increased diffusion contribute only a small fraction to the total transport, particularly for large, sand-bed rivers which are the focus here. Further study of the increased diffusion of the

larger sizes in suspensions with bed forms, in isolation from density stratification effects, is required in order to further improve the proposed method.

Table 1 shows that the method of Wu et al. tends to over-predict the fraction in transport of the larger grain-sizes, i.e. the fine and medium sands. In general, it is seen that the proposed method performs comparably the Wu method for both the mean and the standard deviation of the discrepancy ratio, at least for this particular data set. The advantage of the proposed method is that it is more physically based and provides much more information, including the vertical velocity and concentration profiles, and serves as a predictor of hydraulic resistance.

## **CONCLUSIONS**

New methods are proposed for the prediction of the flow depth, grain-size specific near-bed concentration and bed-material suspended sediment transport rate in sand-bed rivers. The salient improvements delineated here all relate to the need to modify existing formulations in order to encompass the full range of sand-bed streams, and in particular large, low-slope sand-bed streams. They can be summarized as follows: a) the inclusion of density stratification effects, which have been shown in the companion paper (Wright and Parker, in press a) to be particularly relevant for large, low-slope, sand-bed rivers; b) a new predictor for near-bed entrainment rate into suspension which extends the relation of Garcia and Parker (1991) to the range of large, low-slope sand-bed rivers, and c) a new predictor for form drag based on that of Engelund and Hansen (1967) which again includes in its range of validity large, low-slope sand-bed rivers.

Predictions from the new relations were compared to measurements from the Mississippi, Atchafalaya, and Red Rivers, and shown to perform well. Accounting for stratification effects results in improvement over the Brownlie (1983) relation at large depths. For predicting sediment transport, the new relations were shown to perform comparably to the recent more empirical approach of Wu et al. (2000), at least for this particular dataset, while providing more information including the vertical velocity and concentration profiles.

## **ACKNOWLEDGEMENTS**

This research was funded by National Science Foundation Grant CTS-0096916. The second author wishes to thank M. H. Garcia, S. R. McLean, C. Paola, J. D. Smith and P. Wiberg for many stimulating discussions about concepts related to the content of this paper.

## **REFERENCES**

- ASCE (1975). *Sedimentation Engineering*, V.A. Vanoni, ed., New York.
- Bennett, J.P. (1995). "Algorithm for resistance to flow and transport in sand-bed channels." *J. Hydraulic Eng.*, 121(8), 578-590.
- Brownlie, W. (1983). "Flow depth in sand-bed channels.", *J. Hydraulic Eng.*, 109(7), 959-990.
- Colby, B. R. (1957). "Relationship of unmeasured sediment discharge to mean velocity." *Trans. American Geophysical Union*, 38(5), 708-717.

- Colby, B.R., and Hembree, C.H. (1956). "Computations of Total Sediment Discharge Niobrara River Near Cody, Nebraska." *U.S. Geol. Survey Water-Supply Paper 1357*.
- Einstein, H.A. (1950). "The bed load function in open channel flows." *U.S. Dept. of Agriculture, Technical Bulletin No. 1026*.
- Einstein, H. A. and Chien, N. (1953). "Can the rate of wash load be predicted from the bed-load function?" *Trans. American Geophysical Union*, 34(6), 876-882.
- Einstein, H.A., and Chien, N. (1955). "Effects of Heavy Sediment Concentration Near the Bed on Velocity and Sediment Distribution." *MRD Sediment Series No. 8*, University of California, Institute of Engineering Research, Berkeley, California.
- Engelund, F. (1970). "Instability of erodible beds." *J. Fluid Mechanics*, 42(2), 225-244.
- Engelund, F., and Hansen, E. (1967). "A monograph on sediment transport in alluvial streams." *Technical University of Denmark*.
- Garcia, L.P. (1995). "Transport of sands in deep rivers." *Doctoral Dissertation*, Colorado State University, Fort Collins, CO.
- Garcia, M., and Parker, G. (1991). "Entrainment of bed sediment into suspension.", *J. Hydraulic Eng.*, 117(4), 414-435.
- Graf, W.H., and Cellino, M. (2002). "Suspension flows in open channels; experimental study", *J. Hydraulic Res.*, 40(4), 435-447.
- Greimann, B.P., Muste, M., and Holly, F.M. Jr. (1999). "Two-phase formulation of suspended sediment transport", *J. Hydraulic Res.*, 37(4), 479-500.
- Henderson, F.M. (1966). *Open Channel Flow*. MacMillan, New York.

- Jordan, P.R. (1965). "Fluvial sediment of the Mississippi River at St. Louis, Missouri." *U.S. Geol. Survey Water-Supply Paper 1802*.
- Julien, P.Y., and Klaasen, G.J. (1995). "Sand-dune geometry of large rivers during floods." *J. Hydraulic Eng.*, 121(9), 657-663.
- McLean, S.R. (1991). "Depth-integrated suspended-load calculations." *J. Hydraulic Eng.*, 117(11), 1440-1458.
- McLean, S.R. (1992). "On the calculation of suspended load for noncohesive sediments." *J. Geophysical Res.*, 97(C4), 5759-5770.
- Molinas, A., and Wu, B. (2000). "Comparison of fractional bed-material load computation methods in sand-bed channels." *Earth Surf. Proc. and Landforms*, 25, 1045-1068.
- Nordin, C.F., and Dempster, G.R. (1963). "Vertical distribution of velocity and suspended sediment Middle Rio Grande New Mexico." *U.S. Geol. Survey Prof. Paper 462-B*.
- Raudkivi, A.J. (1976). *Loose Boundary Hydraulics*. Pergamom Press, Oxford, U. K.
- Samaga, B.R., Ranga Raju, K.G., and Garde, R.J. (1986). "Suspended load transport of sediment mixtures." *J. Hydraulic Eng.*, 112(11), 1019-1035.
- Scott, L.H., and Stephens, H.D. (1966). "Special sediment investigations Mississippi river at St. Louis, Missouri, 1961-1963." *U.S. Geol. Survey Water-Supply Paper 1819-J*.
- Smith, J.D. (1970). "Stability of a sand bed subjected to a shear flow of low Froude number." *J. Geophysical Res.*, 75(30), 5928-5940.

- Smith, J.D., and McLean, S.R. (1977). "Spatially averaged flow over a wavy surface." *J. Geophysical Res.*, 82(12), 1735-1746.
- Toffaletti, F.B. (1968). "A procedure for computation of the total river sand discharge and detailed distribution, bed to surface." *Technical Report No. 5*, Committee on Channel Stabilization, Corps of Engineers.
- van Rijn, L.C. (1984). "Sediment transport, part II: suspended load transport." *J. Hydraulic Eng.*, 110(11), 1613-1641.
- Vanoni, V.A. (1974). "Factors determining bed forms of alluvial streams." *J. Hydraulics Div. ASCE*, 100(3), 363-377.
- Wright, S., and Parker, G. (in press a). "Density stratification effects in sand-bed rivers", *J. Hydraulic Eng.*
- Wright, S., and Parker, G. (in press b). "Grain-size specific suspended sediment transport and flow resistance in larges sand-bed rivers", Proceedings of the *Symposium on Sedimentation and Sediment Transport*, September 1-6, 2002, Monte Verita, Switzerland.
- Wu, W., Wang, S.S.Y., and Jia, Y. (2000). "Nonuniform sediment transport in alluvial rivers.", *J. Hydraulic Res.*, 38(6), 427-434.

## NOTATION

- A* constant in the Garcia-Parker entrainment relation;
- B* constant in the newly proposed entrainment relation;
- b* hiding/exposure exponent in the newly proposed entrainment relation;
- C<sub>i</sub>* local sediment concentration by volume of grain-size *i*;

$C_{5t}$	total concentration by volume at 5% of flow depth;
$C_{5i}$	concentration by volume of grain-size $i$ at 5% of flow depth;
$C_{ai}$	concentration by volume of grain-size $i$ at near-bed point $a$ ;
$C_m$	total discharge-weighted sand concentration;
$D_i$	diameter of grain-size $i$ ;
$D_{50}$	median diameter of bed material;
$D_{90}$	grain diameter which 90% of bed material is finer;
$E_{si}$	entrainment of grain-size $i$ at 5% of flow depth;
$F_{bi}$	fraction of grain-size $i$ in bed material;
$F_{ti}$	fraction of grain-size $i$ in suspended transport;
$Fr$	Froude number;
$g$	gravitational acceleration;
$h$	flow depth;
$h_{sk}$	flow depth due to skin friction;
$I$	suspended sediment transport integral;
$K_m$	eddy viscosity;
$K_{mo}$	eddy viscosity of an equivalent clear-water flow;
$k_s$	equivalent sand-grain roughness height;
$k_c$	composite (form and skin) roughness height;
$n$	number of grain-sizes in suspension;
$q$	discharge per unit width;
$q_{si}$	suspended sediment transport rate per unit width of grain-size $i$ ;
$q_*$	dimensionless discharge per unit width;

$R$	submerged specific gravity;
$Re_{pi}$	particle Reynolds number of grain-size $i$ ;
$Ri_f$	flux Richardson number;
$S_o$	slope;
$u$	streamwise flow velocity;
$u_*$	shear velocity;
$u_{*sk}$	shear velocity due to skin friction;
$U$	depth-averaged velocity;
$v_{si}$	settling velocity of grain-size $i$ ;
$X_i$	entrainment parameter of grain-size $i$ ;
$y$	vertical distance from bed;
$Z_{Ri}$	Rouse number for grain-size $i$ ;
$\alpha$	simplified stratification adjustment;
$\kappa$	von Karman constant;
$\kappa_a$	apparent von Karman parameter estimated from the full velocity profile;
$\lambda$	parameter characterizing mixture suppression of entrainment;
$\eta$	dimensionless distance from bed, $y/h$ ;
$\eta_o$	dimensionless distance from bed where $u=0$ ;
$\eta_a$	dimensionless distance from bed at near-bed point $a$ ;
$\sigma_\phi$	standard deviation of bed material on sedimentological $\phi$ -scale;
$\sigma_g$	standard deviation of bed material;
$\tau_*$	dimensionless bed shear stress (Shields stress);

$\tau_{*sk}$  Shields stress due to skin friction;

## TABLES

Table 1 Mean and standard deviation (in parentheses) of the discrepancy ratio (ratio of predicted to measured value) for the large river dataset of Toffaleti (1968).

	$C_m$	<i>very fine sand</i> <sup>1</sup> $F_{ii}$	<i>fine sand</i> $F_{ii}$	<i>medium sand</i> $F_{ii}$
Proposed method	1.2 (1.3)	1.3 (0.59)	0.84 (0.60)	0.31 (0.39)
Wu et al. (2000)	1.3 (2.8)	0.84 (0.38)	1.7 (1.2)	1.9 (2.2)

<sup>1</sup> very fine: 0.0625-0.125 mm, fine: 0.125-0.25 mm, medium: 0.25-0.50 mm

## **FIGURES**

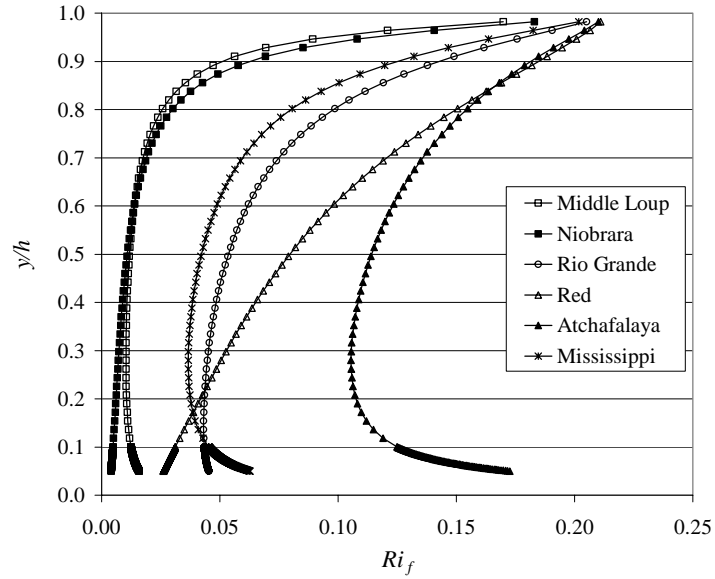


Figure 1 Flux Richardson number profiles for a high flow event for six sand-bed rivers based on model calculations presented in the companion paper (Wright and Parker, in press a).

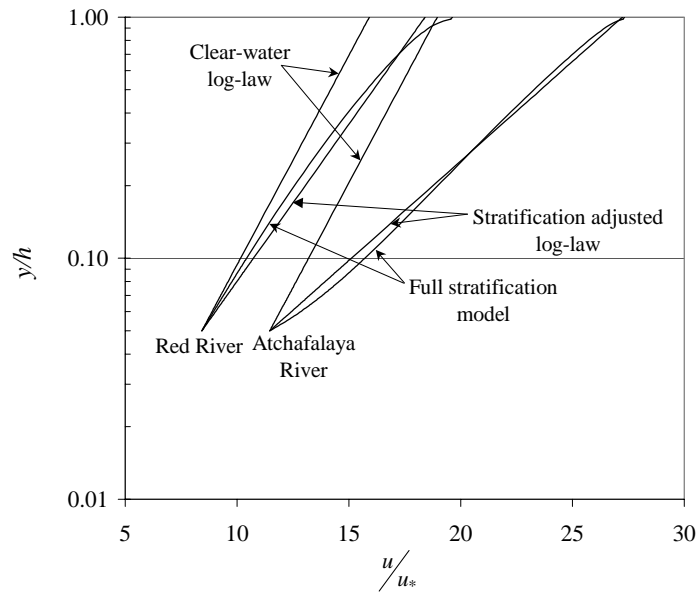


Figure 2 Velocity profiles for the Red and Atchafalaya Rivers, showing the difference between the clear-water log-law, the full stratification model profile from the companion paper, and the stratification adjusted log-law.

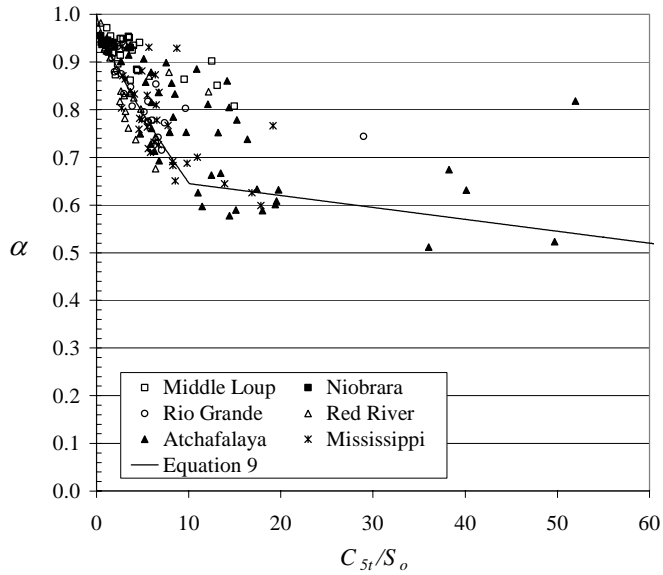


Figure 3 Depth-averaged reduction in eddy viscosity versus the ratio of near-bed concentration to slope based on model calculations presented in the companion paper (Wright and Parker, in press a).

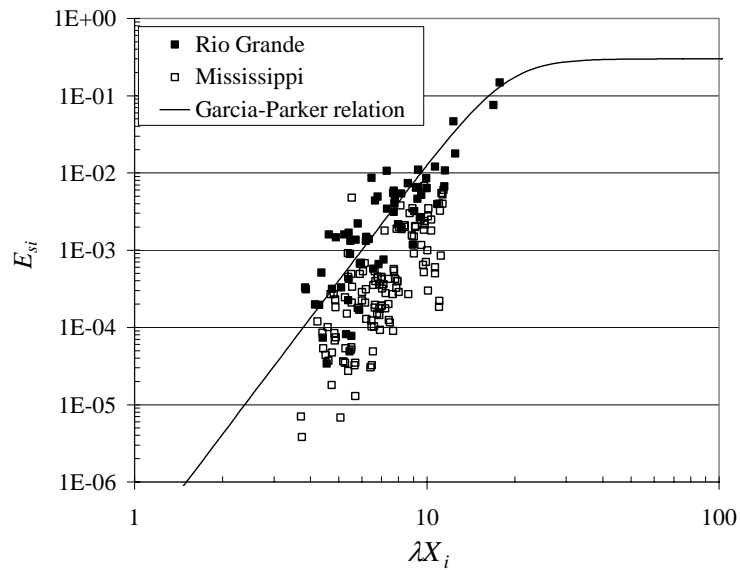


Figure 4 Sediment entrainment versus the Garcia and Parker (1991) entrainment parameter for the Rio Grande and Mississippi Rivers, illustrating the difference between relatively deep and shallow flows.

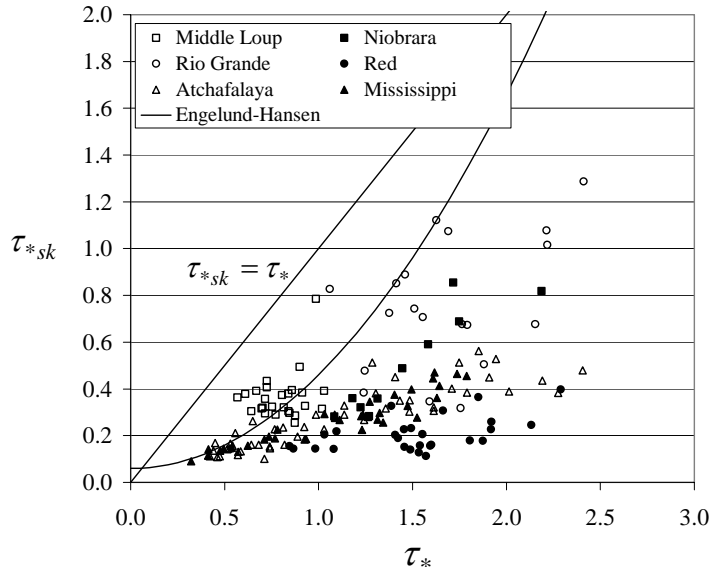


Figure 5 Total Shields stress versus Shields stress due to skin friction (as computed by the Einstein decomposition, Eq. 15) for several sand-bed rivers, along with the relation proposed by Engelund and Hansen (1967). Note the difference in behavior between deep and shallow flows particularly at high Shields stress.

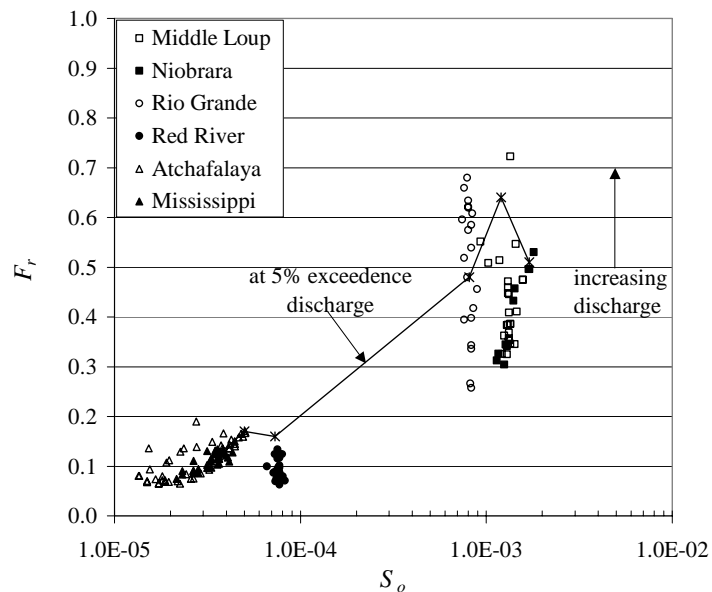


Figure 6 Froude number versus slope for several sand-bed rivers.

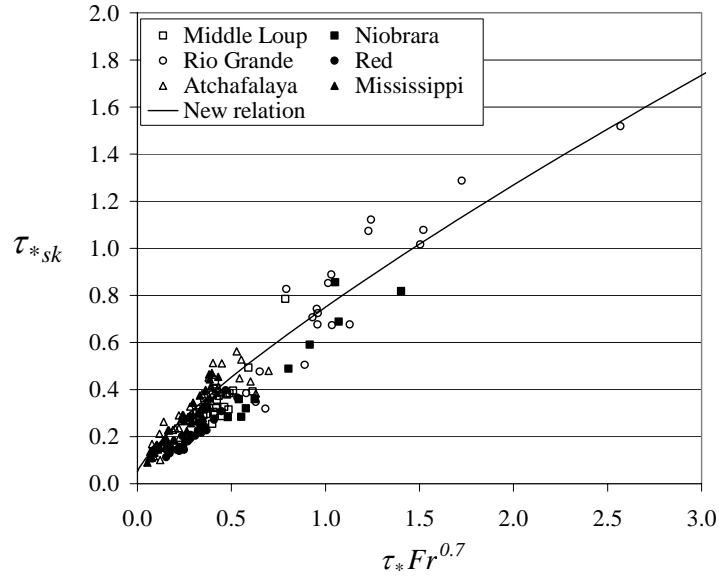


Figure 7 Newly proposed relation between total and skin friction Shields stress, incorporating the Froude number to collapse the difference between deep and shallow flows.

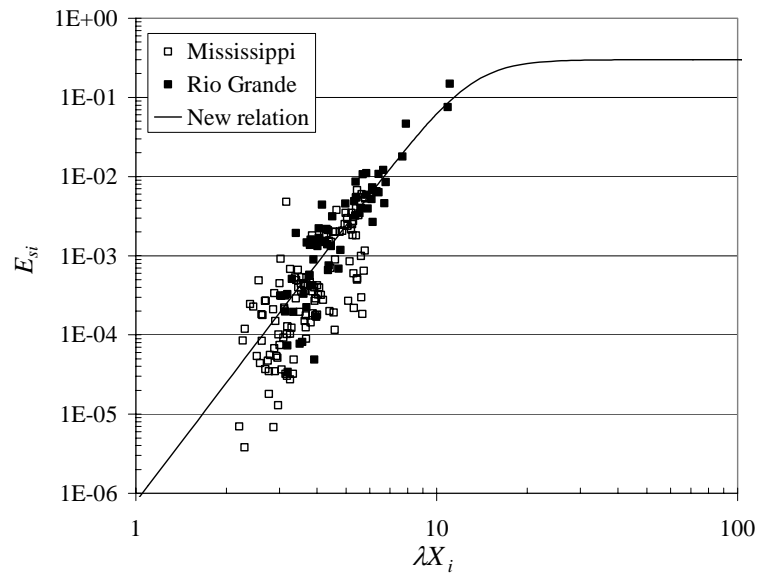


Figure 8 Newly proposed entrainment relation for sediment mixtures.

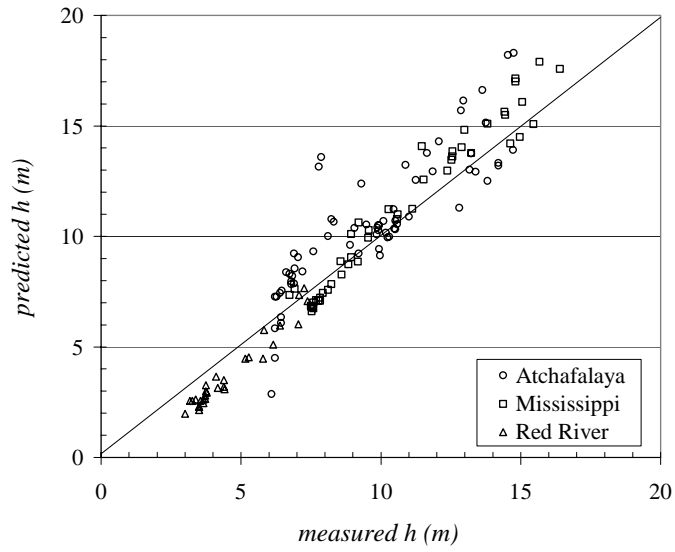


Figure 9 Predicted versus measured depth for the newly proposed depth-discharge predictor for the Toffaleti (1968) large river data.

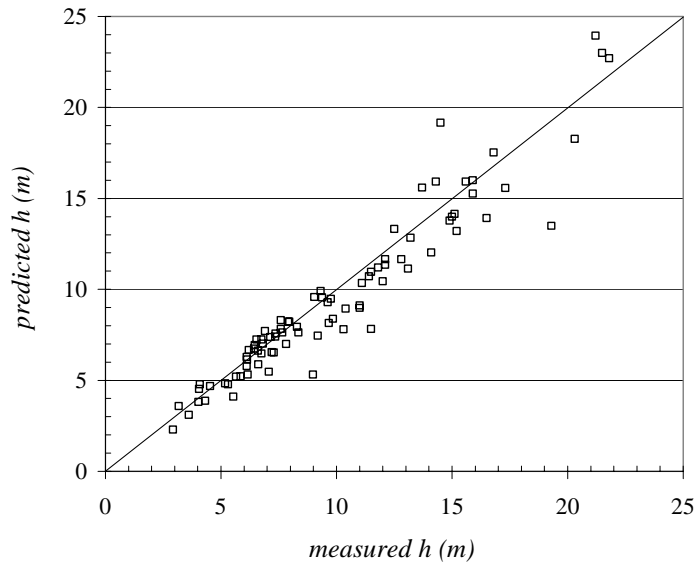


Figure 10 Predicted versus measured depth for the newly proposed depth-discharge predictor for the Garcia (1995) Mississippi basin data.

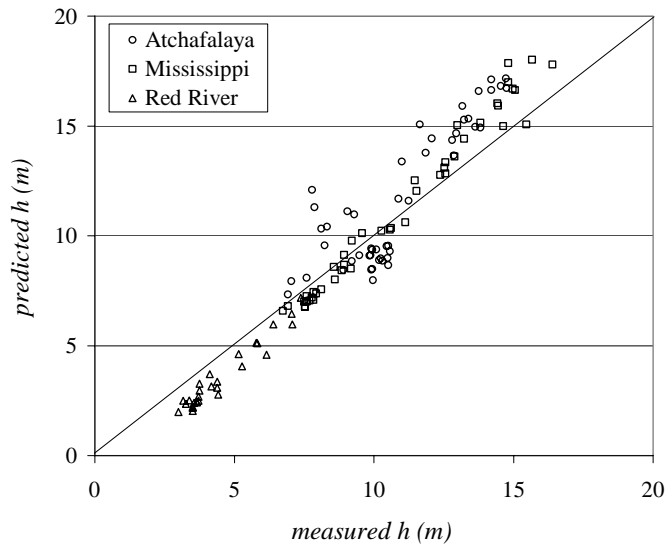


Figure 11 Predicted versus measured depth for the Brownlie (1983) lower-regime equation applied to the Toffaleti (1968) large river data. Note the over prediction at large depth, which is accounted for by the stratification correction in the proposed method.

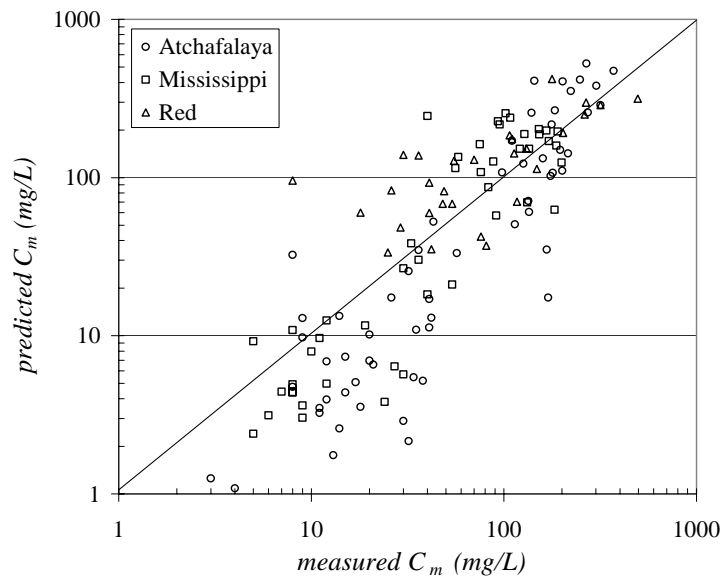


Figure 12 Predicted versus measured total discharge-weighted concentration of sand for the Toffaleti (1968) large river data.

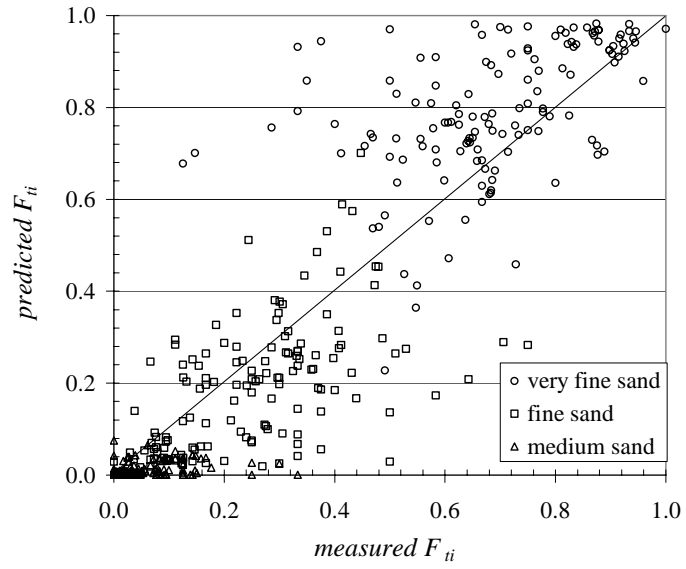


Figure 13 Predicted versus measured content fractions  $F_{ti}$  in the suspended bed-material load for the Toffaleti (1968) large river data.

**CHAPTER 3: MODELING DOWNSTREAM FINING IN SAND-BED  
RIVERS I: FORMULATION**

Scott Wright and Gary Parker

## **ABSTRACT**

In this paper a numerical modeling formulation is presented for simulation of the development of the longitudinal profile and bed sediment distribution in sand-bed rivers. The objective of the model application, which is presented in the companion paper, Wright and Parker (submitted) is to study the development of two characteristics of large, low-slope, sand-bed rivers: 1) a downstream decrease in bed slope (i.e. concave upward longitudinal profile) and 2) a downstream decrease in characteristic bed sediment diameter (e.g. the median bed surface size  $D_{50}$ ). Three mechanisms that lead to an upward concave profile and downstream fining are included in the modeling formulation: 1) a delta prograding into standing water at the downstream boundary, 2) sea-level rise, and 3) tectonic subsidence. In the companion paper, Wright and Parker (submitted), the model is applied to simulate the development of the longitudinal profile and downstream fining in sand-bed rivers flowing into the ocean during the past 5,000 years of relatively slow sea-level rise.

## **INTRODUCTION**

A well-known characteristic of many rivers is a decrease in the grain diameter of the bed (e.g. the median bed surface size  $D_{50}$ ) in the downstream direction. This characteristic, often termed downstream fining, is typically accompanied by a downstream decrease in bed slope, i.e. a concave upward longitudinal profile. These characteristics are well documented in the literature for the case of gravel-bed streams (see e.g. ASCE in press) and thus a long list of references is not provided here. Two examples of these phenomena in large, sand-bed streams are shown in Figures 1 and 2,

pertaining respectively to the lower Mississippi River, USA and the middle Fly River, Papua New Guinea. The longitudinal profile for the Mississippi was taken from the river crossings profile of Figure 56 of Fisk (1944), and the bed sediment data is from USCOE (1935). The Fly profile and bed sediment data are from Dietrich et al. (1999) and Pickup et al. (1979). The primary objective of the analysis presented here and in the companion paper, Wright and Parker (submitted) is to model the processes leading to the simultaneous development of a concave upward longitudinal profile and downstream fining in large, suspended-load dominated rivers such as the Mississippi and Fly.

The subject of downstream fining in bed-load dominated gravel-bed rivers has been the focus of several modeling studies, such as Parker (1991a and 1991b), Hoey and Ferguson (1994, 1997), Pizzuto (1995), and Cui et al. (1996); Parker and Cui (1998), Cui and Parker (1998) and Robinson and Slingerland (1998) studied bimodal gravel-sand mixtures. These studies focused on the effects of selective bed-load transport, abrasion, tributary inputs, tectonic subsidence, hydraulic geometry, water discharge, and sediment feed rate on downstream fining. Downstream fining in purely sand-bed rivers has received relatively less attention. Rana et al. (1973) applied a simple model of sorting by selective transport of finer grain-sizes, assuming that the upward concave longitudinal profile is an independent variable. The downstream fining is then computed by assuming constant water discharge and constant total bed material discharge throughout the reach. Deigaard (1980) presented a more complex model which imposed mass balance of bed sediment and assumed uniform flow, and applied it to several field cases. This model allows the longitudinal profile to evolve; however, an upward concave profile was used as the initial condition, which quickly drives the development of downstream fining.

The model developed here seeks to improve on these previous models of downstream fining in sand-bed rivers in several ways. First and foremost, it is desired to simulate the simultaneous development of the longitudinal profile and downstream fining. To this end, the model includes several mechanisms which can drive this development. Sinha and Parker (1996) identified wavelike progradation of the entire profile and aggradation due to subsidence as mechanisms which lead to an upward concave profile. Similar to the wavelike profile progradation, here the downstream boundary is allowed to prograde as a delta into standing water, which also results in a concave upward profile (Swenson et al., 2000; Kostic and Parker, 2003a,b). The model formulation presented here also allows for subsidence and sea-level rise, both of which drive aggradation and lead to an upward concave profile. The upward concave profile drives the development of downstream fining through a downstream decrease in transport capacity and the selective transport of finer sizes (or selective deposition of larger sizes). Finally, the model employs recently developed relations for hydraulic resistance and grain-size specific suspended-sediment transport in sand-bed rivers. Flow momentum balance is treated in terms of a backwater formulation.

## **MODEL DESCRIPTION**

### **Primary governing equations**

The modeling formulation presented here is similar in general form, with several differences, to some previous models of river morphodynamics, including those of van Niekerk et al. (1992), Hoey and Ferguson (1994), Cui et al. (1996), and Rahuel et al.

(1989), among others. Flow is assumed one-dimensional and quasi-steady in a rectangular channel with no floodplain and no tributaries:

$$\frac{\partial}{\partial x} \left[ \frac{1}{2} \frac{Q^2}{B^2 H^2} + gH + g\eta \right] + gS_f = 0 \quad (1)$$

where  $H$  is flow depth,  $B$  is channel width,  $Q=BUH$  is water discharge,  $U$  is mean velocity,  $\eta$  is channel bed elevation,  $S_f$  is friction slope,  $g$  is gravity and  $x$  is the streamwise coordinate. Conservation of mass for bed sediment is given by the standard Exner equation, on a grain-size specific basis (see e.g. Parker and Sutherland 1990, Parker 1991a, Hoey and Ferguson 1994):

$$B_a (1 - \lambda_p) \left[ \sigma + \frac{\partial \eta}{\partial t} \right] = -I_Q \frac{\partial Q_s}{\partial x} \quad (2)$$

$$B_a (1 - \lambda_p) \frac{\partial (L_a F_{bk})}{\partial t} = -I_Q \frac{\partial Q_{sk}}{\partial x} + F_{lk} \left[ I_Q \frac{\partial Q_s}{\partial x} + B_a (1 - \lambda_p) \frac{\partial L_a}{\partial t} \right] \quad (3)$$

where  $B_a$  is the active width (to be discussed in more detail in the companion paper),  $\lambda_p$  is bed sediment porosity (set equal to 0.4 here),  $\sigma$  is tectonic subsidence rate (so that a negative value corresponds to uplift),  $I_Q$  is the flow intermittency factor characterizing the fraction of time the river is in flood,  $Q_s$  is total (suspended and bed-load) bed-material sediment transport rate,  $Q_{sk}$  is the bed-material transport rate of grain-size interval  $k$ ,  $t$  is time,  $L_a$  is active layer thickness, and  $F_{bk}$  and  $F_{lk}$  denote the fraction of sediment within grain-size interval  $k$  in the active layer and at the interface between the active layer and substrate, respectively. Bed-material is assumed to consist of sand sizes only; grain

diameters smaller than 0.062 mm are considered washload and are thus not allowed to interact with the bed (e.g. Raudkivi, 1976). This point is considered in more detail in the companion paper, Wright and Parker (submitted).

The flow intermittency factor  $I_Q$ , originally introduced by Paola et al. (1992), is used as a simple method to account for flow variability. Geomorphic change occurs primarily during large events which occur infrequently, so that simulating low flow conditions is unnecessary. The intermittency factor allows for the use of a single discharge, for example bankfull flow, to characterize the hydrologic regime. Determination of the factor is discussed in detail in a subsequent section.

For a bed covered in dunes, the active layer thickness has typically been assumed to scale with the dune height or water depth (Deigaard 1980, Rahuel et al. 1989). This assumption is adopted here. The active layer thickness is specified as one dune height, and the dune height is predicted by the relation of Julien and Klaasen (1995). This assumption is addressed through sensitivity analysis of this parameter.

Specification of the interface fraction  $F_{Ik}$  can have a significant effect on model results, as will be shown through sensitivity analysis. During erosion, the interface fraction  $F_{Ik}$  is taken from the substrate distribution. For the case of aggradation, which is the case considered here, the situation is less clear. Hoey and Ferguson (1994) proposed a relation of the following form:

$$F_{Ik} = cF_{ik} + (1 - c)F_{bk} \quad (4)$$

where  $F_{ik}$  is the fraction in transport of grain-size interval  $k$ . For gravel sorting in a flume, Toro-Escobar et al. (1996) obtained the experimental result  $c=0.7$ , which indicates that sediment at the interface is weighted toward the material in transport (in their case as

bed-load only). This is a result of a sieving process whereby the deposited smaller sizes work directly through the surface layer to the interface during deposition. For a sand-bed covered in dunes, it is doubtful that deposited material would be sieved all the way through to the interface (i.e. one dune height). Thus the assumption of  $c=0$  has been adopted for all simulations, which specifies the transfer of active layer sediment only to the substrate during aggradation. The parameter  $c$  is, however included in the sensitivity analysis.

Several constitutive relations are required to close the system of equations (1), (2) and (3). The friction slope and grain-size specific suspended-sediment transport rate are specified using the new formulations of Wright and Parker (in press(b)). These formulations modify previous relations in order to extend their applicability to the case of large, low-slope, sand-bed rivers. Also, the new formulation accounts for the effects of density stratification which were shown by Wright and Parker (in press(a)) to be particularly important for low-slope rivers. Since the focus of this paper is modeling large, low-slope sand-bed rivers, the analysis would not have been possible without the new formulations. Grain-size specific bed-load transport rate is computed using the relation of Ashida and Michiue (1972).

Finally, the formulation presented here makes several assumptions which render the model applicable to long reaches of rivers subject to gradual changes. These assumptions include quasi-steady flow and the equilibrium suspension approximation for sediment transport. The formulation is not applicable to short reaches with rapid variations.

### Prograding delta boundary

Sinha and Parker (1986) showed that wavelike progradation of the entire longitudinal profile can lead to the development of a concave upward profile. A similar mechanism is accounted for here by allowing the downstream boundary to prograde. The derivation to be summarized here has its origin in the models of Swenson et al. (2000) and Kostic and Parker (2003a,b). A definition sketch for the prograding delta face is given in Figure 3. In the following equations, the subscript  $fs$  denotes foreset and  $bs$  denotes bottom slope. Two moving boundaries are involved, the top and bottom of the foreset deposit. The migration rate of the top (point  $s$  in Figure 3) is given by integrating (2) across the delta face:

$$B_a (1 - \lambda_p) \left[ \int_{x_s}^{x_b} \sigma dx + \int_{x_s}^{x_b} \frac{\partial \eta_{fs}}{\partial t} dx \right] = - \int_{x_s}^{x_b} I_Q \frac{\partial Q_s}{\partial x} dx \quad (5)$$

The slope across the foreset is assumed constant,  $S_{fs}$ , so that  $\eta_{fs} = \eta_s - S_{fs}(x - x_s)$  and thus:

$$\frac{\partial \eta_{fs}}{\partial t} = \frac{\partial \eta}{\partial t} \Big|_{x_s} - S_{os} \dot{x}_s + S_{fs} \dot{x}_s \quad (6)$$

where  $S_{os} = -\frac{\partial \eta}{\partial x} \Big|_{x_s}$  is the slope of the river at the top of the foreset, and  $\dot{x}_s = \frac{\partial x_s}{\partial t}$  is the migration rate of the top of the foreset. Substitution of (6) into (5), specifying zero sediment transport at the bottom of the foreset ( $Q_s \Big|_{x_b} = 0$ , so that all incoming bed-material sediment goes toward prograding the delta face), assuming  $\sigma = const$  over the foreset, and performing the integration yields:

$$(x_b - x_s) \left[ \sigma + \frac{\partial \eta}{\partial t} \Big|_{x_s} + (S_{fs} - S_{os}) \dot{x}_s \right] = \frac{I_\varrho Q_s \Big|_{x_s}}{B_a (1 - \lambda_p)} \quad (7)$$

The migration of the bottom of the foreset, point  $b$  in Figure 3, is determined using the relation between  $\eta_b$  and  $\eta_s$ :

$$\eta_b = \eta_{bs} \Big|_{x_b} = \eta_s - S_{fs} (x_b - x_s) \quad (8)$$

Taking the time derivative and assuming the delta is prograding over a fixed bottom slope ( $\frac{\partial \eta_{bs}}{\partial t} = 0$ ) of constant slope yields:

$$-S_{bs} \dot{x}_b = \frac{\partial \eta}{\partial t} \Big|_{x_s} - S_{os} \dot{x}_s - S_{fs} (\dot{x}_b - \dot{x}_s) \quad (9)$$

where  $S_{bs}$  is the bottom slope and  $\dot{x}_b = \frac{\partial x_b}{\partial t}$  is the migration rate of the bottom of the foreset. Equations (7) and (9) provide the additional relations necessary for tracking the two moving boundaries associated with the delta face.

### **Moving boundary formulation**

The solution of the set of equations (1), (2), (3), (7) and (9) requires tracking two moving boundaries. This can be accomplished either by using a fixed grid and tracking the boundaries on this grid or by using a deforming grid which changes with the moving boundaries. Here the latter approach is used. To this end, the following coordinate transformation is applied (Landau 1950):

$$\hat{t} = t \quad \text{and} \quad \hat{x} = \frac{x}{x_s} \quad (10)$$

Using the chain rule and recalling that  $x_s = x_s(t)$  yields:

$$\frac{\partial}{\partial x} = \frac{1}{x_s} \frac{\partial}{\partial \hat{x}} \quad \text{and} \quad \frac{\partial}{\partial t} = \frac{\partial}{\partial \hat{t}} - \hat{x} \frac{\dot{x}_s}{x_s} \frac{\partial}{\partial \hat{x}} \quad (11)$$

Applying the transformation to (1), (2), and (3) results in the following:

$$\frac{1}{x_s} \frac{\partial}{\partial \hat{x}} \left[ \frac{1}{2} \frac{Q^2}{B^2 H^2} + gH + g\eta \right] + gS_f = 0 \quad (12)$$

$$B_a (1 - \lambda_p) \left[ \sigma + \frac{\partial \eta}{\partial \hat{t}} - \hat{x} \frac{\dot{x}_s}{x_s} \frac{\partial \eta}{\partial \hat{x}} \right] = - \frac{I_Q}{x_s} \frac{\partial Q_s}{\partial x} \quad (13)$$

$$B_a (1 - \lambda_p) \left[ \frac{\partial(L_a F_{bk})}{\partial \hat{t}} - \hat{x} \frac{\dot{x}_s}{x_s} \frac{\partial(L_a F_{bk})}{\partial \hat{x}} \right] = - \frac{I_Q}{x_s} \frac{\partial Q_{sk}}{\partial x} + F_{tk} \left[ \frac{I_Q}{x_s} \frac{\partial Q_s}{\partial x} + B_a (1 - \lambda_p) \left\{ \frac{\partial L_a}{\partial \hat{t}} - \hat{x} \frac{\dot{x}_s}{x_s} \frac{\partial L_a}{\partial \hat{x}} \right\} \right] \quad (14)$$

The equations for the moving boundary migration rates, (7) and (9), transform to:

$$\dot{x}_s = \frac{1}{S_{fs}} \left[ \frac{1}{x_b - x_s} \frac{I_Q Q_s \Big|_{\hat{x}=1}}{B_a (1 - \lambda_p)} - (x_b - x_s) \sigma - \frac{\partial \eta}{\partial \hat{t}} \Big|_{\hat{x}=1} \right] \quad (15)$$

$$\dot{x}_b = \frac{S_{fs} \dot{x}_s + \frac{\partial \eta}{\partial \hat{t}} \Big|_{\hat{x}=1}}{S_{fs} - S_{bs}} \quad (16)$$

The equation set (12)-(16) comprise the essential formulation of the model, which may be solved numerically for the five unknowns:  $H$ ,  $\eta$ ,  $F_{bk}$ ,  $\dot{x}_s$ , and  $\dot{x}_b$ . For a grid of  $N$  computational points and  $K$  grain-size intervals, there are  $2+(N-1)(2+K)$  equations and  $2+N(2+K)$  unknowns. Therefore  $2+K$  boundary conditions are required to close the system. The boundary conditions are the depth at the downstream end of the reach ( $H|_{\hat{x}=1}$ ), the incoming grain-size specific sediment load at the upstream end of the reach ( $Q_{tk}|_{\hat{x}=0}$ ), and the condition  $\sum_k F_{bk}|_{\hat{x}=0} = I$  (Rahuel et al. 1989). The depth at the

downstream end of the reach is in turn specified in terms of the difference between the specified elevation  $\xi$  of standing water into which the river flows (and which may change in time) and the bed elevation at the downstream end of the reach ( $\eta|_{\hat{x}=l}$ ); i.e.

$$H|_{\hat{x}=l} = \xi - \eta|_{\hat{x}=l} \quad (17)$$

Initial conditions include the initial bed elevation  $\eta(x, t=0)$ , depth  $H(x, t=0)$ , and active layer grain-size distribution  $F_{bk}(x, t=0)$ .

### Numerical solution scheme

The system of equations is discretized using four-point finite differences, typically referred to as a generalized Preissmann scheme (Lyn and Goodwin, 1987):

$$f \cong \theta[\phi f_{i+1}^{n+1} + (1-\phi)f_i^{n+1}] + (1-\theta)[\phi f_{i+1}^n + (1-\phi)f_i^n] \quad (18)$$

$$\frac{\partial f}{\partial t} \cong \frac{1}{\Delta t} [\phi(f_{i+1}^{n+1} - f_{i+1}^n) + (1-\phi)(f_i^{n+1} - f_i^n)] \quad (19)$$

$$\frac{\partial f}{\partial x} \cong \frac{1}{\Delta x} [\theta(f_{i+1}^{n+1} - f_i^{n+1}) + (1-\theta)(f_{i+1}^n - f_i^n)] \quad (20)$$

where  $f$  is any unknown,  $i$  and  $n$  denote space and time level,  $\Delta x$  and  $\Delta t$  denote space and time step, and  $\phi$  and  $\theta$  are the space and time weighting factors which range between zero and one. For the conventional choice space centering  $\phi=0.5$ , the scheme is subject to the Courant stability constraint of  $\theta \geq 0.5$  (Lyn and Goodwin, 1987). Lyn (1987) showed the potential for stability problems for this choice of weighting factors (for unsteady flow, uniform sediment). However, for the conditions studied here, the choice of  $\phi=0.5$  and  $\theta=0.55$  did not lead to stability problems. The implicit scheme and fully coupled solution allows for the use of large time steps, which are essential for simulating the long periods of interest here.

Applying (18)-(20) to (12)-(16) results in a set of  $2+N(2+K)$  non-linear algebraic equations. The system is solved using a standard Newton iteration (e.g. Atkinson 1989). Because of the inclusion of the delta moving boundaries, the linearized set of equations is not block-diagonal and a double sweep algorithm cannot be used. Efficient Gaussian elimination is accomplished using the FORTRAN IMSL routine DLSLRG.

### **Flow intermittency factor**

The flow intermittency factor,  $I_Q$  in (2) and (3), provides a simple method for condensing simulation time, allowing for the use of a constant flow and large time step. It is desired here to simulate profile development over thousands of years, which makes modeling individual flood events (for example with a daily time step) impractical. The model reach parameters (detailed in the companion paper) are designed around bankfull conditions, thus the intermittency factor should correspond approximately to the bankfull flow. The goal here is to use the intermittency factor to supply the correct amount of sediment to the reach while using a constant flow. It is thus defined as the fraction of time required for a given constant flow to transport the same amount of sediment as the actual hydrograph, for example on an annual basis.

Data from several sand-bed rivers (Toffaletti 1968) were used to compute  $I_Q$ : the Atchafalaya River at Simmesport, LA, the Mississippi River at St. Louis, MO, and Tarbert Landing, LA, and the Red River at Alexandria, LA. For each location, the flow-duration curve (from USGS daily flows) and the sediment rating curve (power-law relationship between flow and suspended bed-material sediment discharge) were determined. From these, the amount of sediment transported annually by each flow increment was computed and summed for the annual load (i.e. integration of flow-

duration and rating curves). Wolman and Miller (1952) showed that moderately high flows, such as the flood occurring once every year or two, tend to transport the most sediment over the long-term because the highest flows occur too infrequently. This tendency was also apparent in the data analyzed here. An example of this is shown in Figure 4, which plots the amount of sediment transported annually by each flow increment for the Mississippi River at Tarbert Landing.

For each location, the flow which transports the most sediment annually (i.e. the peak in Figure 4) was selected and the amount of time required for this flow to transport the annual load was determined. This fraction represents the intermittency factor. The flow which transports the most sediment was chosen because it provides the smallest  $I_Q$ , i.e. the most reduction in simulation time, and it is expected to correspond approximately to the bankfull flow. This was confirmed by computing the 2-year flow, which has been shown to be approximately bankfull for many rivers (Leopold and Maddock 1953), for the locations with enough peak flow data, using standard methods (Beard 1962). The results of the analysis are summarized in Table 1, where  $Q_{max}$  is the flow that transports the most sediment and  $Q_2$  is the two-year flow. The results range from  $I_Q=0.27 - 0.35$ , indicating that a constant  $Q_{max}$  would transport the annual load in about one-third of a year on average. For all simulations presented in the companion paper,  $I_Q=0.3$  was used.

## CONCLUSIONS

A model formulation has been presented for the simulation of the development of the longitudinal profile and downstream fining in sand-bed rivers. The companion paper, Wright and Parker (submitted) presents several applications of the model. The model

uses a backwater formulation for the hydraulics, mass conservation of bed sediment on a grain-size specific basis, a moving boundary formulation for tracking the development of a delta prograding into standing water, and a four-point implicit finite difference numerical scheme for solution.

Several assumptions are made which limit model applicability to the past 5,000 years of relatively stable sea-level. According to the model of Holocene river development promoted by Blum and Tornqvist (2000) and Aslan and Autin (1999), based on data from the Rhine-Meuse, Texas Gulf Coast, and Lower Mississippi Valley, rapid sea-level rise ( $\sim 10$  mm/yr) from about 20 kry B.P. to 5 kyr B.P. may have been accompanied by a rapidly aggrading floodplain with multi-channel streams, frequent avulsion, crevasse splays, and poorly drained backswamps. The past 5,000 years of little or no sea-level rise ( $\sim 1$  mm/yr) had slower rates of floodplain aggradation, leading to meander-belt development and overbank deposition. The model formulation is applicable to the period of slower aggradation during the past 5,000 years only, for several reasons. First, flow is assumed in a single channel with no floodplain, which leads to the implicit assumption that overbank floodplain deposition keeps pace with channel aggradation. The single channel assumption is not valid for the period of multi-channel flows. The overbank deposition assumption is not valid for the conditions of rapid sea-level rise when the floodplain was being built by channel avulsion, crevasse splays, and the filling of poorly-drained floodplain lakes. Also, discharge and sediment load conditions during glacial melting likely differed significantly from loads during stable sea-level. Finally, the closure relationships for hydraulic resistance and sediment transport capacity were developed empirically from data for modern, single-thread,

meandering, sand-bed rivers. Thus these relationships may not be applicable to the avulsing, multi-channel streams of the period of rapid sea-level rise.

This material is based on work supported by the National Science Foundation under Agreement Number CTS-0096916, "Mechanics of downstream fining in long reaches of large, low-slope sand-bed rivers." In addition, this work was also supported in part by the STC program of the National Science Foundation under Agreement Number EAR-0120914. This paper is a publication of the National Center for Earth-surface Dynamics.

## REFERENCES

- Ashida, K., and Michiue, M., 1972. "Study on hydraulic resistance and bedload transport rate in alluvial streams" *Transactions, Japan Society of Civil Engineering* 206, 59-69.
- Atkinson, K.E., 1989. *An Introduction to Numerical Analysis*, John Wiley and Sons, New York.
- Beard, L.C., 1962. *Statistical Methods in Hydrology*, U.S. Army Engineer District, Corps of Engineers, Sacramento, California.
- Cui, Y., Parker, G., and Paola, C., 1996. "Numerical simulation of aggradation and downstream fining" *Journal of Hydraulic Research* 34(2), 185-204.
- Cui, Y. and Parker, G., 1998. "The arrested gravel front: stable gravel-sand transitions in rivers. Part 2: General numerical solutions" *Journal of Hydraulic Research*, 36(2), 159-182.

- Deigaard, R., 1980. "Longitudinal and transverse sorting of grain sizes in alluvial rivers"  
Paper No. 26, Institute of Hydrodynamics and Hydraulic Engineering, Technical  
University of Denmark.
- Dietrich, W.E., Day, G. and Parker, G., 1999. "The Fly River, Papua New Guinea:  
inferences about river dynamics, floodplain sedimentation and fate of sediment"  
In *Varieties of Fluvial Form*, Miller, A.J. and Gupta, A., eds., John Wiley and  
Sons, New York, 345-376.
- Fisk, H.N., 1944. "Geological investigations of the alluvial valley of the lower  
Mississippi River" U.S. Army Corp of Engineers, Mississippi River  
Commission, Vicksburg, MS.
- Hoey, T.B., and Ferguson, R., 1994. "Numerical simulation of downstream fining by  
selective transport in gravel bed rivers: Model development and illustration"  
*Water Resources Research* 30(7), 2251-2260.
- Hoey, T.B., and Ferguson, R., 1997. "Controls of strength and rate of downstream fining  
above a river base level" *Water Resources Research* 33(11), 2601-2608.
- Julien, P.Y., and Klaasen, G.J., 1995. "Sand-dune geometry of large rivers during  
floods." *J. Hydraulic Eng.*, 121(9), 657-663.
- Kostic, S., and Parker, G., 2003a. "Progradational sand-mud deltas in lakes and  
reservoirs. Part 1. Theory and numerical modeling" *Journal of Hydraulic  
Research* 41(2), 127-140.
- Kostic, S., and Parker, G., 2003b. "Progradational sand-mud deltas in lakes and  
reservoirs. Part 2. Experiment and numerical simulation" *Journal of Hydraulic  
Research* 41(2), 141-152.

- Landau, H.G., 1950. "Heat conduction in a melting solid" *Quarterly of Applied Mathematics* 8, 81-94.
- Leopold, L.B. and Maddock, T. 1953. "The hydraulic geometry of stream channels and some physiographic implications" *U.S. Geological Survey Professional Paper* 252.
- Lyn, D.A., 1987. "Unsteady sediment-transport modeling" *Journal of Hydraulic Engineering* 113(1), 1-15.
- Lyn, D.A., and Goodwin, P., 1987. "Stability of a general Preissmann scheme" *Journal of Hydraulic Engineering* 113(1), 16-28.
- Paola, C., Heller, P.L., and Angevine, C.L., 1992. "The large-scale dynamics of grain-size variation in alluvial basins, 1: Theory" *Basin Research* 4, 73-90.
- Parker, G., and Sutherland, A.J., 1990. "Fluvial armor" *Journal of Hydraulic Research* 28(5), 529-544.
- Parker, G., 1991a. "Selective sorting and abrasion of river gravel. I: Theory" *Journal of Hydraulic Engineering* 117(2), 131-149.
- Parker, G., 1991b. "Selective sorting and abrasion of river gravel. II: Applications" *Journal of Hydraulic Engineering* 117(2), 150-171.
- Parker, G. and Cui, Y., 1998. "The arrested gravel front: stable gravel-sand transitions in rivers. Part 1: Simplified analytical solutions" *Journal of Hydraulic Research*, 36(1), 75-100.
- Pickup, G., Higgins, R.J., and Warner, R.F., 1979. "Impact of waste rock disposal from the proposed Ok Tedi mine on sedimentation processes in the Fly River and its

- tributaries, Papua New Guinea” *Report*, Department of Minerals and Energy and Office of Environment and Conservation, 138 pp.
- Pizzuto, J.E., 1995. “Downstream fining in a network of gravel-bedded rivers” *Water Resources Research* 31(3), 753-759.
- Rahuel, J.L., Holly, F.M., Chollet, J.P., Belleudy, P.J., and Yang, G., 1989. “Modeling of riverbed evolution for bedload sediment mixtures” *Journal of Hydraulic Engineering* 115(11), 1521-1542.
- Rana, S.A., Simons, D.B., and Mahmood, K., 1973. “Analysis of sediment sorting in alluvial channels” *ASCE Journal of the Hydraulics Division* 99(HY11), 1967-1980.
- Raudkivi, A.J., 1976. “Loose Boundary Hydraulics” Oxford, Pergamom Press, 397 p.
- Robinson, R.A.J., and Slingerland, R.L., 1998. “Origin of fluvial grain-size trends in a foreland basin: the Pocono formation on the Central Appalachian Basin” *Journal of Sedimentary Research* 68(3), 473-486.
- Sinha, S.K., and Parker, G., 1996. “Causes of concavity in longitudinal profiles of rivers” *Water Resources Research* 32(5), 1417-1428.
- Swenson, J.B., Voller, V.R., Paola, C., Parker, G., and Marr, J., 2000. “Fluvio-deltaic sedimentation: A generalized Stefan problem” *European Journal of Applied Math.* 11, 433-452.
- Toffaletti, F.B. (1968). “A procedure for computation of the total river sand discharge and detailed distribution, bed to surface.” *Technical Report No. 5*, Committee on Channel Stabilization, Corps of Engineers.

- Toro-Escobar, C.M., Parker, G., and Paola, C., 1996. "Transfer function for the deposition of poorly sorted gravel in response to streambed aggradation" *Journal of Hydraulic Research* 34(1), 35-53.
- USCOE, 1935. "Studies of river bed materials and their movement, with special reference to the lower Mississippi River" Paper 17 of the U.S. Waterways Experiment Station, Vicksburg, MS.
- van Niekerk, A., Vogel, K.R., Slingerland, R.L., and Bridge, J.S., 1992. "Routing of heterogeneous sediments over movable bed: model development" *Journal of Hydraulic Engineering* 118(2), 246-259.
- Wolman, M.G., and Miller, J.P., 1960. "Magnitude and frequency of forces in geomorphic processes" *Journal of Geology* 68(1), 54-74.
- Wright, S.A., and Parker, G., in press (a). "Density stratification effects in sand-bed rivers" *Journal of Hydraulic Engineering*.
- Wright, S.A., and Parker, G., in press (b). "Resistance and suspended load in sand-bed rivers: simplified stratification model" *Journal of Hydraulic Engineering*.
- Wright, S.A., and Parker, G., submitted. "Modeling downstream fining in sand-bed rivers II: application" *Journal of Hydraulic Research*.

## NOTATION

- $B$  channel width [L]
- $B_a$  active width [L]
- $c$  partitioning coefficient for active layer-substrate interface grain-size distribution
- $D_{50}$  median diameter of bed sediment [L]

$F_{bk}$	fraction of bed sediment within grain-size interval $k$
$F_{Ik}$	fraction of sediment at active layer-substrate interface within grain-size interval $k$
$g$	gravitational acceleration [ $L T^{-2}$ ]
$H$	water depth [L]
$i$	space level in numerical scheme
$I_Q$	flow intermittency factor
$K$	number of grain-size intervals
$L_a$	active layer thickness [L]
$n$	time level in numerical scheme
$N$	number of computational points
$Q$	water discharge [ $L^3 T^{-1}$ ]
$Q_s$	total sediment transport rate [ $L^3 T^{-1}$ ]
$Q_{sk}$	sediment transport rate of grain-size interval $k$ [ $L^3 T^{-1}$ ]
$S_f$	friction slope [ $L L^{-1}$ ]
$S_o$	river bed slope [ $L L^{-1}$ ]
$S_{fs}$	foreset slope [ $L L^{-1}$ ]
$S_{os}$	river bed slope at the top of the foreset, point $x_s$ [ $L L^{-1}$ ]
$S_{bs}$	bottom slope [ $L L^{-1}$ ]
$t$	time [T]
$\hat{t}$	time in moving boundary coordinates [T]
$U$	mean velocity [ $L T^{-1}$ ]
$x$	streamwise space coordinate [L]
$\hat{x}$	space in moving boundary coordinates

$x_s$	location of the upstream boundary of the foreset [L]
$x_b$	location of the downstream boundary of the foreset [L]
$\dot{x}_s$	migration rate of the top of the foreset, point $x_s$ [L T <sup>-1</sup> ]
$\dot{x}_b$	migration rate of the bottom of the foreset, point $x_b$ [L T <sup>-1</sup> ]
$\Delta x$	space step [L]
$\Delta t$	time step [T]
$\phi$	space weighting factor for numerical scheme
$\eta$	bed elevation [L]
$\eta_{fs}$	bed elevation within the foreset [L]
$\eta_s$	bed elevation at the top of the foreset, point $x_s$ [L]
$\eta_b$	bed elevation at the bottom of the foreset, point $x_b$ [L]
$\eta_{bs}$	bed elevation within the bottom slope [L]
$\lambda_p$	bed sediment porosity
$\theta$	time weighting factor for numerical scheme
$\sigma$	tectonic subsidence or uplift rate [L T <sup>-1</sup> ]
$\xi$	elevation of standing water into which the river flows [L]

## TABLES

Table 1 Information used for computing the flow intermittency factor. In the rating curves,  $Q_s$  is in  $mg/s$ ,  $Q$  in  $m^3/s$ .  $Mmt$  is million metric tons.

<i>Location</i>	<i>Rating curve</i>	$Q_{max}$ ( $m^3/s$ )	$Q_s$ annual ( $Mmt$ )	$I_Q$	$Q_2$ ( $m^3/s$ )
Atchafalaya River at Simmesport, LA	$Q_s = 0.57Q^{2.39}$ $R^2=0.93$	11,700	33.6	0.35	10,900
Mississippi River at St. Louis, MO	$Q_s = 1.69Q^{2.23}$ $R^2=0.81$	11,600	18.5	0.30	14,600
Mississippi River at Tarbert Landing, MS	$Q_s = 0.044Q^{2.48}$ $R^2=0.86$	25,600	40.6	0.34	N/A
Red River at Alexandria, LA	$Q_s = 26.9Q^{2.31}$ $R^2=0.90$	2,500	15.8	0.26	2,800

## **FIGURES**

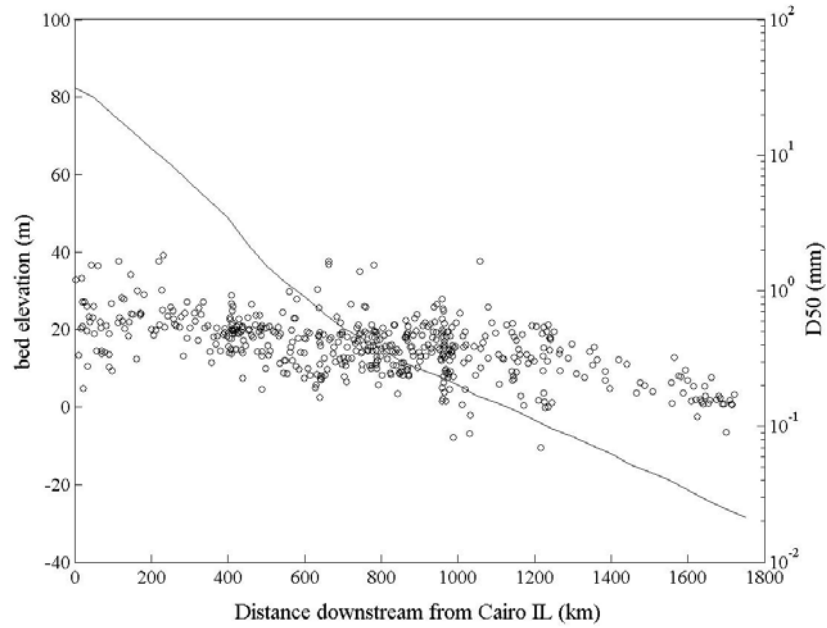


Figure 1 Bed elevation (line) and median bed sediment diameter (circles) for the Lower Mississippi River, illustrating an upward concave longitudinal profile and downstream fining.

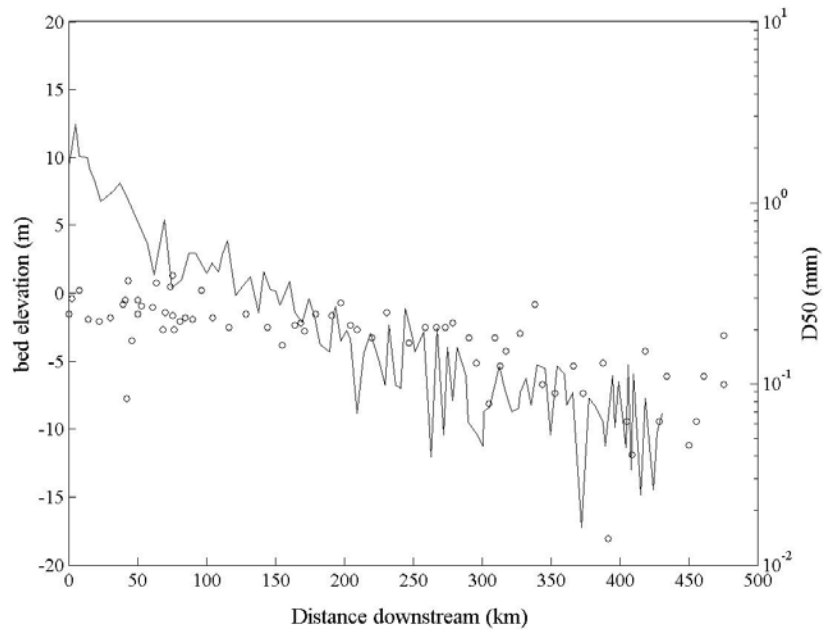


Figure 2 Bed elevation (line) and median bed sediment diameter (circles) for the Fly River in Papua New Guinea.

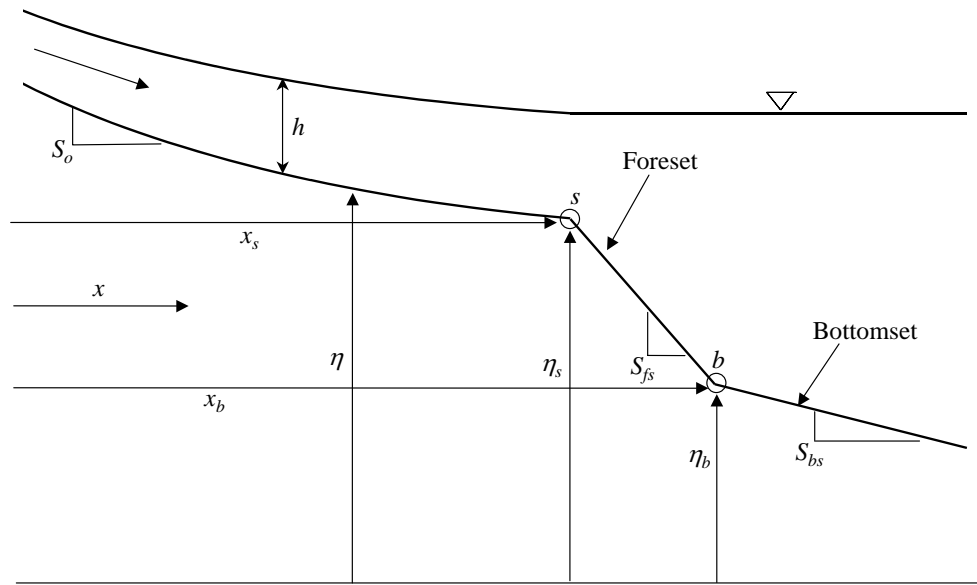


Figure 3 Definition sketch for model with prograding delta at downstream boundary.

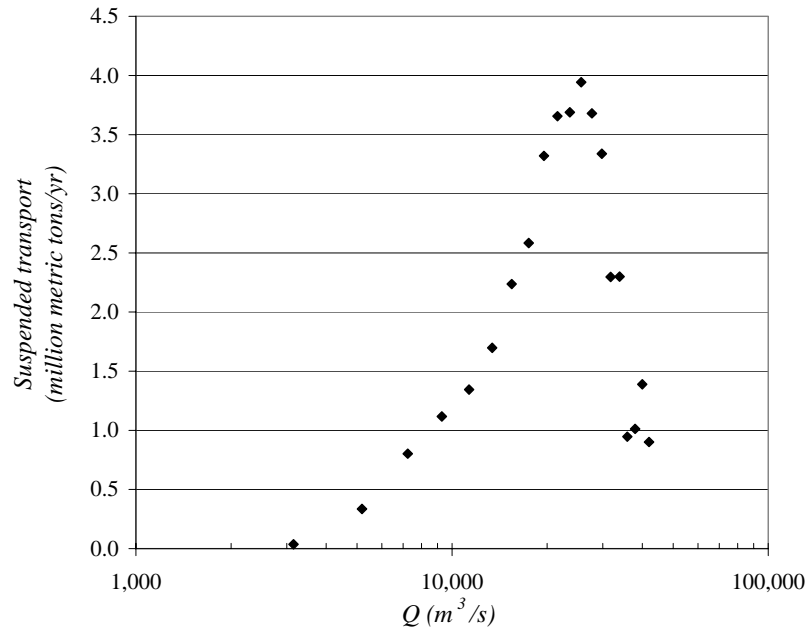


Figure 4 Annual suspended bed-material load versus flow for the Mississippi River at Tarbert Landing, MS.

**CHAPTER 4: MODELING DOWNSTREAM FINING IN SAND-BED  
RIVERS II: APPLICATION**

Scott Wright and Gary Parker

## **ABSTRACT**

In this paper the model presented in the companion paper, Wright and Parker (submitted) is applied to a generic river reach typical of a large, sand-bed river flowing into the ocean in order to investigate the mechanisms controlling longitudinal profile development and downstream fining. Three mechanisms which drive downstream fining are studied: a delta prograding into standing water, sea-level rise, and tectonic subsidence. Various rates of sea-level rise (typical of the late Holocene) and tectonic subsidence are modeled in order to quantify their effects on the degree of profile concavity and downstream fining. Also, several other physical mechanisms which may affect fining are studied, including the relative importance of the suspended versus bed load, the effect of the loss of sediment overbank, and the influence of the delta bottom slope. Finally, sensitivity analysis is used to show that the grain-size distribution at the interface between the active layer and substrate has a significant effect on downstream fining.

## **INTRODUCTION**

In the companion paper (Wright and Parker, submitted), a formulation was presented for modeling the development of the longitudinal profile and downstream variation in bed sediment characteristics of large, low-slope sand-bed rivers. Many rivers exhibit a downstream decrease in bed slope and bed sediment median grain-diameter in the downstream direction, as illustrated in Figures 1 and 2 of the companion paper (Wright and Parker, submitted). In this paper, the model is applied to conditions typical of sand-bed rivers flowing into the ocean in order to study the mechanisms driving the

phenomena, and the processes controlling the strength of downstream fining and profile concavity.

The model formulation contains several assumptions which may limit its applicability to the past 5,000 years of relatively stable sea-level. According to the model of Holocene river development promoted by Blum and Tornqvist (2000) and Aslan and Autin (1999), based on data from the Rhine-Meuse, Texas Gulf Coast, and Lower Mississippi Valley, rapid sea-level rise (~10 mm/yr) from about 20 kry B.P. to 5 kyr B.P. was accompanied by a rapidly aggrading floodplain with multi-channel streams, frequent avulsion, crevasse splays, and poorly drained backswamps. The past 5,000 years of little or no sea-level rise (~1 mm/yr) lead to slower rates of floodplain aggradation, meander-belt development and overbank deposition. The model formulation is applicable to the period of slower aggradation of the past 5,000 years only for several reasons. First, flow is assumed in a single channel with no floodplain, which leads to the implicit assumption that overbank floodplain deposition keeps pace with channel aggradation. The single channel assumption is not directly valid for the period of multi-channel flows. The overbank deposition assumption is not valid for the conditions of rapid sea-level rise when the floodplain was being built by channel avulsion, crevasse splays, and the filling of poorly-drained floodplain lakes. Also, discharge and sediment load conditions during glacial melting likely differed significantly from loads during stable sea-level in such rivers as the Mississippi. Finally, the closure relationships for hydraulic resistance and sediment transport capacity were developed empirically from data for modern, single-thread, meandering, sand-bed rivers. Thus these relationships may not be applicable to the avulsing, multi-channel streams of the period of rapid sea-level rise.

The strategy for model simulation is to study the mechanisms controlling the development of the longitudinal profile and downstream fining in a generalized manner. Thus, the model was applied to a generic river reach with conditions typical of large, suspension-dominated sand-bed rivers flowing to the ocean. The generic river reach was subjected to several forcing mechanisms that drive fining, including a prograding delta, sea-level rise, and subsidence. Each mechanism drives aggradation accompanied by size selective transport which leads to a concave upward profile and downstream fining. For these simulations, all other model parameters were held constant. Though the objective of the modeling was not to simulate any particular river, the results of several of the simulations are compared to the cases of the Mississippi River, USA and the Fly River, Papua New Guinea in terms of dimensionless reach-averaged profile concavity and downstream fining.

The second phase of simulations is designed to study the effects of various physical processes, for a single driving mechanism case. For these simulations, the case of a sea-level rise rate of 1 mm/yr was chosen. The physical processes investigated include the relative importance of bedload versus suspended load sorting, the effect of the active width, the importance of the loss of sediment to overbank deposition, and the effect of density stratification. Finally, a subsequent section investigates the sensitivity of the model to two specified model parameters.

## MODEL PRELIMINARIES

### Generic study reach

The objective of the model applications is to explore the development of downstream fining in large, low-slope, sand-bed rivers in response to various forcing mechanisms. Therefore a reach of river with parameters typical of large sand-bed rivers flowing into the ocean was constructed for application of the model. The reach is based loosely on several datasets on sand-bed rivers and hydraulic geometry relations (ASCE, in press).

The study reach has a bankfull discharge of  $10,000 \text{ m}^3/\text{s}$ , and bankfull channel width equal to  $500 \text{ m}$ . The initial bed slope is constant and equal to  $8 \times 10^{-5}$ , and the total initial reach length is  $500 \text{ km}$ . There are no tributaries entering the reach, so that the discharge and width are constant. The initial bed elevations are set so that a water surface elevation of zero at the downstream end corresponds to uniform flow. The initial bed and water surface profiles are shown in Figure 1, where the flow is uniform with a constant depth of  $12.3 \text{ m}$ . The bed sediment (active layer) grain-size distribution is initially constant over the reach and log-normally distributed with median diameter of  $0.4 \text{ mm}$ , and geometric standard deviation equal to  $1.7$ . For all model runs the incoming sediment load and grain size distribution are constant in time and equal to those associated with the initial transport capacity at the upstream end. The size distributions of the initial bed material and incoming sediment load are shown in Figure 2. The total concentration of the incoming bed material load is  $131 \text{ mg/L}$ .

The model accounts only for conservation of bed material load, and ascribes no role for wash load except for the implicit assumption that floodplain construction can

keep pace with channel bed aggradation. While the cutoff size between bed material load and wash load is known to be a dynamic variable (e.g. Paola and Parker, 2000), for simplicity a cutoff size of  $0.0625\text{ mm}$  is used here (e.g. Raudkivi, 1976). With this in mind, the bed material load in the present model consists entirely of sand.

The slope of the delta face (foreset) was set to  $5^\circ$  which is within the range of typical foreset slopes for a sand delta (Borland, 1971; Kostic et al., 2002). The bottom slope was given a value of  $0.1^\circ$ , i.e. a value that is reasonably typical of the continental shelf on passive margins such as the Atlantic margin of the USA, the margin of the northern Gulf of Mexico and that of the Gulf of Papua, (e.g. Harris, 1994; O'Grady, 2001).

For all of the simulations performed, the reach was broken into 21 computational points, the grain-size distribution was discretized into 50 size intervals, and a time step of 100 years was used. This large time step was made possible by the use of the flow intermittency factor and the fully coupled, implicit numerical scheme.

### **Active width**

The active width has been introduced to account for the fact that the river may aggrade over a width greater than just the channel width, such as the meander-belt width. Lateral migration dictates that the channel will move back and forth across the meander-belt width, resulting in aggradation over this entire width over the long time periods considered here. The active width provides a simple method for accounting for this process. The model does not account for rapid aggradation and avulsion, a process that may result in aggradation over the entire floodplain width (if it is greater than a single meander-belt width) over long time periods. For the majority of the simulations

presented, the active width has been set to ten times the channel width, which may correspond roughly to a meander belt width for most rivers. Also, simulations were performed for a range of active widths, from one channel width to twenty channel widths, to study the effects on downstream fining.

In point of fact, most of the sediment depositing within the meander belt or floodplain can be expected to be in the range that is here considered to be wash load, i.e. material finer than  $0.0625\text{ mm}$ . A detailed accounting of wash load routing and floodplain formation is beyond the scope of the present analysis. Implicit in the present analysis is the assumption that the rate of aggradation of the channel bed is sufficiently slow so that floodplain construction can keep up with it without major planform instabilities.

## **RESULTS I: DRIVING MECHANISMS**

### **Prograding delta**

The first mechanism to be studied which drives downstream fining is the delta prograding into standing water. The prograding delta sets up a backwater profile which induces aggradation and leads to a concave upward profile, size selective transport, and downstream fining. For this simulation, sea-level rise and subsidence are both zero. The results are presented in Figures 3, 4, and 5, which show the longitudinal profile, downstream variation in median bed sediment ( $D_{50}$ ), and bed slope ( $S_o$ ), respectively, at times 500, 2000 and 5000 years. The downstream fining develops in the first 3000 years or so and persists for the remainder of the simulation (10,000 years total). Figure 4 indicates that after 5,000 years of simulation time, the  $D_{50}$  of the bed decreases from 0.40

mm at the upstream end to 0.32 mm at the downstream boundary. This fining is accompanied by a decrease in bed slope (i.e. an upward concave profile) from  $8.2 \times 10^{-5}$  at the upstream end to  $6.4 \times 10^{-5}$  at the downstream boundary.

### **Sea-level rise**

Another mechanism which leads to aggradation and downstream fining is sea-level rise. Sea-level rise was modeled by increasing the downstream water surface elevation  $\xi$  of standing water into which the river flows. It was desired to approximate eustatic sea-level rise rates typical of the gradual rates of the past 5,000 years. The model here is designed to simulate slow aggradation and a single-thread meandering profile, conditions more typical of the late Holocene. Thus a range of sea-level rise rates up to a maximum of 2 mm/yr (e.g. Bard et al. 1990, Milne et al. 2002, Aslan and Autin 1999) were simulated for a 5,000 year time period.

The results of the sea-level rise simulations are presented in Figures 6, 7, and 8. The figures show the results after 5,000 years for the longitudinal profile and downstream variation in  $D_{50}$  and  $S_o$ , respectively, for several rates of sea-level rise. Note that the case of zero sea-level rise corresponds to the case of delta progradation only presented in the previous section. As expected, the degree of profile concavity and downstream fining increase with increasing sea-level rise. For example, for the 2 mm/yr case  $D_{50}$  decreases from 0.40 mm upstream to 0.19 mm at the downstream boundary, while for the 0.5 mm/yr case  $D_{50}$  is reduced to 0.28 mm at the downstream boundary. Similarly, for the 2 mm/yr case  $S_o$  decreases from  $8.4 \times 10^{-5}$  upstream to  $3.7 \times 10^{-5}$  at the downstream boundary, while for the 0.5 mm/yr case  $S_o$  is reduced from  $8.2 \times 10^{-5}$  upstream to  $5.8 \times 10^{-5}$  at the downstream boundary.

## Tectonic subsidence

Tectonic subsidence has a similar effect as sea-level rise by creating space for aggradation, so that selective transport leads to downstream fining. A range of subsidence rates were simulated up to a maximum of 1 mm/yr (i.e. the same range as that used by Paola et al. 1992), again for a 5000 year time period. For all simulations, subsidence was assumed constant (piston-style subsidence) over the reach. The simulation results (longitudinal profile,  $D_{50}$ , and  $S_o$ ) are shown in Figures 9, 10, and 11. The results are quite similar to the sea-level rise results, in that the degree of concavity and downstream fining increase with increasing subsidence.

## Comparison with field cases

The simulation results presented thus far provide a general comparison of three driving mechanisms for conditions typical of large, sand-bed rivers. It is also desired to provide a rough comparison of the model results with field cases, to see if the model predictions are the same order of magnitude as the field cases. To this end, the following reach-averaged, dimensionless measures of profile concavity ( $PC$ ) and downstream fining ( $DF$ ) are defined:

$$PC = H \overline{\frac{d^2\eta}{dx^2}} \quad (1)$$

$$DF = -\overline{\frac{dD_{50}}{dx}} \quad (2)$$

where the overbar denotes averaging over the entire reach.

The profile concavity,  $PC$ , and downstream fining,  $DF$ , were computed for the simulation results presented in the previous sections and for the cases of the Mississippi

and Fly Rivers, whose profiles and fining are shown in Figures 1 and 2 of the companion paper, Wright and Parker (submitted). These results are presented in Figures 12 and 13, which indicate that the degree of concavity and downstream fining of the simulations are of the same order of magnitude as the Mississippi and Fly. This provides confidence that a model of this type could be applied successfully to a particular field case. This has not been pursued here for a variety of reasons. First, the primary goal here is to develop the model and test it for simple cases. Also, as will be shown in the sensitivity analysis, the model is quite sensitive to a parameter which is not presently well constrained. Finally, application to a particular field case requires data that may not be available for most rivers, such as the initial longitudinal profile (e.g. at the transition from braiding to meandering) and incoming sediment load throughout the Holocene.

## **RESULTS II: IMPORTANCE OF OTHER MECHANISMS**

### **Bed load versus suspended load**

Large, sand-bed rivers tend to transport the majority of their sediment load in suspension. However, both bed load and suspended load result in size selective transport and thus will contribute to downstream fining. For bed load, the Ashida and Michiue (1972) relation introduces size selective transport through a dependence of the critical shear stress on particle diameter. Suspended load results in size selective transport through the near-bed concentration predictor and, more importantly, because smaller sizes have lower settling velocities and thus are transported at a higher rate than their larger brethren once in suspension. This is illustrated in Figure 14, where the initial size distributions of the bed, suspended, and total bed material loads are shown (bed load

accounts for about 12% of total load). The bed load distribution is nearly identical to the initial bed material distribution (Figure 2) indicating that bed load sorting should be relatively weak. This is because the sorting effects come through the critical shear stress, which is much smaller than the total stress for bankfull conditions leading to near equal mobility conditions.

To illustrate how bed load and suspended load contribute to the overall amount of downstream fining, simulations were performed with and without bed load. The case of 1 mm/yr sea-level rise and an active width equal to ten channel widths was used. Figure 15 shows the  $D_{50}$  profiles at 5,000 years of simulation time. The results show that the bed load retards the fining that would develop due to suspended load sorting only. This is expected given the distributions of Figure 14. The bed load contributes a distribution roughly equivalent to the bed material, thus decreasing the overall size selectivity of the total load. The overall fining, as measured by (22), is approximately 10% greater with bed load excluded from the simulation.

### **Active width**

The active width is defined here as the width over which channel-driven aggradation takes place. It is included in recognition that aggradation may occur over a width greater than the channel width only as the river migrates over its floodplain (e.g. Howard, 1992). For a meandering river, channel-driven aggradation (i.e. aggradation driven by the sediment transport divergence based on channel hydraulics, as opposed to overbank floodplain deposition) may take place over the entire meander-belt width. As the channel migrates back and forth across the meander-belt and aggrades, the elevation of the entire width of the meander-belt is raised. The active width can also account for a

river occupying a multitude of positions through time. For example, the Mississippi River is known to have occupied five separate meander-belts during the Holocene (Aslan and Autin 1999). Thus the total amount of channel-driven aggradation would be distributed over the entire width of the five meander-belt widths.

For the simulation results presented thus far, the active width was set equal to ten channel widths. This may be considered a typical meander-belt width for a large, sand-bed river. The sensitivity of the results is investigated here by assigning the active width values of one, five, ten, and twenty channel widths. Again, the case of 1 mm/yr sea-level rise is used for illustration. The longitudinal profiles and downstream fining profiles for the four widths are shown in Figures 16 and 17, respectively. The figures illustrate the dramatic effect that the active width has on the results. For an active width equal to one channel width, the amount of aggradation is much greater and would almost certainly result in avulsion, which this model is not equipped to handle. Also for this case, the aggradation easily keeps pace with the sea-level rise, leading to less downstream decrease in slope and thus less downstream fining. The remaining simulations illustrate the increase in fining with increasing active width. This is because the greater width results in less aggradation, creating a stronger backwater effect as sea-level rises. The greater decrease in slope in the downstream direction with increasing active width accentuate size selective transport and result in greater downstream fining.

### **Overbank sediment loss**

Though the model in its current state treats channel processes only, a rough estimate of the effects of the loss of sediment overbank can be made. The sediment sizes lost overbank will be highly biased to the finer sizes, as these are the sizes that ride

highest in the water column. Thus overbank processes may be expected to decrease the overall downstream fining by removing these finer sizes. To make a very rough estimate of this effect without treating overbank processes in detail, a simulation was performed where it was assumed that all sediment in the upper ten percent of the flow depth was lost to the floodplain. Clearly this is not the case in reality, however, it is a conservative assumption that allows of an order of magnitude estimate of the effect of overbank sediment loss. The analysis is made possible by the use of the Wright and Parker (in press b) suspended sediment predictor, which treats the details of the vertical concentration profile using a modified Rouse formulation.

The size distributions of the bed-material sediment in the upper ten percent of the flow and over the entire flow depth are compared in Figure 18. This illustrates that the upper ten percent is dominated by finer sizes. In terms of transport rates, the upper ten percent accounts for only about three percent of the total transport. Simulations using 1 mm/yr sea-level rise and an active width equal to ten channel widths, with and without overbank loss, yielded very slight differences in downstream fining. Reach-averaged fining rates from (22) differed by only about one percent, indicating that the loss of sediment overbank is not a primary controlling process in downstream fining. However, this should be considered a first order estimate, given the simplicity of the method used in the evaluation. While the method does account for the loss of the finer sizes, it does not account for relative differences in this loss in the downstream direction, which may be the most important factor. For example, an attenuating floodwave may result in longer periods of overbank flow in downstream reaches and thus more sediment lost to the floodplain (Y. Cui, personal communication). More definitive results on the effect of

overbank processes await a model with a more complex treatment of channel-floodplain interaction.

### **Delta bottom slope**

For the model applications presented thus far the bottom slope,  $S_{bs}$  in Figure 3 of the companion paper, was set to  $0.1^\circ$ , a slope representative of the continental shelf. The bottom slope affects the progradation rate and shape of the delta. To investigate its effect on downstream fining, simulations were also performed with bottom slopes of  $1^\circ$  and  $0.03^\circ (5 \times 10^{-4})$ . The  $1^\circ$  slope is representative of a steeper shelf slope, while the  $0.03^\circ$  slope is meant to represent flow into an estuary or reservoir where the bottom slope would be mild. Again, the base case of 1 mm/year sea-level rise, no subsidence, and an active width of ten channel widths was used. The resulting longitudinal profiles and downstream fining are shown in Figures 19 and 20, respectively. As the bottom slope decreases, there is less space for deposition on the foreset delta face. Thus for the lower bottom slopes the delta progrades faster and the elevation of the topset-foreset break is lower in elevation. This results in a greater backwater effect, greater downstream decreases in slope (increased concavity) and sediment transport capacity, and greater downstream fining (Figure 20).

### **Density stratification**

The formulations used for hydraulic resistance and suspended-sediment transport rate include the effects of density stratification, which have been shown to be particularly important for large, low-slope, sand-bed rivers (Wright and Parker, in press a, b). The density gradient resulting from the vertical concentration gradient induces a buoyancy force which inhibits turbulent mixing. Wright and Parker (in press a) showed that the

reduction in turbulent mixing results in decreased sediment transport (less upward vertical flux of sediment) and decreased median size of the suspension (greatest effect is on largest sizes since they have largest concentration gradients), as opposed to the without stratification case.

To test the effects of density stratification on model predictions of downstream fining, a simulation was performed with the stratification effects removed from the hydraulic resistance and suspended-sediment transport relations. Again, the case of 1 mm/yr sea-level rise and an active width equal to ten channel widths was used. Without stratification, the uniform flow depth increases from 12.3 m to 14.7 m, the sediment transport capacity of the reach increases from 132 mg/L to 161 mg/L, and the median size of the transported sediment increases from 0.167 mm to 0.176 mm. These changes affect the initial and boundary conditions because the initial condition is uniform flow and the incoming sediment load is set to the capacity at the most upstream point. The resulting longitudinal profiles and downstream variations in bed  $D_{50}$  are shown in Figures 21 and 22. The increased incoming load results in increased aggradation and delta progradation, but the effects on downstream fining are not great. This is because density stratification has a greater effect on the total suspended-sediment transport rate than on the grain-size distribution of the suspension.

## **SENSITIVITY ANALYSIS**

The model formulation contains many empirical parameters which must be specified. The sediment transport and hydraulic resistance relations, for example, contain several parameters which were determined from field and laboratory data. It is not the

goal here to study these parameters, as they are better constrained by data than some other parameters. The two parameters chosen for study here are the two considered to be the least constrained by data or theory. They are the active layer thickness,  $L_a$ , and the relation for partitioning sediment at the interface between the active layer and the substrate during aggradation,  $F_{Ik}$ .

During aggradation, sediment is transferred from the active layer to the underlying substrate. The formulation presented in the companion paper partitions this sediment between the transported material ( $F_{tk}$ ) and the material in the active layer ( $F_{bk}$ ):

$$F_{Ik} = cF_{tk} + (1 - c)F_{bk} \quad (3)$$

The only experimental evaluation of the partitioning constant,  $c$ , is that of Toro-Escobar, et al. (1996), who found  $c=0.7$  for laboratory experiments of downstream fining of gravels. The weighting of the interface fraction toward the transported material was attributed to a sieving mechanism whereby finer material in transport moves directly through the active layer to the substrate. For sand beds, there are no experimental results to provide guidance. Here the choice of  $c=0$  was adopted for all model simulations because the sieving mechanism is expected to be greatly hindered in a sand-bed river versus a gravel bed because 1) the bed material grain-size distribution is more narrow and, 2) the active layer thickness is significantly larger (one dune height vs.  $D_{90}$ ). This choice dictates that during aggradation, only material from the active layer is transferred to the substrate.

To test the sensitivity of the model to this partitioning,  $c$  was varied between 0 and 0.7, i.e. the gravel case was considered a maximum value for  $c$ . The case of 1 mm/yr sea-level rise was again used as the base case. The results, in terms of the fining measure

defined in (2), are shown in Figure 23. In the figure,  $DF_o$  is the fining rate for the base case of  $c=0$ . The results indicate that the partitioning of sediment at the active layer/substrate interface can have a significant effect on the degree of downstream fining predicted by the model. The choice of  $c=0$ , which transfers active layer sediment only to the substrate during aggradation, results in the greatest downstream fining. The choice  $c=0.7$ , which has been found experimentally for gravels, yields approximately one-half the amount of downstream fining as compared to  $c=0$ . This type of sensitivity to a parameter that is not very well constrained by data makes application of the model to a particular field case difficult. Model results could most likely be made to match the field data simply by adjusting  $c$ . Thus there is a clear need for further experimental and theoretical research into bed sediment mixing mechanics, whether it be to better constrain a parameter such as  $c$  for sand-beds, or to support the probabilistic formulation for Exner recently presented by Parker et al. (2000). Recent progress in this area has been made by Blom (2003).

Several relations have been used by various authors for specifying the active layer thickness. Deigaard (1980) and Rahuel et al. (1989) assumed the thickness to be proportional to water depth, with a proportionality constant between 0.1 and 0.2, suggesting that the active layer has a thickness of about a dune height for sand-bed rivers. This line of reasoning has been followed here, where  $L_a$  was set equal to one dune height, with the height predicted by the Julien and Klaasen (1995) relation. The sensitivity of the model to the active layer thickness was tested by varying the thickness from one-half to twice the dune height. It was found that the model results are relatively insensitive to

active layer thickness. The degree of downstream fining was found to vary by less than 1% from the base case of  $L_a$  equal to one dune height.

## CONCLUSIONS

The companion paper, Wright and Parker (submitted) presented a numerical model for the simulation of the simultaneous development of the longitudinal profile and bed sediment distribution in sand-bed rivers. This paper presents results from application of the model to a generic model reach designed to be representative of large, low-slope, sand-bed rivers. The results of the model simulations lead to the following observations and conclusions:

- A delta prograding into standing water at the downstream boundary leads to the development of a backwater profile. The resulting aggradation leads to a downstream decrease in slope (upward concave longitudinal profile), and size selective transport results in downstream fining of bed sediment.
- Sea-level rise and tectonic subsidence create space for aggradation, leading to increased profile concavity and downstream fining. The degree of concavity and fining increase with increasing sea-level rise and subsidence.
- The degree of dimensionless, reach-averaged, profile concavity and downstream fining predicted by the model for the generic large, sand-bed river are of the same order of magnitude as the Mississippi and Fly Rivers, for sea-level rise and subsidence rates typical of the late Holocene.
- Size selective transport due to the suspended load dominates the sorting process compared to bed load.

- The width over which aggradation occurs, termed the active width here, has a significant effect on the model results. An active width of one channel width leads to rapid aggradation which would most likely lead to avulsion, which the model is not equipped to handle. Active widths typical of meander belt widths (i.e. about ten channel widths) lead to significantly less aggradation and greater downstream fining. This is because as active width increases, sea-level rise and/or subsidence outpaces aggradation leading to a greater backwater effect and selective transport.
- During overbank flows, the finest sizes in transport may be lost to floodplain deposition. A very crude analysis here indicates that this process has a minor effect on downstream fining. However, more definitive results on this effect await a more complex model of channel-floodplain interaction.
- The bottom slope of the prograding delta can have a significant effect on the profile concavity and downstream fining. As the bottom slope decreases, the degree of concavity and downstream fining increase.
- The model was shown to be quite sensitive to the size distribution of sediment transferred at the interface between the active layer and substrate as the bed aggrades. During aggradation, the sediment transferred to the substrate may be a mixture of the sediment in transport and the sediment in the active layer. This partitioning is not well constrained for sand transport. Further research into this process would significantly improve models of this type.

This material is based on work supported by the National Science Foundation under Agreement Number CTS-0096916, “Mechanics of downstream fining in long reaches of large, low-slope sand-bed rivers.” In addition, this work was also supported in

part by the STC program of the National Science Foundation under Agreement Number EAR-0120914. This paper is a publication of the National Center for Earth-surface Dynamics.

## REFERENCES

ASCE, in press. New Manual 54.

Ashida, K., and Michiue, M., 1972. "Study on hydraulic resistance and bedload transport rate in alluvial streams" *Transactions, Japan Society of Civil Engineering* 206, 59-69.

Aslan, A., and Autin, W.J., 1999. "Evolution of the Holocene Mississippi River floodplain, Ferriday, Louisiana: Insights on the origin of fine-grained floodplains" *Journal of Sedimentary Research* 69(4), 800-815.

Bard, E., Hamelin, B., and Fairbanks, R.G., 1990. "U-Th ages obtained by mass spectrometry in corals from Barbados: sea level during the past 130,000 years", *Nature* 346, 456-458.

Blom, A., 2003. "A vertical sorting model for rivers with non-uniform sediment and dunes", Ph.D. thesis, University of Twente, the Netherlands, 267 p.

Blum, M.D. and Tornqvist, T.E., 2000. "Fluvial responses to climate and sea-level change: a review and look forward", *Sedimentology* 47 (Suppl. 1), 2-48.

Borland, W.M., 1971. "Reservoir sedimentation" Chapter 25, *River Mechanics*, Shen, H.W., ed., H.W. Shen, Publisher., 29-1 – 29-24.

- Deigaard, R., 1980. "Longitudinal and transverse sorting of grain sizes in alluvial rivers"  
Paper No. 26, Institute of Hydrodynamics and Hydraulic Engineering, Technical  
University of Denmark.
- Harris, P. T., 1994. "Incised valleys and backstepping deltaic deposits in a foreland-basin  
setting, Torres Strait and Gulf of Papua, Australia" In SEPM Special Publication  
No. 51, *Incised-valley Systems: Origin and Sedimentary Sequences*, ISBN 1-  
56576-015-8, 99-107.
- Howard, A.D., 1992. "Modelling channel migration and floodplain development in  
meandering streams" in *Lowland Flood Plain Rivers*, Carling, P.A. and Petts,  
G.E., eds., 1-41.
- Julien, P.Y., and Klaasen, G.J., 1995. "Sand-dune geometry of large rivers during  
floods." *J. Hydraulic Eng.*, 121(9), 657-663.
- Kostic, S., Parker, G. and Marr, J. G., 2002. "Role of turbidity currents in setting the  
foreset slope of clinoforms prograding into standing fresh water" *J. Sedimentary  
Research*, 72(3), 353-362.
- Milne, G.A., Mitrovica, J.X., and Schrag, D.P., 2001. "Estimating past continental ice  
volume from sea-level data" *Quaternary Science Reviews* 21, 361-376.
- O'Grady, D.B., 2001. "Sedimentary geomorphology of siliciclastic continental slopes"  
Ph.D thesis, University of Colorado, 189 p.
- Paola, C. and Parker, G., 2000. "Criterion for cutoff size of bed material load versus  
wash load in sand bed streams" *Eos Trans. AGU*, 81 (48), Fall Meet. Suppl.,  
Abstract H11C-29.

- Parker, G., Paola, C., and Leclair, S., 2000. “Probabilistic Exner sediment continuity equation for mixtures with no active layer” *Journal of Hydraulic Engineering* 126(11), 818-826.
- Rahuel, J.L., Holly, F.M., Chollet, J.P., Belleudy, P.J., and Yang, G., 1989. “Modeling of riverbed evolution for bedload sediment mixtures” *Journal of Hydraulic Engineering* 115(11), 1521-1542.
- Raudkivi, A.J., 1976. “Loose Boundary Hydraulics” Oxford, Pergamom Press, 397 p.
- Toro-Escobar, C.M., Parker, G., and Paola, C., 1996. “Transfer function for the deposition of poorly sorted gravel in response to streambed aggradation” *Journal of Hydraulic Research* 34(1), 35-53.
- Wright, S.A, and Parker, G., submitted. “Modeling downstream fining in sand-bed rivers I: formulation” *Journal of Hydraulic Research*.

## NOTATION

$c$	partitioning coefficient for active layer-substrate interface grain-size distribution
$D_{50}$	median diameter of bed sediment [L]
$D_{90}$	diameter of which 90% of bed material is finer [L]
$DF$	dimensionless, reach-averaged measure of downstream fining
$DF_o$	dimensionless, reach-averaged measure of downstream fining for the case $c=0$
$F_{bk}$	fraction of bed sediment within grain-size interval $k$
$F_{lk}$	fraction of sediment at active layer-substrate interface within grain-size interval $k$
$F_{tk}$	fraction of grain-size interval $k$ in transport
$H$	water depth [L]

$L_a$	active layer thickness [L]
$PC$	dimensionless, reach-averaged measure of longitudinal profile concavity
$S_{bs}$	bottom slope [L/L]
$S_o$	river bed slope [L/L]
$x$	streamwise space coordinate [L]
$\eta$	bed elevation [L]
$\xi$	elevation of standing water into which the river flows [L].

## **FIGURES**

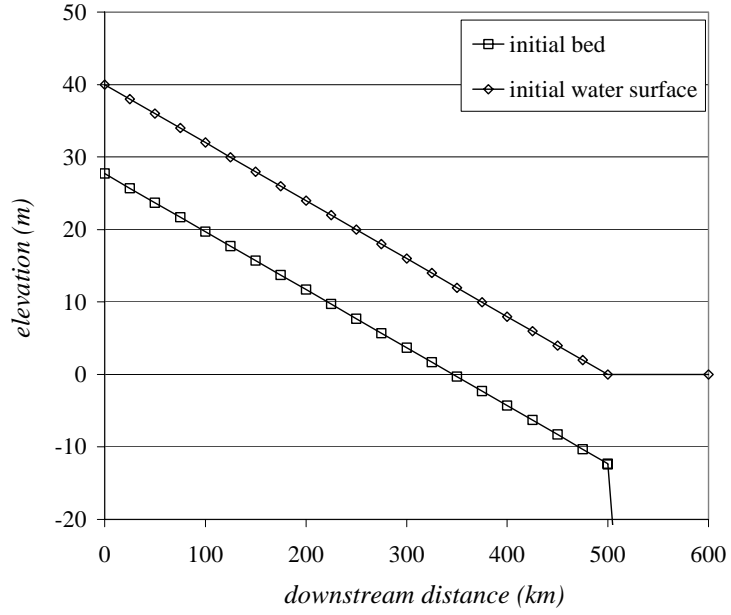


Figure 1 Initial bed and water surface elevation for all model runs.

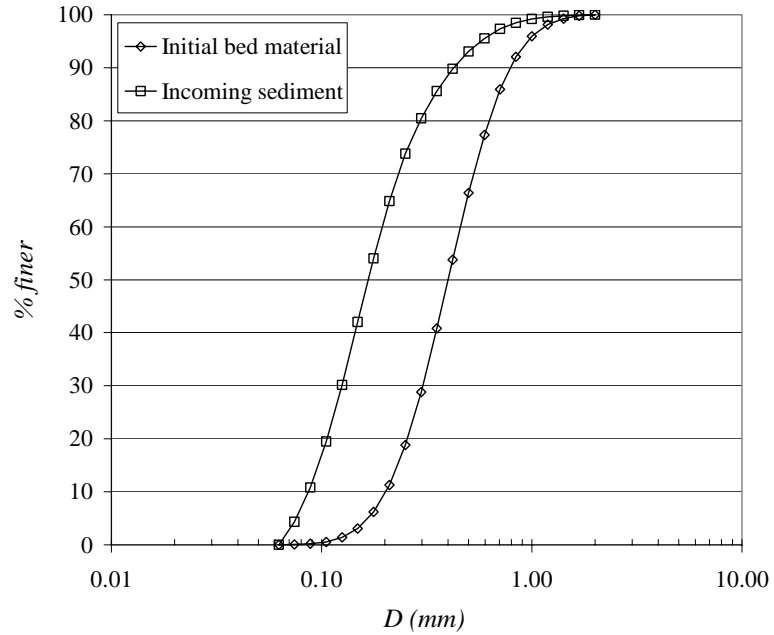


Figure 2 Initial bed material and incoming sediment grain-size distributions. The initial bed material distribution is constant throughout the reach.

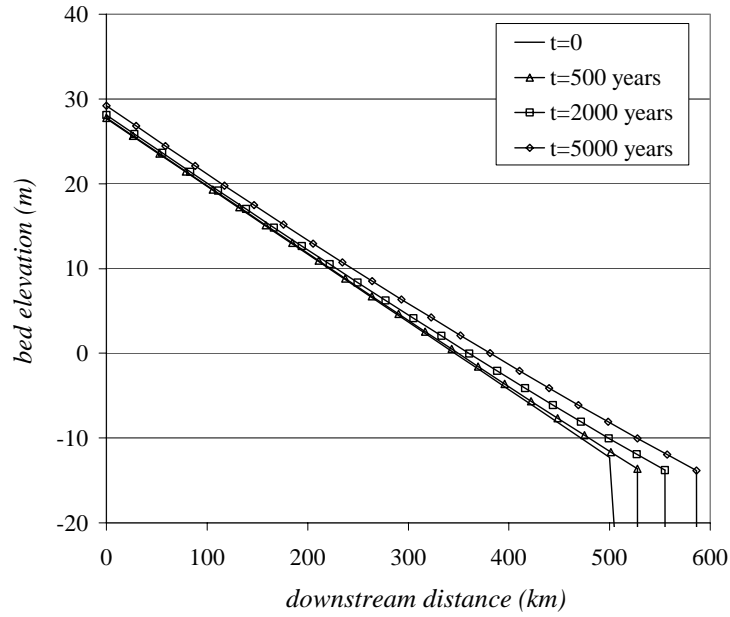


Figure 3 Simulated time evolution of the longitudinal profile for the case of delta progradation only.

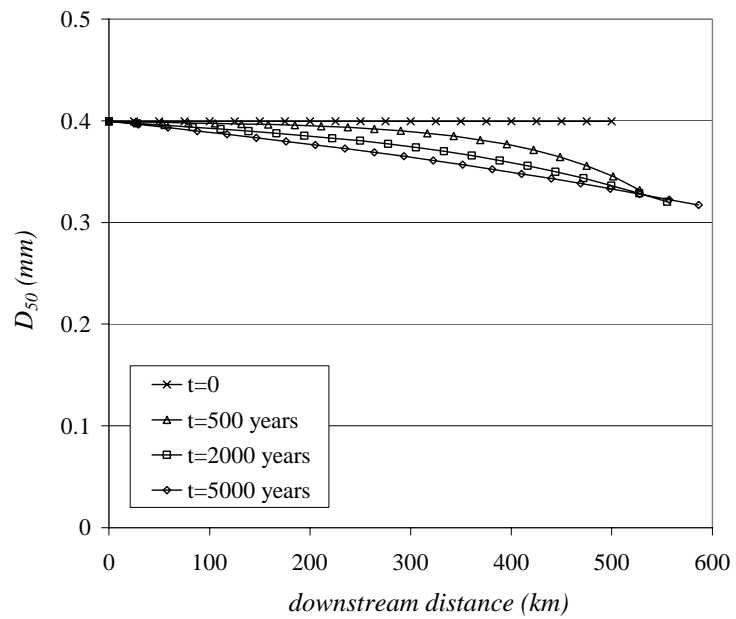


Figure 4 Simulated time evolution of the downstream variation in median bed sediment diameter for the case of delta progradation only.

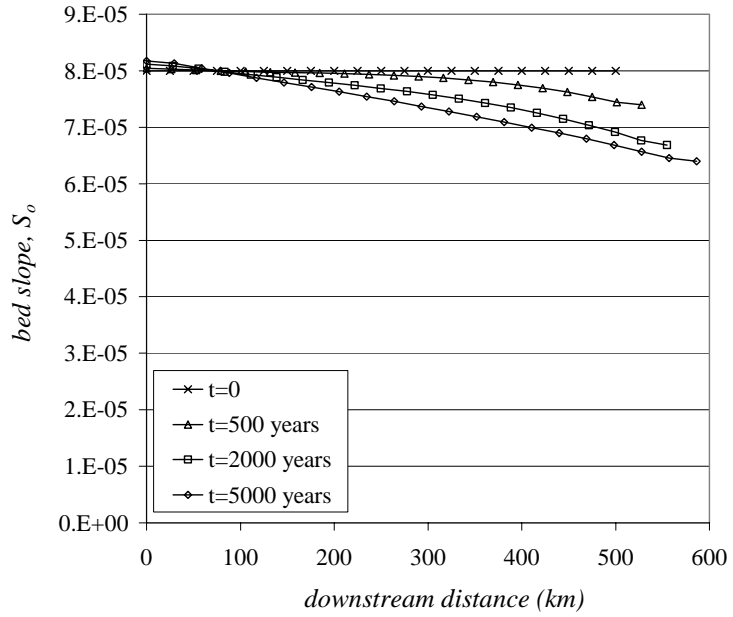


Figure 5 Simulated time evolution of the downstream variation in bed slope for the case of delta progradation only.

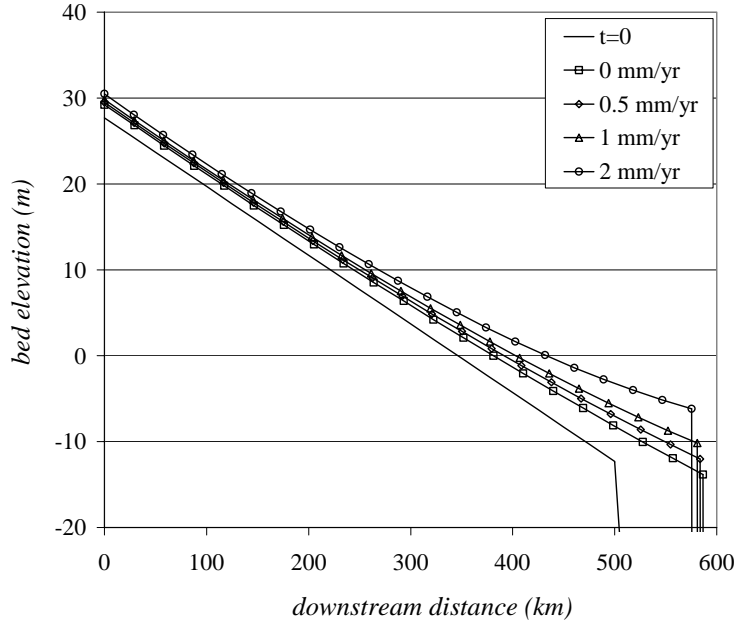


Figure 6 Simulated longitudinal profiles at  $t=5,000$  years for a range of rates of sea-level rise.

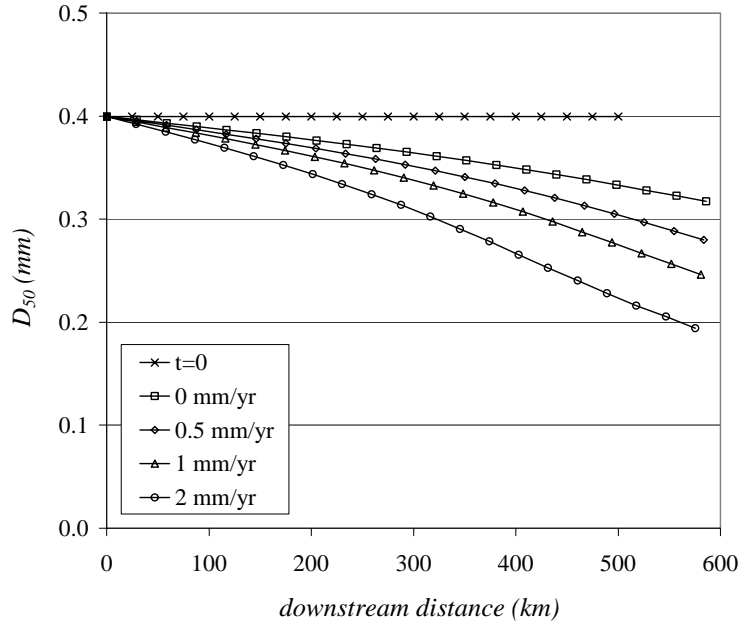


Figure 7 Simulated downstream variation in median bed sediment diameter at  $t=5,000$  years for a range of rates of sea-level rise.

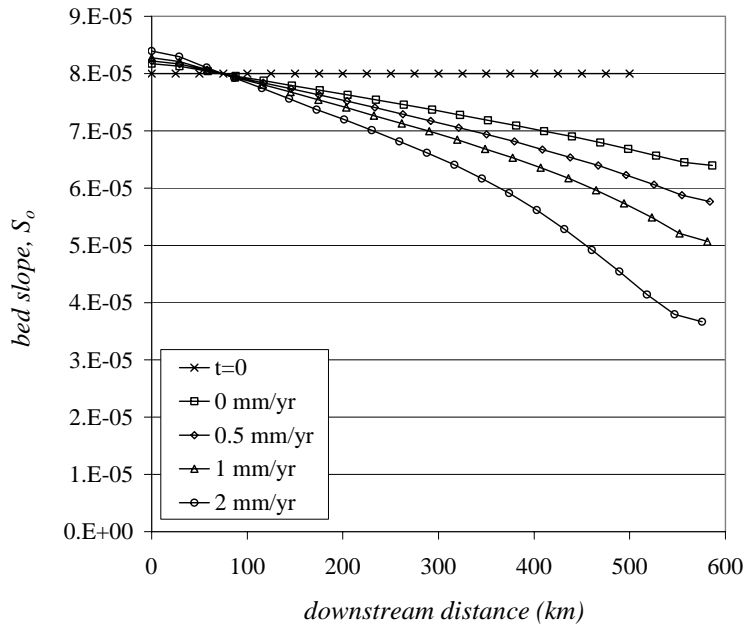


Figure 8 Simulated downstream variation in bed slope at  $t=5,000$  years for a range of rates of sea-level rise.

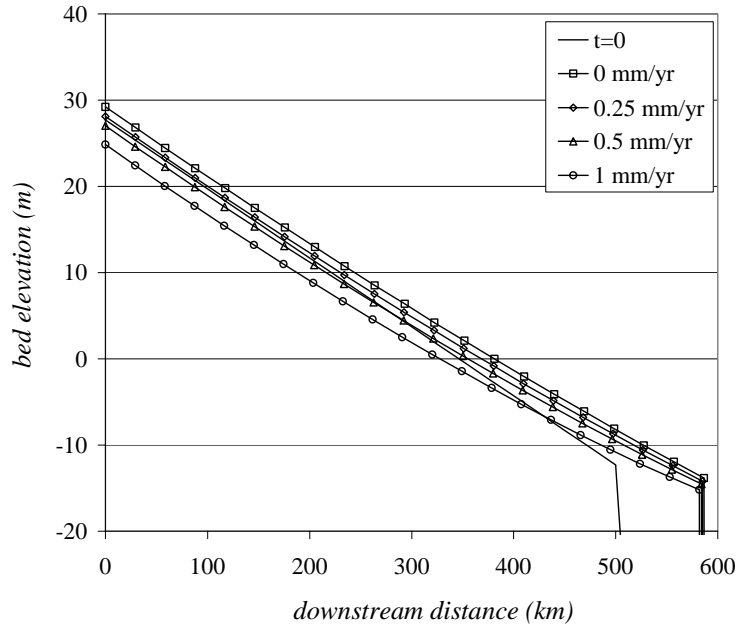


Figure 9 Simulated longitudinal profiles at  $t=5,000$  years for a range of subsidence rates.

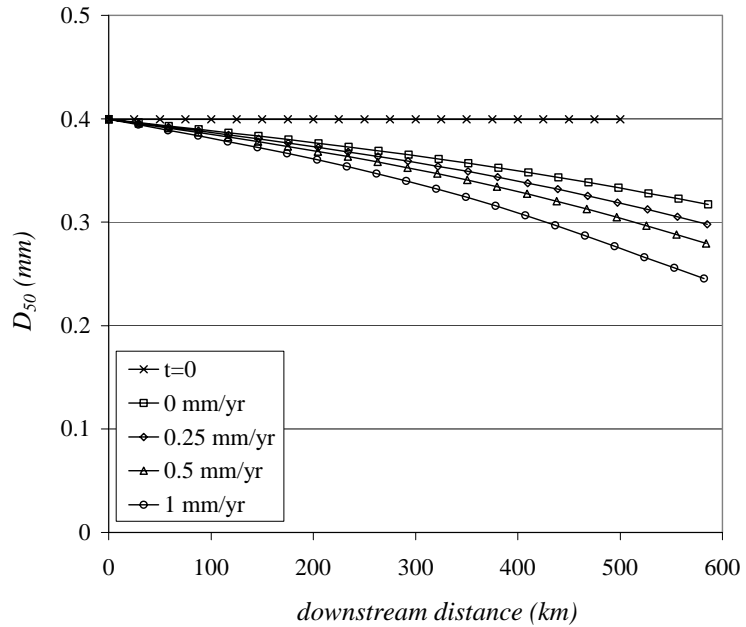


Figure 10 Simulated downstream variation in median bed sediment diameter at  $t=5,000$  years for a range of subsidence rates.

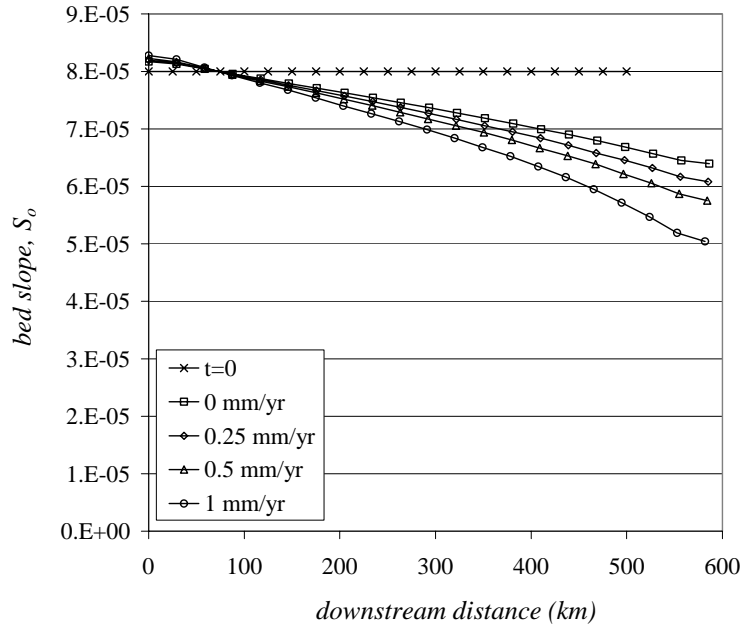


Figure 11 Simulated downstream variation in bed slope at  $t=5,000$  years for a range of subsidence rates.

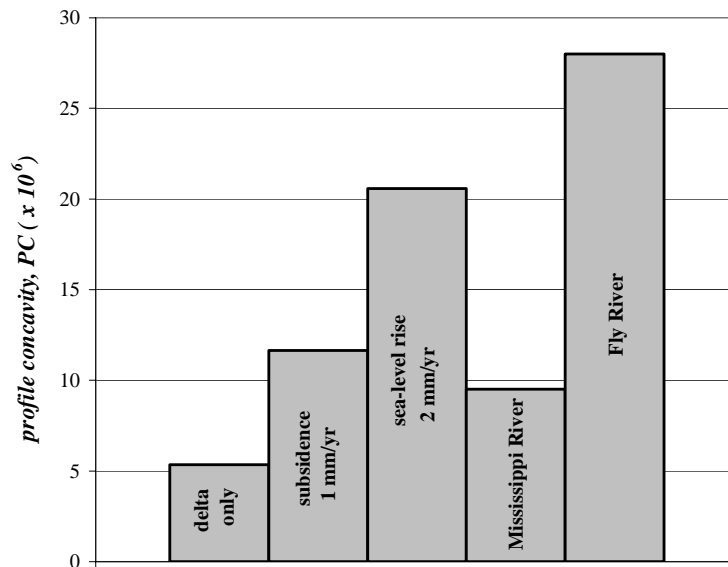


Figure 12 Comparison of dimensionless, reach-averaged, longitudinal profile concavity for several model simulations and the Mississippi and Fly Rivers.

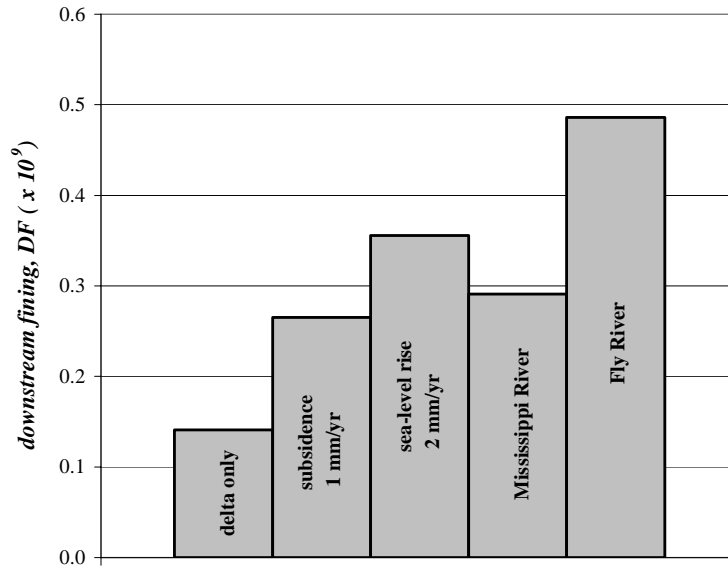


Figure 13 Comparison of dimensionless, reach-averaged, downstream fining for several model simulations and the Mississippi and Fly Rivers.

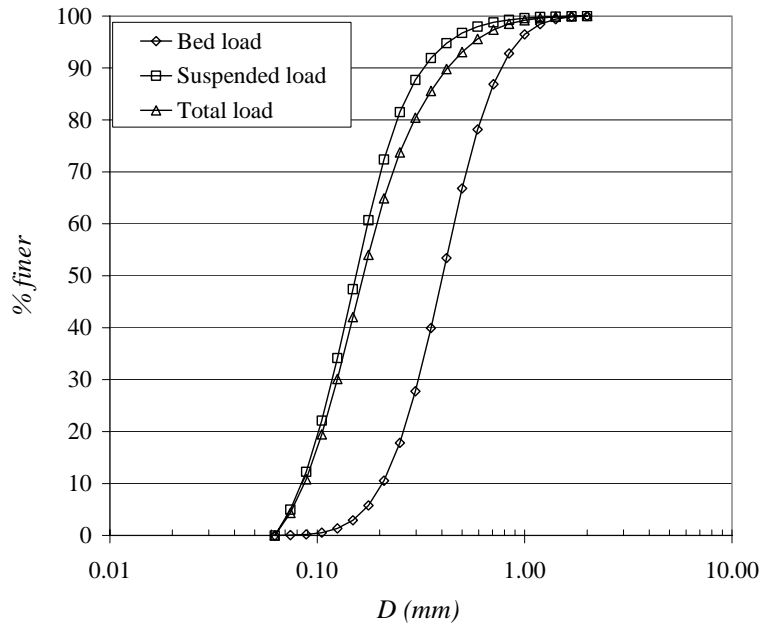


Figure 14 Grain-size distributions of the bed, suspended, and total loads throughout the reach at the initial condition.

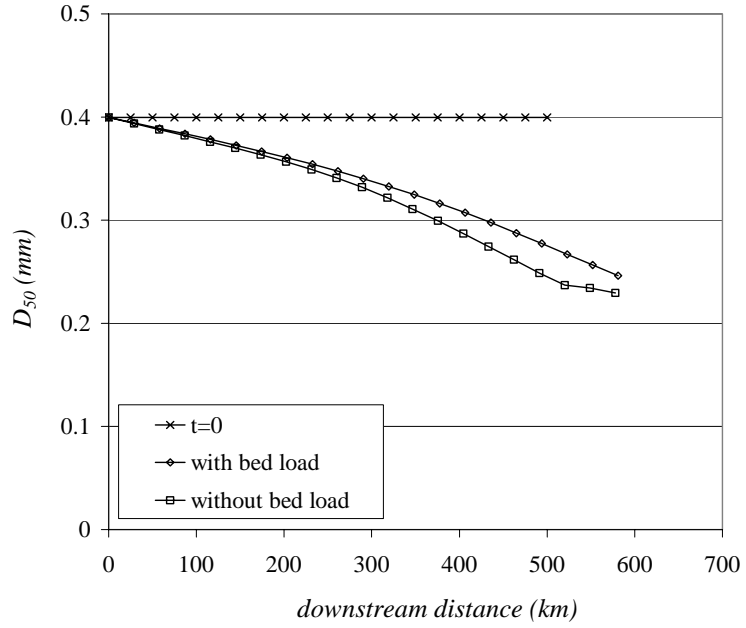


Figure 15 Simulated downstream variation in median bed sediment diameter at  $t=5,000$  years for the case with and without bed load (1 mm/year sea-level rise, no subsidence).

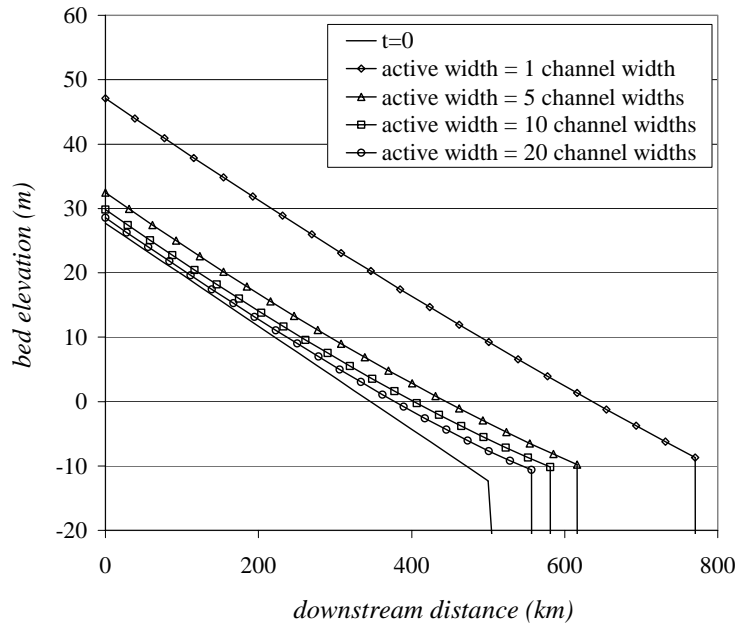


Figure 16 Simulated longitudinal profiles at  $t=5,000$  years for a range of active widths (1 mm/year sea-level rise, no subsidence).

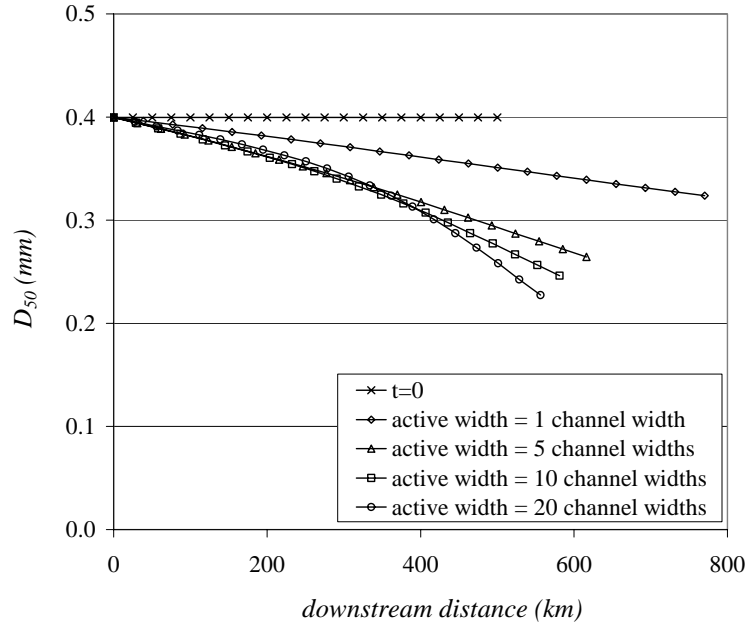


Figure 17 Simulated downstream variation in median bed sediment diameter at  $t=5,000$  years for a range of active widths (1 mm/year sea-level rise, no subsidence).

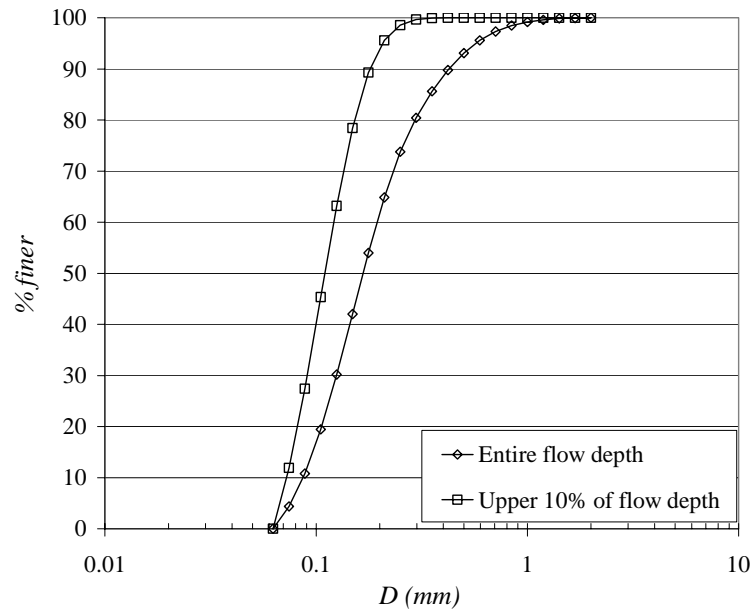


Figure 18 Grain-size distributions of suspended-sediment over the entire flow depth and over the upper ten percent of the flow depth.

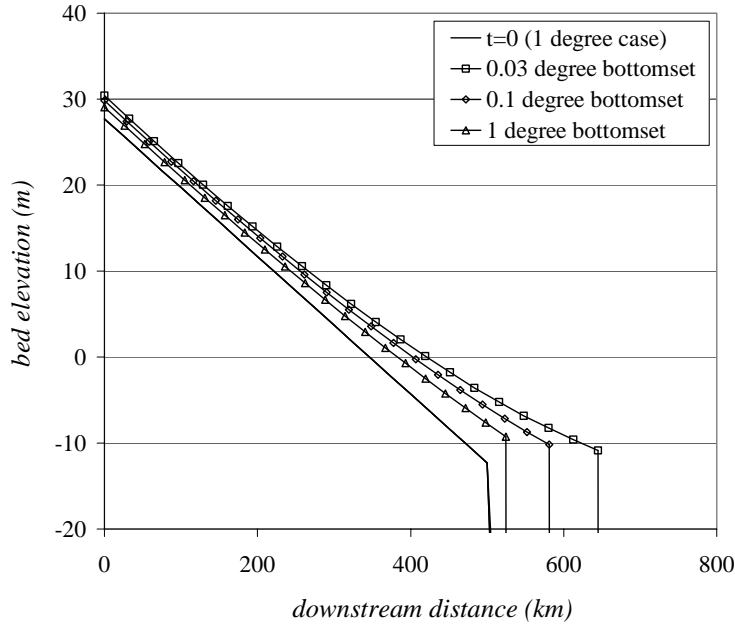


Figure 19 Simulated longitudinal profiles at t=5,000 years for several bottom slopes (1 mm/year sea-level rise, no subsidence).

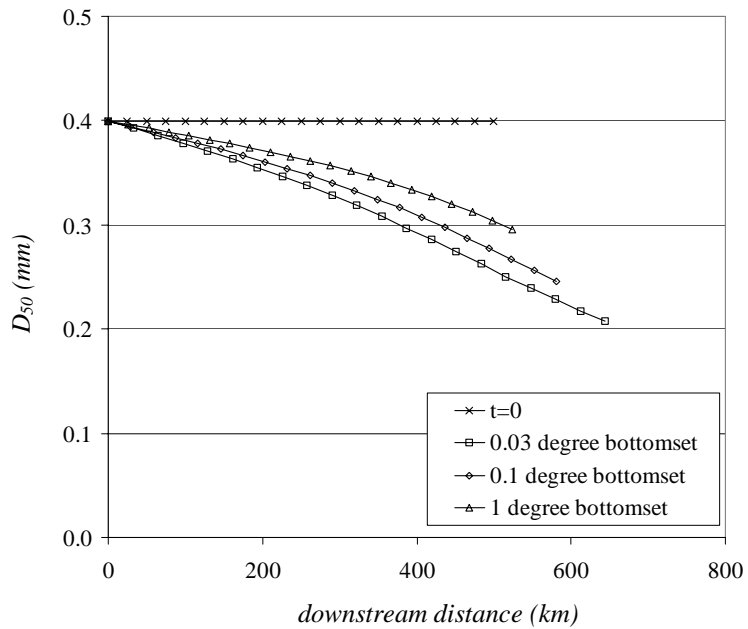


Figure 20 Simulated downstream variation in median bed sediment diameter at t=5,000 years for several bottom slopes (1 mm/year sea-level rise, no subsidence).

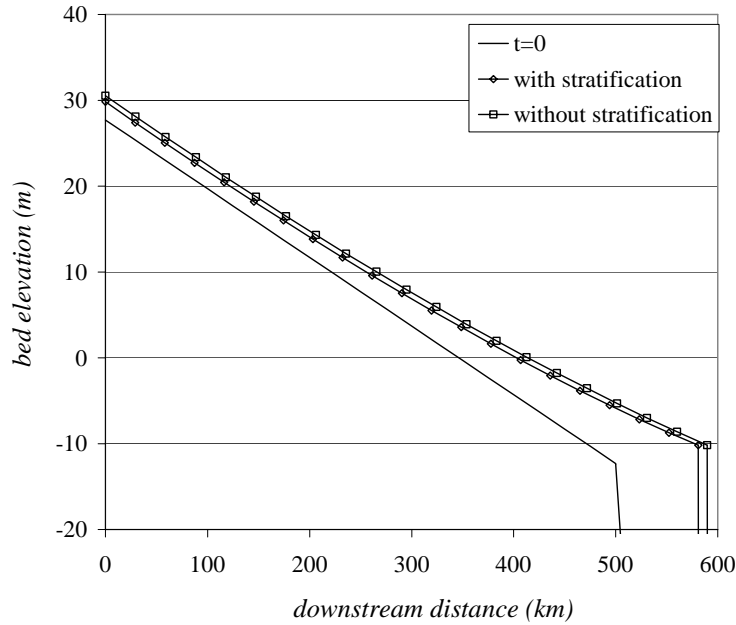


Figure 21 Simulated longitudinal profiles at  $t=5,000$  years for the cases with and without density stratification effects (1 mm/year sea-level rise, no subsidence).

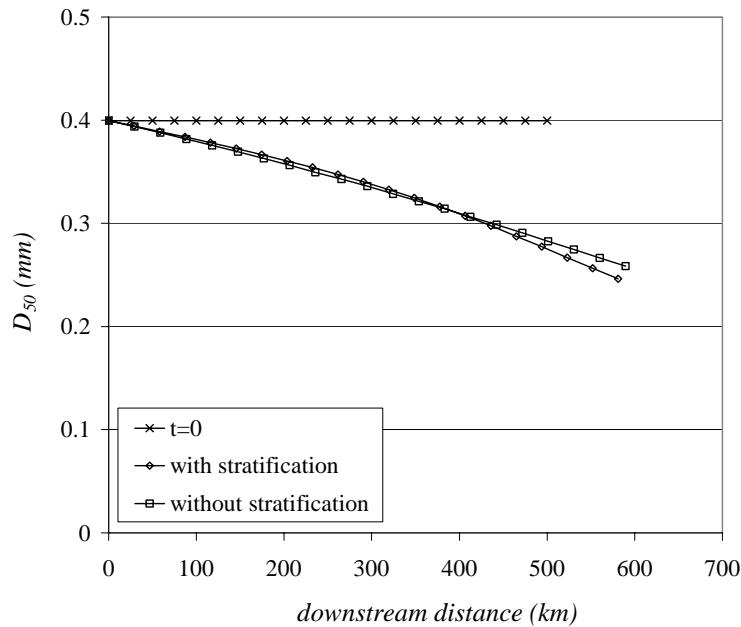


Figure 22 Simulated downstream variation in median bed sediment diameter at  $t=5,000$  years for the cases with and without density stratification effects (1 mm/year sea-level rise, no subsidence).

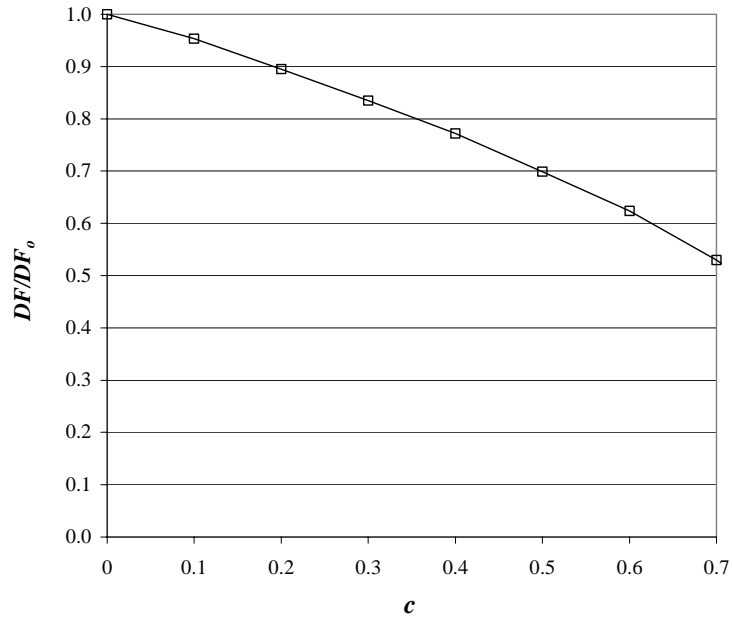


Figure 23 Effect of parameter  $c$ , which controls the partitioning of sediment between transported sediment and active layer sediment, on downstream fining (1 mm/year sea-level rise, no subsidence).  $DF$  is reach-averaged downstream fining;  $DF_0$  is for the case  $c=0$ .